Università della Svizzera italiana

Faculty of Biomedical sciences

Protein profiling of various human samples in Parkinson's Disease and related conditions:

new biomarkers of disease

Elena Vacchi

Thesis director: Prof. Dr. med. Alain Kaelin-Lang

Thesis co-director: PD Dr. med. Giorgia Melli

Internal expert: Prof. Vittorio Limongelli

External expert: Prof. Dr. med. Gabor Kovacs

Mentor: Prof. Dr. med Davide Rossi

Abstract

Parkinson's disease (PD) is the second most frequent neurodegenerative disorder of the elderly, characterized by selective dysfunction and progressive loss of dopaminergic neurons in the substantia nigra-pars compacta, associated with pathologically α-Synuclein (αSyn) deposits in the brain and peripheral organs. To date, PD remains without effective causal treatment and a definitive diagnostic test. Thus, the discovery of biomarkers is essential for better and more efficient treatment of the patients and the development of specific disease-modifying therapies.

With the aim to identify a biomarker for PD and develop a not invasive and reliable diagnostic test, I investigate two peripheral tissues, skin and blood tissues, both easily accessible and of high interest for PD's biomarkers research. Indeed, the skin contains peripheral autonomic nerves strongly involved at early stages of PD, while blood contains subpopulations of EVs produced by central nervous system cells carrying information about brain pathology and involved in immune and inflammatory pathways.

A longitudinal case-control study was performed enrolling patients with PD (n=30), age-matched healthy control (n=22), and atypical parkinsonism (AP, n=23). In skin biopsy, multiple forms of pathological αSyn and intraepidermal nerve fiber density (IENFD) reduction were investigated, and the diagnostic accuracy was evaluated for each of them. Moreover, these parameters were measured longitudinally at baseline and after two years to assess their capability to predict disease progression. In blood, distinctive plasmatic extracellular vesicles (EVs) subpopulations were characterized by simultaneous immunophenotyping 37 different membrane proteins. The diagnostic accuracy of the most expressed was determined, and a diagnostic model based on EV surface markers expression was built via supervised machine learning algorithms.

A higher expression of all the pathological αSyn forms and an overt small fiber neuropathy were found in PD skin compared to healthy subjects and patients with tauopathies. A progression of denervation, not of pathological αSyn, was seen in PD at two years-follow-up: lower IENFD at baseline was associated with a cognitive and motor decline in PD. Moreover, a skin biopsy-derived compound marker, resulting from a linear discrimination analysis model of all the parameters, stratified patients with accuracy (77.8%), including the discrimination between PD and other types of synucleinopathies (84.6%).

In blood, a higher amount of EV was identified in PD. 17 out of 37 EV-surface markers were statistically differentially expressed between groups, most of which were related to inflammatory/immune response. A random forest diagnostic model based on these EV markers expression correctly classified 88.9% of patients with reliable diagnostic performance after internal and external validations.

In conclusion, skin and blood analysis provided relevant results, potentially impacting clinical practice. Both are minimally invasive tests for patients and can be repeated over time to follow up the course of the disease. While for EV, the field is new and needs further investigation, for skin, the next step should be a multicentric standardization of the technique.

1. Introduction 4
1.1 Parkinson's disease 4
1.2 Biomarkers of Parkinson's Disease 6
1.3 α-Synuclein 8
1.4 Extracellular Vesicles 11
2. Aims of the project and study design 14
3. Cervical skin denervation associates with αSyn aggregates in PD 15
Methods 15
Results 18
Figures and tables 21
4. αSyn oligomers and small nerve fiber pathology in skin biopsy are biomarkers of PD 27
Methods 28
Results 31
Figures and Tables 33
5. Immune profiling of plasma-derived EVs identifies PD 44
Methods 45
Results 48
Figures and Tables 51
6. Profiling Inflammatory EVs in Plasma and CSF: An Optimized Diagnostic Model for PD 62
Methods 63
Results 65
Figures and Tables 67
7. Discussion 77
8. Conclusion 86
9. Bibliography 87
10. Abbreviations 95
11. List of publications and other activities 96

1. Introduction

1.1 Parkinson's disease

Parkinson's disease (PD) is a neurodegenerative disorder characterized by selective dysfunction and progressive loss of dopaminergic neurons, especially in the substantia nigra-pars compacta, associated with pathological α-Synuclein (αSyn) deposit in the brain and peripheral organs. It is the second most frequent neurodegenerative disorder of the elderly, and it is estimated that more than 5 million people worldwide, over age 60, have PD [1,2]. Moreover, with the increase in life span and the consequent aging of the world population, the number of PD patients is expected to increase in the next few years [3]. Although the pathology was described for the first time in 1817, after two centuries, PD remains without definitive diagnostic biomarkers and disease-modifying therapies [4].

1.1.1 Epidemiology and etiopathogenesis

PD affects 1% of the people above 60 years [5]. The prevalence is higher in Europe and America compared to other countries [6] and ranges from 1 to 2 per 1000 in unselected populations [5]. Incidence data are influenced by misdiagnosis and under-diagnosis of the disease, but it is estimated around 10-20 per 100,000 inhabitants [5].

The risk of developing PD is multifactorial, probably due to the interplay between environmental and genetic elements. In line with other neurodegenerative disorders, age is the major known risk factor: prevalence and incidence rise with age and culminate around 80 years of age [6]. Thus, with the increase in life span and the consequent aging of the world population, PD is estimated to increase more than 50% by 2030 [1,6]. The median age of onset is 60 years, whereas, considering the whole PD population, only 4% of patients have an early start under 50 [7]. In addition, the incidence is also influenced by gender: men have a higher probability of developing PD than women, with a male/female ratio of 3:2 [6].

Epidemiological studies have found several environmental factors able to alter the risk of developing PD. Among these, pesticide exposure, rural living, and head injury have been associated with an increased risk, while smoking, coffee drinking, and non-steroidal anti-inflammatory drug use with a decreased risk [8]. Although there is a correlation between environmental factors and pathology, cause-effect associations have not been demonstrated yet; thus, additional studies are needed. Finally, although PD is defined as a sporadic and non-genetic disease, 5-10% of cases are inherited [9]. Genome-wide association studies have identified several genes associated with the pathology: mutations of SNCA, LRRK2, VPS35, DNAJC31, EIF4G1, and CHCHD2 genes are linked with autosomal dominant forms of PD; while mutations of PARK2, PINK1, and PARK7 genes have been linked to autosomal recessive forms of the disease [10]. The list of mutations linked to PD is growing and accounts for 2-3% of the late-onset cases and 50% of early-onset forms [10].

1.1.2 Clinical features

PD is primarily described as a movement disorder characterized by bradykinesia, muscular rigidity, rest tremor, and postural and gait impairment [11]. Nevertheless, the appearance of motor symptoms occurs about 10-15 years after the actual onset of the disease [4,6]. The premotor or prodromal phase of PD is characterized by unspecific and heterogeneous symptoms that involve especially the autonomic and peripheral nervous system (PNS). Indeed, at the early stages of the disease, PD patients display symptoms like gastrointestinal dysfunction and constipation [12], reduced cardiac uptake [13,14], urinary and sexual dysfunctions [13], reduced salivation, over-production of sweat and sebum, fatigue, pain, stiffness, depression, sleep disorder and defective thermoregulation [13,15]. These symptoms remain unnoticed and misinterpreted for a long time [15]. Since it has been demonstrated that motor symptoms appear when most of the dopaminergic neurons in the substantia nigra of the brain have already been lost [16], the premotor phase represents the best time window to test potential disease-modifying therapy able to arrest or delay the development and progression of the disease [4,6].

After the manifestation of the early motor symptoms, generally bradykinesia, rigidity, and tremor, the pathology tends to get progressively worse, developing urinary dysfunction, orthostatic hypotension, dementia, dysphagia, postural instability, freezing of gait, and falls [4,6]. Moreover, while early signs can be handled with symptomatic therapies, like Levodopa or dopamine agonist, as the pathology advance, these treatments lose effectiveness and start to induce long-term related complications, like motor and non-motor fluctuations, dyskinesia, and psychosis, that clinically characterized the late-stage of PD [4,6].

1.1.3 Atypical parkinsonisms and Lewy Bodies disorders

Atypical Parkinsonisms (AP) are progressive neurodegenerative diseases that share clinical features typical of PD. In addition, like PD, AP are characterized by multisystem degeneration and abnormal protein deposition in brain tissue and peripheral organs. Based on the histopathological analysis of the predominant protein aggregates within the brain, these disorders can be subdivided into synucleinopathies, which include multiple system atrophy (MSA) and Lewy body spectrum disorders (LBSD), and tauopathies, which comprise progressive supranuclear palsy (PSP) and corticobasal degeneration (CBD). Since the similarity at both clinical and molecular levels, the differential diagnosis between PD and AP is challenging for clinicians.

MSA is clinically characterized by a variable combination of autonomic failure, parkinsonism, cerebellar ataxia, and/or corticospinal tract dysfunction[17]. Based on the motor phenotype, MSA is clinically classified into those with predominant parkinsonism (MSA-P) or cerebellar ataxia (MSA-C) [17]. The median age of onset is 58 years, while the mean disease duration is between 7–9 years, showing a faster progression than PD, typical of the AP [18]. From a molecular point of view, MSA displays neuronal loss, gliosis, myelin pallor, and axonal degeneration, especially in the substantia nigra, dorsolateral zone of the caudal putamen, vermis, cerebellar hemisphere, and inferior olivary nucleus[18]. Finally, the neuropathological hallmark of MSA is the presence of cytoplasmic inclusions in oligodendrocytes, termed glial cytoplasmic inclusions (GCIs), which are mainly composed of αSyn. The main areas involved

in GCI accumulation are the pyramidal, extrapyramidal, corticocerebellar, and preganglionic autonomic systems[18].

The Lewy body spectrum disorders (LBSD) group comprise, besides PD, Parkinson's disease dementia (PDD), and dementia with Lewy bodies (DLB)[19]. They share neuropathological and clinical features with both PD and Alzheimer's disease. Classically, PDD can be distinguished from DLB by the timing of symptom onset: PDD is diagnosed if an individual had already a well-established PD diagnosis before the onset of dementia; while DLB is diagnosed if the dementia is already present at the beginning of the parkinsonian symptoms[20]. DLB manifests dementia, fluctuating cognition, and visual hallucinations at the beginning of the disease. Both are characterized by Lewy bodies (LBs) and Lewy Neurites (LNs) in which αSyn is the main component but, differently from PDD, DLB show also β-amyloid and Tau deposits[20].

Progressive Supranuclear Palsy (PSP) is the most common AP. It is characterized by supranuclear ophthalmoplegia, postural instability, dysarthria, executive dysfunction, dysphagia[21]. Often PSP patients show an asymmetric onset, tremor, and moderate initial response to levodopa, complicating the differential diagnosis with PD[21]. Neuropathologically, PSP displays the accumulation of neurofibrillary tangles composed of tau protein and neuropil threads in the subthalamic nucleus, striatum, pallidum, brainstem regions, medulla oblongata, dentate nucleus, and in the cerebral cortex. In addition, PSP also shows tufted astrocytes and oligodendroglial coiled bodies[22].

Corticobasal Degeneration (CBD), like PSP, is a tauopathy clinically characterized by asymmetric dystonia, apraxia, myoclonus, pyramidal signs, and cortical sensory loss[23]. CBD pathology includes astrocytic plaques, tau accumulation in axons and oligodendrocytic cell processes, and coiled bodies in oligodendroglia [22]. The neuronal and glial tau pathology initially involved the frontoparietal and motor cortical areas and the striatum, and subsequently other subcortical nuclei and the brainstem.

1.2 Biomarkers of Parkinson's Disease

The definitive diagnosis of PD is possible only with a post-mortem pathological examination [6] that highlights moderate/severe neurodegeneration in the substantia nigra associated with the presence of Lewy pathology in surviving neurons in the absence of other pathologies able to induce parkinsonism [24]. To date, diagnostic tests able to identify patients at the early stages of the disease are missing. The clinical diagnosis, based only on motor symptoms manifestation, has significant limitations: it is for later stages and do not consider prodromal autonomic and peripheral symptoms; it has a high rate of misdiagnosis and under-diagnosis, especially at the beginning of the disease when PD may be confused with other parkinsonisms movement disorders. Thus, identifying specific and early biomarkers for PD is critical for developing effective disease-modifying therapies, and by discriminating PD from atypical parkinsonisms (AP), for the proper diagnosis and management of patients.

1.2.1 Imaging biomarkers

At the beginning of the disease, the progressive reduction of dopamine due to the loss of dopaminergic neurons is balanced out by compensation mechanisms, such as increased sensitivity of dopamine receptors [25]. Thus, it does not immediately result in clinical motor symptoms, which instead manifest themselves when about 60% of neurons have already been lost [25,26].

The loss of dopaminergic neurons and the structural changes in the substantia nigra can be monitored *in vivo* by positron emission tomography, magnetic resonance imaging, single-photon emission computed tomography, or transcranial sonography [6]. These imaging technologies can differentiate PD from other movement disorders without dopaminergic neurodegeneration, such as essential tremor, but not from AP, like MSA or PSP that are characterized by presynaptic dopaminergic terminals deficit [6]. Moreover, dopaminergic imaging results abnormal only after a substantial loss of neurons, thus can't be used for early diagnosis [6].

Imaging technologies can also estimate the abnormal accumulation of protein or iron in the brain, the activity of aromatic amino acid, or the level of vesicular monoamine transporter, all factors involved in PD pathogenesis [27]. However, the results obtained from these studies are not unequivocal and do not show enough sensitivity and specificity to use them for diagnostic purposes. Up to date, imaging technologies can only support the clinical diagnosis that remains the gold standard for diagnosing PD in vivo [27].

1.2.2 Genetic biomarkers

The first gene associated with PD diagnosis was identified in Italian and Greek families in 1997 [28,29]. The mutated gene was SNCA which encodes for αSyn protein [29]. From that time onward, the list of the genes linked to PD has grown substantially.

Besides the different genes able to induce PD, each of them can undergo multiple mutations with variable penetrance and expressivity. Each patient has alternative polymorphisms that alter the susceptibility and the genetic risk of developing PD [27]. As a consequence of this variability, each single patient results clinically and neuropathologically different from the other: for example, PD patients with a mutation in PARKIN or PINK1 proteins show dopaminergic degeneration in the brain with rare or completely absent LBs pathology, differently from patients with a mutation in GBA protein that display a widespread, abundant presence of LBs[30].

Thus, although known genes are linked to PD, the situation is much more complicated, and univocal genetic biomarkers don't seem feasible. Moreover, genetic biomarkers are helpful especially for familial PD, which are easier to identify: they usually have a juvenile-onset, other cases in the family, and account for only 5-10% of all the PD subjects. However, the study of genes involved in PD development can help identify protein biomarkers for disease diagnosis or prognostic evaluation.

1.2.3. Biochemical biomarkers

Many molecules directly involved in the pathogenesis of the disease, such as dopamine metabolites, oxidative damage markers, inflammatory markers, miscellaneous markers, and protein markers, have been analyzed in multiple tissues and body fluids as PD biomarkers. Despite this, none of them resulted in clinically valuable [27].

The discovery of the genetic link between SNCA and PD and the subsequent finding of αSyn as the main component of LBs and LNs [2,31], has led αSyn to be the most studied biomarker. In the absence of an imaging tracer able to detect and measure pathological αSyn directly in living patients' brains, now the focus is predominantly on αSyn detection in the PNS of peripheral tissues.

Moreover, another research field of great interest focuses on extracellular vesicles (EVs) and their molecular profile. Indeed, EVs are a heterogeneous population of secreted membrane particles involved in physiological cell to cell communication, transmission of biological signals, and regulation of many pathophysiological processes, including immune responses and inflammation [32]. Due to the release of EVs into the bloodstream from endothelial and microglial cells responding to central nervous system (CNS) diseases as well as from neuronal cells, and due to the expression of surface markers which allow their tracking to the cell of origin, EVs are relevant tools for diagnostic purposes and biomarker discovery, in PD [33].

1.3 α-Synuclein

αSyn is an intrinsically disordered neuronal protein highly expressed in the brain at presynaptic terminals [2,31]. In physiological conditions, αSyn exists as stable, unfolded monomers but can adopt multiple conformations and interact with biological membranes and proteins [34,35]. Its function is not entirely elucidated, but it has a role in regulating neurotransmitter release, synaptic function, and plasticity [35]. In pathological conditions, αSyn forms misfolded aggregates, representing the pathological hallmark of a family of neurodegenerative diseases collectively known as synucleinopathies, including PD, DLB, MSA, and pure autonomic failure. PD and DLB display intraneuronal aggregates, LBs and LNs; MSA shows principally abundant GCI; while pure autonomic failure is characterized by αSyn deposits in peripheral autonomic ganglia and nerves [35].

1.3.1 αSyn aggregation

The pathological process of physiological αSyn to intracellular insoluble deposits (LBs, LNs, GCI) has not been completely elucidated yet [36,37]. In the cytosol, αSyn predominantly exists as monomers, with an α-helical conformation that can interact and form unstable dimers. In pathological conditions, αSyn can be subjected to post-translational modification and/or changes in the conformation that leads the protein to self-aggregation and generation of more stable structures, named oligomers, and fibrils, of varying morphologies and dimensions [36,37]. Oligomers and fibrils are considered the main toxic elements able to induce neurodegeneration: they can disrupt membrane integrity, intracellular calcium homeostasis, synaptic transmission, signaling, endoplasmic reticulum–Golgi trafficking, and cause

mitochondrial dysfunction [36,37]. A cell mechanism to contain and mitigate the toxic effect of these elements, that cannot be eliminated, is to deposit and isolate them in cytoplasmic low-toxic and low-dynamic structures: LBs, LNs, and GCI [36,37].

1.3.2 Neuroanatomical Stages of Alpha Synuclein Accumulation in Parkinson's Disease

In 2003, Braak and colleagues developed a staging system to describe the progressive distribution of pathological αSyn in the brain. αSyn aggregates appear first in the olfactory bulb and the dorsal motor nucleus of the vagal nerve (DMV) [38,39]. In the visceromotor neurons of DMV, it is possible to observe both spindle-shaped and globular somatic inclusions, which are respectively LNs and LBs. Whereas LNs are prevalently present in the unmyelinated and long axons of the projection cells of DMV in the medulla [38,39] . In stage 2, retrograde axonal and trans-neuronal transport via descending fibers drive Lewy pathology from the nucleus of the vagal nerve to the lower raphe nuclei, magnocellular portions of the reticular formation, and the locus coeruleus [38,39]. During stages 2 and 3, neurons in the spinal cord, targets of the lower brainstem nuclei projections, develop Lewy pathology. In particular, neuronal cells of the intermediate-lateral nucleus in layer 7 are affected in stage 2, while the large nociceptive projection neurons in layer 1 and the motoneurons in layer 9 are involved in stage 3 [38-40]. In stage 3, Lewy pathology also diffuses into the mesencephalic tegmentum and basal portions of the prosencephalon. At stage 4, LBs and LNs are found in the forebrain, particularly in the transentorhinal region in the anteromedial temporal lobe. At this point, aggregated αSyn gradually spreads throughout the entire neocortex: in high-order sensory association areas and prefrontal fields of the neocortex, such as subgenual, insular, and anterior cingulate areas (stage 5) and in the first-order sensory association areas, primary sensory and premotor/motor fields (stage 6) [38,39].

After 4 years, in 2007, Braak proposed a peripheral origin of PD. Since αSyn aggregates appear first in the olfactory bulb and the DMV, it was postulated that PD possibly originates also from the PNS gastro-enteric synapses, and it invades the CNS via retrograde axonal transport [41]. Many clinical observations and experimental settings have supported this hypothesis. αSyn can be detected in the gut of PD patients up to 20 years before the diagnosis [42], and truncal vagotomy appeared to lower the risk of developing PD by 40–50% after 10–20 years [43]. In a transgenic rat model with excess levels of αSyn, the injection of αSyn fibrils into the duodenum fully recapitulated the trans-synaptic propagation through the vagus nerve to DMV, through the sympathetic connectome to the celiac ganglion and IML, and then rostrally to the brainstem with involvement of locus ceruleus and substantia nigra. This model also provided the first evidence of a secondary anterograde transport to the stomach and heart [44].

Few years after the publications, several studies demonstrated that the Braak's staging system was not valid for all patients. Indeed, a number of PD subjects do not present pathology in the DMV, whereas they had clear pathology in the locus cereleus, substantia nigra and amygdala, making impossible to classify these patients with the "Braak Model" [45].

1.3.3 Brain- vs. Body-first hypothesis

In 2019, Borghammer and colleagues, proposed the "brain- vs. body-first" model, trying to combine the two main hypothesis of synucleinopathies origin and spreading [45].

This model suggests the presence of two different types of PD: in the brain-first type αSyn pathology appears in the CNS, in particular in the amygdala, followed by the substantia nigra, and locus coeruleus, without the prior involvement of the autonomic nervous system; while in the body-first type, αSyn aggregates appear first in the enteric or peripheral autonomic nervous system, followed by a propagation to the CNS via the vagus and the sympathetic spreading route to the sympathetic trunk and heart, and a subsequently development of "brain-first" phenotype [45,46]. From a clinical point of view, the body-first type is associated with REM sleep behavior disorder (RBD) during the prodromal phase and marked autonomic damage before the dopaminergic system involvement, while the brain-first is RBD negative during the prodromal phase and presents a marked involvement of the nigrostriatal system before the autonomic PNS damage [45,46].

This classification seems to be in line with histopathological analysis of post-mortem cases that show two main patterns of Lewy pathology distribution [46]: the caudo-rostral and the amygdala-centred patterns. The caudo-rostral patter is recognisable by: 1) the first formation of αSyn outside the brain, more probably in the enteric nervous system; 2) the autonomic nuclei are the earliest areas affected in the CNS; 3) a higher pathology in the brainstem than in the telencephalon is detectable. The amygdala-centered pattern instead are characterized by 1) the first formation of αSyn is in the amygdala, transentorhinal cortex, or closely connected structures, and in rarer cases in the substantia nigra and locus cereleus; 2) with the disease course, the most abundant pathology remains restricted to the amygdala, entorhinal cortex, and substantia nigra, and relatively less pathology is found in the lower brainstem and spinal autonomic nuclei.

Finally, this model was further refined [46], proposing that in body-first patients, pathological αSyn bilaterally spreads through the vagus nerves and sympathetic connections to the CNS. The propagating of αSyn within the brain results symmetrical, leading to a more aggressive symmetric parkinsonism since the dissemination of αSyn and the nerve loss will be bilateral. In contrast, the brain-first type, starting at a specifying point within the brain, is characterized by an asymmetric dopaminergic loss and parkinsonism due to the presence of pathological αSyn in just one hemisphere. The dissemination of Lewy pathology to both the brainstem nuclei and the contralateral hemisphere requires a longer time, explaining a slower disease progression in the brain-first clinical phenotype [46].

1.3.4 Alpha Synuclein in the Peripheral Nervous System as a Biomarker for Synucleinopathies

The involvement of PNS, either early or later in the course of the disease, has been widely demonstrated in PD and synucleinopathies. In fact, in PD and DLB, αSyn aggregates have been detected throughout the PNS in sympathetic ganglia, enteric nervous system, cardiac and pelvic plexus, submandibular glands, adrenal medulla, and skin [47]. In MSA, αSyn aggregates have been demonstrated in sympathetic ganglia [48], in Schwann cells cytoplasm [49], and skin autonomic nerves [50]; of note, a study on sural biopsy

showed a reduction of small unmyelinated fibers (somatosensory and autonomic) in 23% of MSA cases [51] and mild degeneration of cardiac sympathetic nerves had been described [52]. These findings have important implications for discovering in vivo biomarkers of disease that are so urgently needed for neurodegenerative diseases. A recent systematic review and meta-analysis on determining the most suitable tissue for assessing αSyn deposits in PD found that skin biopsy using anti-phosphorylated αSyn antibodies displayed the best diagnostic accuracy compared to the gastro-intestinal tract, submandibular glands, minor salivary glands, parotid glands, and olfactory epithelium [53]. Indeed, phosphorylated αSyn has been found in skin small fibers nerves innervating autonomic structures [54] in PD, and of note also in RBD patients, suggesting the potential value of skin biopsy as an early biomarker of disease [55,56]. More recently, aggregated αSyn has been demonstrated in skin nerves by conformational antibodies, recognizing oligomeric forms of the protein [50,57], and using proximity ligation assay technology in the skin [58]. In addition, skin biopsy offers the great advantages of being minimally invasive, compared to other biopsy sites like the gastro-enteric system; it can be repeated in time during follow-ups and provides the unique opportunity to access the sympathetic structures in the skin (sweat glands, small arterioles, muscle arrector pili), which animal models have demonstrated as possibly involved early [44]. Of great interest, a skin biopsy can be used to detect small fiber neuropathy. Several clinical studies have shown that PD patients develop a small fiber neuropathy [59] which is the most likely expression of the neurodegenerative process and seems to correlate to disease progression [50,60]. These findings imply a possible role of small fiber neuropathy as a disease biomarker.

1.4 Extracellular Vesicles

EVs are a heterogeneous population of lipid bilayer membrane particles produced by almost all human cells and released into pericellular space and several body fluids. Based on their biogenesis, EVs can be classified into three subtypes: exosomes formed from multivesicular bodies following the endosomal pathway [61], ectosome or microvesicles produced via outward budding of plasma membrane [62], and apoptotic bodies obtained during apoptosis via cellular disassembly [63]. EVs are involved in physiological cell to cell communication, transmission of biological signals, and regulation of many pathophysiological processes, including immune responses and inflammation [64]. On their surface, EVs displayed proteins that can provide information about their biogenesis, cell of origin, trafficking, and uptake by a recipient cell; while inside EVs contains a variety of protein, lipid, mRNA, and miRNA that can influence the physiological state of the recipient cell after the uptake [65]. Both the surface proteins and the cargo change in pathological conditions.

The production of EVs by neuronal cells, the capability of EVs to pass the blood-brain-barrier and reach peripheral body fluids, the expression of surface markers which allow their tracking to the cell of origin and reflect the physio/pathological status of the originated cell, the possibility to easily isolate neuronal EVs with non-invasive techniques, make EVs particularly relevant for the diagnosis of neurodegenerative disorders [66].

1.4.1 EVs function in physiological and pathological conditions

As for EVs produced in all the other parts of the body, brain-EVs' primary function is to exchange information between cells, facilitating communication inside and outside the CNS. In addition, brain-EVs are involved in specific neuronal physiological processes, such as synaptic physiology, trophic support, axon damage regeneration, and regulation of neuroinflammation [67].

In pathological conditions, EVs show a direct involvement in speeding neuronal dysfunction and progression of neurological disorders. In PD, for example, EVs produced by both neurons and glia are involved in the uptake, shuttle, and secretion of pathological proteins and inflammatory factors [67]. *In vivo* and *in vitro* observations show that the propagation of toxic αSyn through EVs can induce pathological αSyn aggregation in a distant area of the brain and different cell subtypes, while the spreading of inflammatory modulators, such let-7, promote inflammation and neurodegeneration [67].

1.4.2 EVs as biomarkers for PD

Several studies have explored the utility of EVs as biomarkers for PD by quantifying brain-derived EVs or measuring specific target proteins in neuronal-derived EVs.

In EVs from cerebrospinal fluid (CSF), PD patients showed a higher amount of αSyn [68] and several miRNAs, such as miR-153 or let-7g-3p [69], than healthy control (HC) subjects. And while the amount of αSyn in EVs did not correlate with disease severity, not making it a promising biomarker, the levels of the miRNAs showed good sensitivity and specificity for tracking PD progression [69]. Although CSF is the optimal body fluid for neurodegenerative disorders biomarkers discovery, as it permeates the cerebral cortex, spinal cord, cerebral ventricles, and medullary canal, receiving EVs mainly from the CNS, the lumbar punction to obtain CSF is invasive, and the content of EVs is low. Consequently, most of the studies were performed in peripheral blood, which, however, contains different subpopulations of EVs that derive mainly from immune cells, platelets, and endothelial cells [70].

The content of blood-derived EVs has been intensely investigated: considering all the different subpopulations, several miRNAs have been observed increased in PD compared to HC, showing a good diagnostic performance (miR331-5p: area under the curve (AUC)=0.85; miR-505: AUC=0.89); while considering the neuronal-derived EVs content of αSyn (AUC=0.65) and DJ-1 (AUC=0.70) the results were less promising [67]. Moreover, as shown by recent work, the detection and combination of multiple markers improved the diagnostic accuracy of neuronal-derived EVs: the simultaneous quantification of both αSyn and clusterin differentiates PD from other proteinopathies and MSA with excellent accuracy (AUC=0.98 and 0.94 respectively) [71]. Despite this, the amount of these proteins found in plasmatic EVs failed to reflect the disease state, suggesting circulating EVs can be used as supporting elements for PD identification.

Finally, EVs can be isolated by other body fluids such as saliva, urine, and tears. A higher amount of DJ-1 and LRRK2 was observed in urine-derived EVs from PD compared to HC, and their amount correlated with cognitive and motor impairment, while in another study, PD showed more phosphorylated αSyn in salivary neuron-derived EVs compared to HC [67].

In conclusion, to date, we can not provide PD patients with an early diagnosis that could slow down the course of the disease and guarantee a better lifestyle. In particular, the only available tests are to support the late clinical diagnosis. Thus, non-invasive tests that can be repeated over time to follow the disease progression and performed at the appareance of the first pre-motor symptoms are necessary to make progress in the treatment of PD.

Some studies have evaluated the pathological αSyn in peripheral tissues, like skin and blood. In skin, most studies were focused on the P-αSyn; however, it lacks the evaluation of other disease-associated αSyn forms, the comparison between different areas in which to perform the skin biopsy, and a longitudinal study to evaluate the variation of the marker over time. In blood, αSyn has been checked as free protein or within neuron-derived EVs; however, it lacks an overall description of the different EVs subpopulations present in the blood of PD patients, which can provide information about brain pathology and neuroinflammation.

2. Aims of the project and study design

The main aim of my Ph.D. project was to find a reliable biomarker for PD in peripheral tissues. Since a practical diagnostic test should be not invasive, we decided to investigate skin and blood tissues, both easily accessible tissues. Furtherly, the skin contains peripheral autonomic nerves that are strongly involved in PD, especially at early stages, while blood contains subpopulations of EVs produced from CNS cells carrying information about brain pathology and represent a privileged window to investigate inflammatory processes involved in PD.

We performed a longitudinal case-control study and enrolled patients with PD, age-matched HC subjects, and AP patients with synucleinopathies and tauopathies.

We analyzed the peripheral intraepidermal sensory innervation in skin biopsies and detected several pathological forms of αSyn protein at different anatomical sites. For each of those parameters was tested the diagnostic accuracy. Moreover, they were measured at baseline and after two years to evaluate them as biomarkers of disease progression.

In blood, distinctive plasmatic EV subpopulations were characterized by simultaneously immunophenotyping 37 different membrane proteins. The profile of most expressed EV markers was analyzed exploiting machine learning algorithms, and the diagnostic accuracy was determined. In addition, to further improve the diagnostic tool potential, we integrated information obtained by CSF-derived EV analysis.

Therefore, the following thesis will be subdivided into four sections, according to the specific studies I contributed:

1. Cervical skin denervation associates with αSyn aggregates in PD;
2. αSyn oligomers and small nerve fiber pathology in skin biopsy are potential biomarkers of PD;
3. Immune profiling of plasma-derived EVs identifies PD;
4. Profiling Inflammatory EVs in plasma and Cerebrospinal fluid: an optimized diagnostic model for PD.

3. Cervical skin denervation associates with αSyn aggregates in PD

With the aim to identify early biomarkers of disease, in this first study, we described the presence of aggregated αSyn in skin biopsies of PD patients.

αSyn and P-αSyn detection by immunohistochemistry was already investigated in cutaneous autonomic nerve fibers of PD [72,73], and patients with AP, like MSA [73,74], and DLB [75], suggesting that skin biopsy could be a diagnostic tool for synucleinopathies. Despite the promising potential obtained, especially with P-αSyn, the increasing evidence of the pathological role of αSyn oligomers/small aggregates in PD has prompted us to investigate these isoforms in the cutaneous PNS with a conformation-specific antibody (5G4) reactive for αSyn aggregates and not to monomers [76,77]. Indeed, while αSyn oligomers/small aggregates are thought to be an early neurotoxic agent that plays a crucial role at the beginning of the neurodegenerative cascade leading to PD [36], the pathogenic role of P-αSyn is more controversial. The marked accumulation of P-αSyn in the LBs may be the result of a cellular defense mechanism to its toxic role and neurodegenerative potential or a secondary deposit event to enhance LBs degradation. Moreover, the P-αSyn antibody could highlight physiological phenomena in response to cellular stresses or insults that, in general, can significantly increase the phosphorylation state of many proteins, including αSyn [78].

In this study, we investigate both the aggregated and phosphorylated αSyn isoforms in skin biopsies from three anatomical sites (cervical area, thigh, and ankle) in PD, AP, and HC. We found aggregated αSyn deposits in dermal nerves, especially in those surrounding sweat glands (SG) and other autonomic structures of the dermis (a spatial distribution resembling that of P-αSyn). They are as sensitive and specific as P-αSyn for the clinical diagnosis of PD: both 5G4 and P-αSyn antibodies showed a reliable diagnostic performance, but of great interest, 5G4 immunofluorescence for cervical site only is just as effective in diagnosing PD as immunofluorescence of samples from all three anatomical sites.

In addition, another crucial emerging point in this scientific field was that most PD patients displayed cutaneous somatic and autonomic denervation [59,60]. Thus, in this study, we measured skin innervation at baseline and its variation with time (follow-up analysis at 12 months) at different anatomical sites as a biomarker of disease progression. We found that cervical skin denervation is a biomarker of PD progression: indeed, cervical skin denervation positively correlates with disease duration and is a marker of disease severity, as shown by the fact that more severely affected patients had more significant denervation at this site on follow-up at 12 months. Thus, cervical skin denervation alone is an interesting potential marker of neurodegeneration and disease progression in PD independently of pathological αSyn deposits.

The results produced have been published in the journal “Annals of Clinical and Translational Neurology” (DOI: 10.1002/acn3.669).

Methods

Subjects

The Cantonal Ethics Committee approved the study protocol, and all enrolled subjects gave written informed consent to the study. Twenty-two consecutive patients with idiopathic PD and 13 with AP followed by the movement disorders outpatient clinic at NSI Lugano were enrolled from July 2015 to December 2017. Inclusion criteria for PD were: a definite clinical diagnosis according to the UK Brain Bank diagnostic criteria, disease duration at least three years, no family history, and no significant cognitive impairment or major dysautonomic symptoms in the history. In seven cases, the diagnosis was supported by 123I-FP-CIT (DaTSCAN; GE Healthcare, Buckinghamshire, UK), showing typical dopaminergic nigrostriatal denervation. Seventeen age-matched HC for PD patients were recruited among hospital staff and patients' partners. The AP group comprised patients in two subgroups: seven with AP with possible synucleinopathy (AP-Syn), including five with probable MSA and two with probable LBD according to published diagnostic criteria [79,80] and six with AP with possible tauopathy (AP-Tau), including four with probable PSP and two with possible corticobasal degeneration (CBD) [81,82]. During the screening visit, all subjects underwent a blood test for known causes of neuropathy (glycated hemoglobin, creatinine, vitamin B12, TSH, serum immunofixation, HIV, HCV, syphilis, and borreliosis), and three subjects (all PD group) who tested positive were excluded. Scores on the following clinical diagnostic instruments were determined: the Hoehn and Yahr Scale (H&Y) [83] and the Movement Disorder Society Unified Parkinson's Disease Rating Scale (MDS-UPDRS) [26], the Mini-Mental State Examination (MMSE) [84], the Montreal Cognitive Assessment (MoCA) [85], the Beck Depression Inventory-II (BDI-II) [86], and the REM sleep Behavior Disorder (RBD) by the RBD Screening Questionnaire [87]. The levodopa equivalent daily dose (LEDD) was calculated for the PD patients [88]. Thirteen of the 19 subjects with PD were reevaluated in a follow-up visit at 12 months (T12) and underwent a second round of skin biopsies and clinical assessment scales as above. Of the remaining six patients, four were lost to follow-up (because of disease progression in one case and personal reasons in three cases), and two were enrolled less than 12 months before the analysis.

Skin biopsy

Each subject underwent six (3 mm-diameter) skin biopsies at three anatomical sites: two biopsies from the skin of the neck at C8 dermatomal level, two from the thigh 10 cm below the trochanter, and two from the leg 10 cm above lateral malleolus, on the side, which was clinically more affected, according to our standard technique [89]. For each anatomical site, one biopsy was fixed in Paraformaldehyde-Lysine-Periodate 2% fixative for immunofluorescence studies, while the other one was frozen, and subsequently, a RIPA extract was prepared for biochemistry analysis.

Skin innervation

Skin innervation was assessed with a standard indirect immunofluorescence technique on 50 µm thin tissue sections stained by free-floating with an antibody specific for the neuronal marker protein gene product 9.5 (PGP9.5, rabbit polyclonal, Abcam, Cambridge UK, 1:1000). Cell nuclei were counterstained for DAPI.

PGP9.5 positive structures were counted to determine the linear intraepidermal nerve fiber density (IENFD) according to published standard protocols and expressed as the number of fibers/mm [90-92]. The same rater, blind to the disease group, assessed all skin biopsies at baseline and follow-ups.

P-αSyn and 5G4 immunofluorescence

Eight nonconsecutive 50 µm skin sections per site were incubated overnight with primary antibodies against PGP9.5, anti-P-αSyn mouse antibody targeting phosphorylated serine 129 of human αSyn (Wako Chemicals, Neuss, Germany, 1:1000) and the 5G4 (Analytik Jena Life Science, Jena, Germany, 1:400). The 5G4 is a mouse monoclonal antibody targeting disease-specific forms of αSyn, including oligomers, and it has been widely used to detect high-molecular-weight αSyn oligomers in brain tissues that are nitrated and display the typical beta-sheet conformation, with less binding to αSyn fibrils and none to physiological, monomeric αSyn[77]. The weak detection of monomeric αSyn by 5G4 is possible because the epitope is not available in an unfolded conformation. The epitope recognized by 5G4 (amino acids 46-53) starts after the interruption of the alpha-helical structure of physiological αSyn at amino acid 43-44 and terminates at amino acid 53, which may harbor an A53T mutation and could influence the aggregating ability of αSyn.
Secondary antibodies were AlexaFluor 488 goat anti-rabbit and AlexaFluor 594 goat anti-mouse (ThermoFisher Scientific, Waltham, USA, 1:400).
Tissue sections were counter-stained for PGP9.5 and DAPI to detect the specific co-localization of P-αSyn and 5G4 within nerves. Sections were viewed under an inverted fluorescence microscope (Nikon Eclipse Ti-E, Tokyo, Japan). At each site across groups, the presence or absence of positive structures (5G4/PGP9.5 or P-αSyn/PGP9.5 or both) was assessed by an independent examiner blinded to the clinical diagnosis. Since most commercial antibodies cross-react to monomeric physiological αSyn in epithelial cells, only structures that show double staining PGP9.5 and P-αSyn/5G4 were considered positive. Unspecific SG acinus intraluminal fluorescent precipitates and SG tubules autofluorescence were carefully excluded. A subject was classified as positive if at least one biopsy site showed nerve fibers immune-reactive to P-αSyn or 5G4. The number of positive biopsy sites per subject was recorded. Co-localization area of P-αSyn/PGP9.5 and 5G4/PGP9.5 was measured in at least 1 SG for location for subject in each group (2-5 subjects for group for location).

Western blot analysis

The total amount of protein in the RIPA extracts, obtained from each skin biopsy, was determined with the QuantiPro BCA assay kit; 30 µg of protein was then subjected to SDS polyacrylamide electrophoresis, transferred to PVDF membranes, and probed with antibody against PGP9.5 and βactin (mouse monoclonal, Sigma Aldrige, Saint Louis, MO, 1:10.000). PGP9.5 quantification in skin extracts was determined by fluorescence intensity with an Odyssey CLx system (Li-cor Biosciences, Lincoln, Nebraska) and normalized to βactin signal for each subject at each site.

Statistical analysis

Comparisons across groups of patients were performed with Welch t-tests. Analyses of denervation at different sites were run with mixed models, including the subject as a random factor. These models are similar to repeated-measure ANOVAs but have the advantage that all subjects do not need to have the same number of repeated measures. Analyses were run in R 3.2.2 with the lmer procedure in the lme4 (1.1-14) library, the glmmadmb procedure in the glmmADMB (0.8.3.3) library, and post-hoc tests (Tukey method) with the lsmeans and difflesmens procedures in the lmerTest (2.0-33) library. Similarly, models of positivity to P-αSyn and 5G4 were run by binomial generalized linear mixed models (GLMMs) fitted with the glmer procedure. Since the process for posthoc tests were not available for GLMMs, we performed comparisons between pairs of levels of the factors of interest with multiple GLMMs including only the levels under scrutiny, while correcting significance with the false discovery rate method according to the Benjamini-Hockberg procedure in the multtest (2.30.0) library of R to account for multiple statistical tests. Analysis of PGP9.5 measurement obtained by Western blot was performed by a repeated measure ANOVA run in SPSS (v.20 IBM Corp, Armonk, NY).

The diagnostic yields of tests performed with each antibody on each body area were estimated by the area under the receiver operating characteristic (ROC) curve. The standard error (SE) and 95% confidence interval (95% CI) of the AUC were assessed by a stratified bootstrap with 2000 repetitions. Bootstrap was also used to compare the AUC of two ROC curves. Analyses were performed with the pROC (1.10.0) library of R.

Results

Patients

The demographic data and clinical assessments in each group are summarized in Table 1. AP-Tau subjects result statistically older than HC (P=0.031), more depressed (P=0.008), and with a more significant cognitive impairment (P=0.002) compared to PD and AP-Syn. AP groups share a more severe disease gravity measured by H&Y than PD subjects (AP-Syn P<0.001, AP-Tau P<0.001).

P-αSyn and 5G4 positive deposits are significantly more expressed in PD

In PD subjects, pathological αSyn was significantly more highly expressed, being detected mainly in dermal nerve fascicles innervating autonomic structures, namely SG, muscle arrector pili (MAP), and arterioles, while no staining of epidermal nerve fibers was found in any group (Fig. 1 and 2). P-αSyn was found to a significantly greater extent in the PD group than in all others ($z \geq 2.64$, $P_{(FDR)} \leq 0.03$); the extent of its presence did not vary significantly among sites (likelihood-ratio test: $X^2_2 = 1.58$, $P = 0.45$) (Fig. 1I–J) or between the two sexes ($X^2_1 = 0.34$, $P = 0.56$). In the PD group, 5G4-positive structures were expressed to a significantly greater extent than in the HC or in the AP-Tau patients ($z \geq 2.87$, $P_{(FDR)} = \leq 0.01$), and AP-Syn patients more than in the AP-Tau ones ($z \geq 2.29$, $P_{(FDR)} = 0.04$). Moreover, AP-Syn patients expressed 5G4 positive structures at similar levels to PD patients ($z \geq 1.98$, $P_{(FDR)} = 0.07$) but to a lesser extent in the cervical

area (Fig. 2I–J). Finally, 5G4 positive structures were more highly expressed in male than in female patients (X^2_1 = 0.4.75, P = 0.03), but at similar levels at all three sites (likelihood-ratio test: X^2_2 = 0.38, P = 0.83).

A major colocalization area was measured in PD for both 5G4 and P-αSyn with a proximal to distal gradient (Fig. 1P and 2P). However, this analysis is limited because SG were unavailable for all subjects, and SG denervation would increase the ratio.

No significant difference in P-αSyn deposits was found at T12 ($|z| \leq 0.95$, $P \geq 0.35$), while temporal changes in the expression of 5G4 deposits between T0 and T12 differed among sites (likelihood-ratio test for the effect of the site x time interaction: X^2_2 = 10.18, P = 0.006). However, post hoc tests did not demonstrate any significant pairwise difference between sites ($|z| \leq 0.04$, $P \geq 0.97$), perhaps because of the small number of skin biopsies available for this analysis.

5G4 versus P-αSyn detection: sensitivity and specificity

When considering at least two positive sites for P-αSyn, we found that nine out of 16 PD (56%) were positive, 0/ 12 in HC, 0/7 in AP-Syn, and 0/6 in AP-Tau; for 5G4 in the PD group, 13/16 were positive (81.3%), 2/14 (14%) in HC, 4/7 in AP-Syn (57.1 %), and 0/7 in AP-Tau.

For PD, P-αSyn had 56% sensitivity and 100% specificity compared to HC, AP-Syn, and AP-Tau; 5G4 had 81% sensitivity and 86%, 43%, and 100% specificity compared to HC, AP-Syn, and AP-Tau respectively. For AP-Syn, 5G4 had 57% sensitivity and 19%, 86%, and 100% specificity compared to PD, HC, and AP-Tau respectively. We calculated the sensitivity and specificity of P-αSyn and 5G4 in diagnosing PD at each anatomical site, as summarized in Fig. 3A. The worst performance was with P-αSyn in the thigh, and the best performance was with 5G4 in the neck (P = 0.054). The diagnostic yield of a combination of tests run with P-αSyn, 5G4, and both antibodies at all anatomical sites was assessed by ROC curves (Fig. 3B). The area under the ROC was 0.839 for P-αSyn (SE = 0.066; 95% CI = 0.699–0.951) and 0.886 for 5G4 (SE = 0.054; 95% CI = 0.759–0.970). The difference between areas was 0.047 (SE = 0.058; 95% CI = 0.067 to 0.164; P = 0.42). The AUC of a test employing both antibodies was 0.863 (SE = 0.069; 95% CI = 0.713–0.983) and did not differ significantly from the AUC of the tests with P-αSyn or 5G4 alone ($P \geq 0.34$). Since the best results were achieved with 5G4 in the neck, we also assessed the diagnostic efficiency of testing both antibodies in the neck only. The AUC was 0.899 for 5G4 (SE = 0.056, 95% CI = 0.774–1.000), 0.753 for P-αSyn (SE = 0.081, 95% CI = 0.589–0.900) and 0.871 for P-αSyn + 5G4 (SE = 0.055, 95% CI = 0.750–0.965).

PD group shows reduced epidermal nerve fibers density at all anatomical sites, and gender affects denervation

In Fig. 4, immunofluorescence images of innervation of the epidermis and dermal autonomic structures are shown for PD and HC. The results of the mixed model analysis of IENFD are summarized in Table 2. In all groups, the IENFD depends significantly on the site of nerve biopsy, with a greater epidermal innervation density in the neck (Tukey post hoc tests: $t72.8 \geq 6.11$, $P < 0.001$) and a proximal-to-distal gradient effect, in accordance with previous reports (Fig. 5C). The IENFD was lower in the PD group than in the HC and AP-Tau groups ($t40.8 < 2.33$, $P < 0.03$), but not the AP-Syn group ($t38.4 = 0.44$, $P = 0.66$), independently of

anatomical site, as indicated by the nonsignificant site x group interaction. The IENFD of AP-Tau patients also tended to be higher than that of AP-Syn ones, although this difference was not statistically significant ($t41.8 = 1.71$, $P = 0.09$) (Fig. 5A). Differences in IENFD among groups also varied according to sex. Indeed, the IENFD was significantly lower in women in the PD group than in healthy women ($t34.9 = 3.4$, $P = 0.002$) and in AP-Tau women ($t36.2 = 4.04$, $P < 0.001$), but not in women in the AP-Syn group ($t36.6 = 1.60$, $P = 0.12$). Women with PD also had lower IENFD values than men with PD ($t35.6 = 2.64$, $P = 0.01$). In addition, the IENFD values of women in the AP-Syn group were lower than those of women in the AP-Tau group ($t37.9 = 2.24$, $P = 0.03$). In contrast, there was no significant difference across groups for male subjects ($t40.1 = 0.93$, $P \geq 0.36$) (Fig. 5B). Age did not significantly affect IENFD values.

Cervical cutaneous denervation is correlated with disease duration and increases over time

Differences between PD patients and HC in the PGP9.5 measurements obtained by Western blot were significantly larger at cervical site, as indicated by the significance of the site x group interaction ($df = 7$, $F = 7.09$, $P = 0.02$, Fig. 5D–E). Cervical skin denervation was correlated with disease duration (Spearman's correlation: $r = 0.59$, $n = 13$, $P = 0.03$, Fig. 5F).

On follow-up at 12 months (T12), skin biopsies showed that, in the PD group, the IENFD was significantly lower than at baseline on the neck (difference = - 12.0 ±- 2.6 SE, $t40.6 = 4.63$, $P < 0.001$ at Tukey post hoc tests) and the thigh (-7.7± 2.4 SE, $t39.6 = 3.24$, $P = 0.002$), but not the leg (- 0.1± 2.2 SE, $t39.6 = 0.03$, $P = 0.98$) (Fig. 5C).

Cervical cutaneous denervation is more pronounced in patients with more severe PD

We split the PD group at T0 into two subgroups according to disease severity (H&Y score). Six patients had more severe disease (H&Y ≥ 3), and 13 had milder disease (H&Y < 3). As shown in Fig. 6, the subjects in the first group were significantly older and had a shorter disease duration (age: $t12.759 = 4.08$, $P = 0.001$; disease duration: $t13.595 = 2.74$, $P = 0.02$). No difference in LEDD was found ($t13.049 = 0.001$, $P = 0.999$). Mixed models accounting for biopsy site and sex showed that, on assessment at T0, the group with more severe PD displayed similar levels of positivity to P-αSyn or 5G4 and similar IENFD values to patients with less severe disease ($|t16.01| \leq 1.25$, $P \geq 0.23$). However, a comparison of the denervation values of the same patients at T0 and T12 in a mixed model accounting for patient sex and disease severity showed a significant worsening of denervation at the cervical site only ($t41.1 = 5.06$, $P < 0.001$; $|t41.1| \leq 1.56$, $P \geq 0.13$ for the other areas) (Fig. 6D). The group with more severe disease is significantly older, and age can affect innervation, but at T12, significant denervation was measured selectively at cervical site only and not at distal sites where we would attend major denervation due to aging since distal axons are more exposed to metabolic and oxidative stress. Finally, IENFD did not correlate at any anatomical site with LEDD at T0 and T12.

Figures and tables

Table 1. Demographic data and clinical scores of patients with PD, AP, and HC.

	PD T0	PD T12	AP-SYN	AP-TAU	HC
Number and gender	19 13 Male, 6 Female	13 10 Male, 3 Female	7 3 Male, 4 Female	6 2 Male, 4 Female	17 9 Male, 8 Female
Median age (years) (quartiles)	66 (56.5/73)	67 (61/80)	72 (66/73.5)	76.5 * (71.5/77.8)	57 (54/72)
Median disease duration (years) (quartiles)	4.5 (3/7.8)	6 (4/9)	5.5 (2.8/7.5)	4 (3.3/4.8)	–
Median H&Y Scale (quartiles)	2 (1/3)	2 (2/2)	5 *** (3.5/5)	4.5 *** (4/5)	–
% Patients treated with L-DOPA	73.7%	69%	–	–	–
LEDD (mg) (quartiles)	587.5 (337.5/762.5)	495 (300/700)	–	–	–
Median Beck Depression Scale (quartiles)	6 (2.5/8.5)	9 (4/12)	8 (3.8/13)	14 ** (11.8/15.5)	–
Median MDS-UPDRS (quartiles)	22.50 (15.3/30.5)	19 (13.5/26)	–	–	–
Median RBD (quartiles)	3 (1.5/4)	3 (2/5)	3 (1.3/4.8)	2.5 (0.3/4.8)	–
Median MMSE (quartiles)	29 (28.5/30)	30 (28/30)	28 (26.3/29)	24 ** (22/28)	–
Median MOCA (quartiles)	27 (23.5/28.5)	27 (20/28)	24.5 (21.5/26)	22 (16/23.5)	–

PD, HC, and AP-Syn groups did not differ in age (Tukey post hoc test: $|t45| \leq 2.02$, $P \geq 0.19$), while the AP-Tau subjects were significantly older than the HC (Tukey post hoc test: $t45 = 2.85$, $P = 0.03$). AP-Tau and AP-Syn had a more severe disease as measured by H&Y compared to PD subjects ($P < 0.001$). The sex ratio did not differ across patient groups (binomial GLM: v2 3 = 3.01, P = 0.39). AP-Tau subjects had significantly lower MMSE scores (Tukey post hoc test: t27 = -3.74, P = 0.002) and significantly higher scores on the BDI-II (Tukey post hoc test: t28 = 3.23, P = 0.01) compared to the PD group. In contrast, AP-Syn subjects had intermediate values of both scores, not differing significantly from either the AP-Tau group or the PD group (Tukey post hoc test: $|t27| \leq 2.05$, $P \geq 0.12$). There was no significant difference in disease duration in the PD, AP-Syn, and AP-Tau groups (Poisson GLM: v2 2 = 1.22, P = 0.54). *P < 0.05; **P < 0.01; ***P < 0.01.

Figure 1. P-αSyn deposits are more expressed in PD.

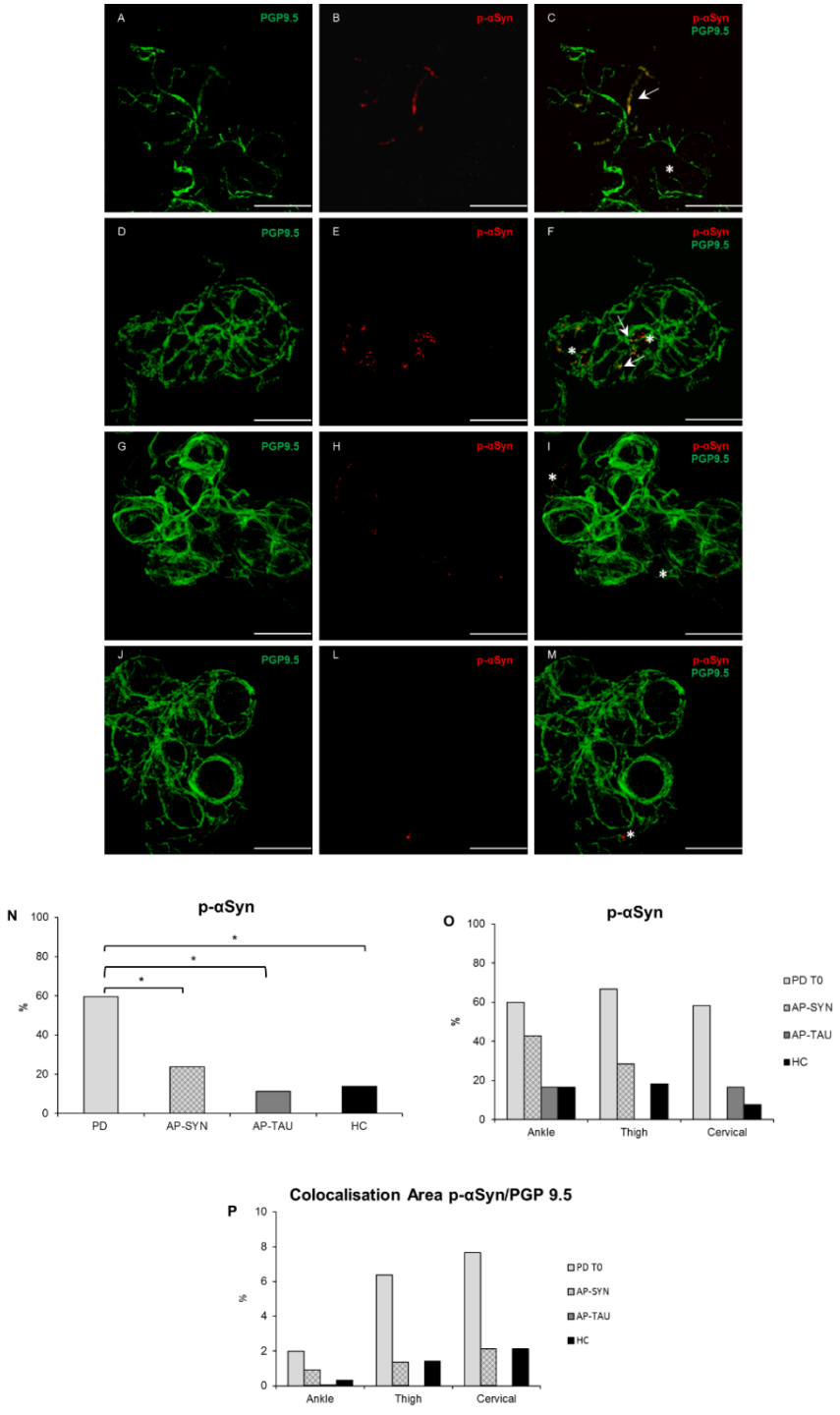

Confocal images of immunofluorescence with PGP9.5 (green) and P-αSyn (red) of dermal nerves around SG in PD T0 (A–B), in AP-Syn (D–E), AP-Tau (G–H), and HC (J–L). In yellow colocalization of P-αSyn and PGP 9.5 (C, F, I, M) along axons. Scale bar 50 µm. White arrows indicate positive structures; asterisks indicate unspecific staining in non-neuronal structures. The percentage of P-αSyn is higher in PD T0 patients compared to other groups (P = 0.028) (N) but is not different among localizations (O). A major colocalization area P-αSyn /PGP9.5 was measured in PD with a proximal to distal gradient (P).

Figure 2. 5G4 deposits are more expressed in PD and AP-Syn patients.

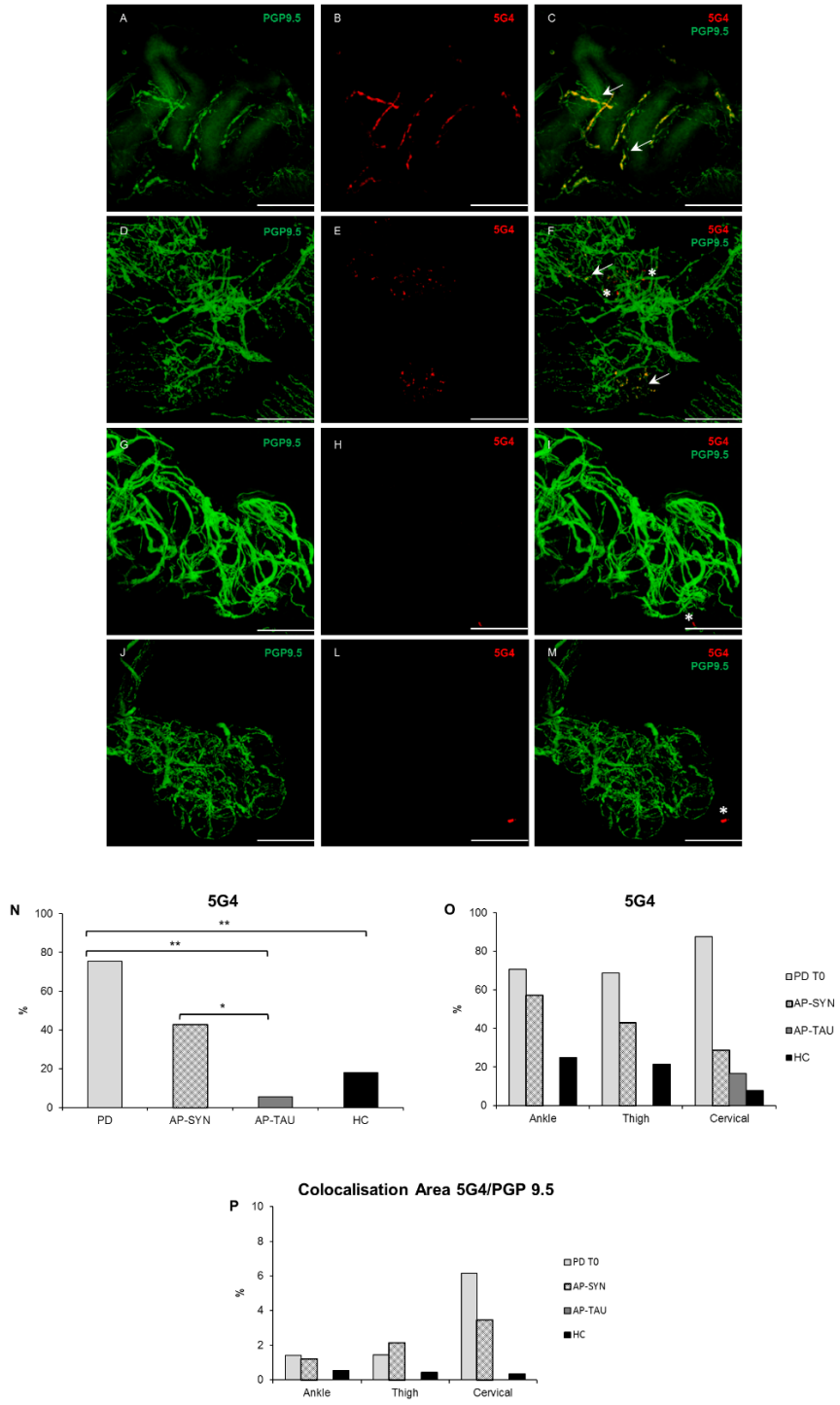

Confocal images of immunofluorescence with PGP9.5 (green) and 5G4 (red) of dermal nerves around SG in PD T0 (A–B), AP-Syn (D–E), AP-Tau (G–H), and HC (J–L). In yellow colocalization of 5G4 and PGP 9.5 (C, F, I, M) along axons. Scale bar 50 µm. White arrows indicate positive structures; asterisks indicate unspecific staining in non-neuronal structures. The percentage of 5G4 is higher in PD T0 compared to HC and AP-Tau (PFDR < 0.012), but not compared to AP-Syn, and in AP-Syn more than in AP-Tau (PFDR = 0.04) (N); no significant differences among localizations but a tendency of higher 5G4 at the cervical site in PD (O). A major colocalization area 5G4/PGP9.5 was measured in PD with a proximal to distal gradient (P).

Figure 3. ROC analysis for P-αSyn and 5G4 in PD.

A

	Site	Sensitivity	Specificity	N° PD T0	N° HC
P-α-Syn	Ankle	0.600	0.833	15	12
P-α-Syn	Thigh	0.600	0.818	15	11
P-α-Syn	Cervical	0.583	0.923	12	13
5G4	Ankle	0.706	0.750	17	12
5G4	Thigh	0.687	0.786	16	14
5G4	Cervical	0.875	0.923	16	13

B

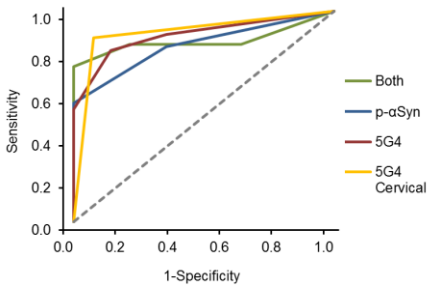

Sensitivity and specificity tests with each antibody in each anatomical site. N° PD T0 and N° HC are the numbers of subjects for which each test is available (A). Comparison of the diagnostic yield of test performed with P-αSyn (blue), 5G4 (red), both markers (green), and 5G4 in the cervical area only (yellow) (B). The statistical power of the ROC curves was: P-αSyn (0.946), 5G4 (0.987), both markers (0.987), and 5G4 in the cervical area only (0.998).

Figure 4. Skin innervation: intraepidermal nerve fiber density (IENFD).

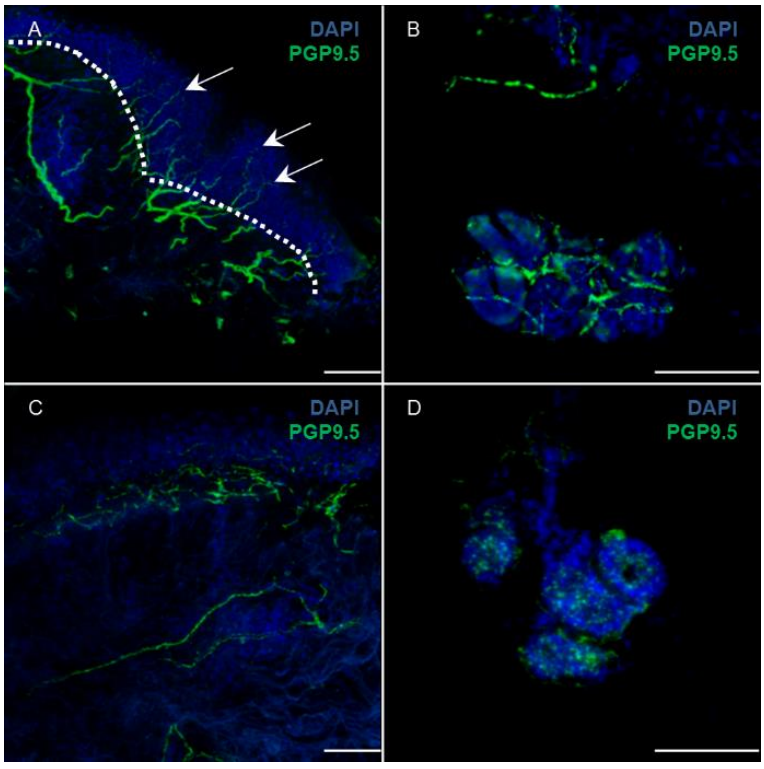

Immunofluorescence staining with anti-PGP9.5 (green) and DAPI (blue) of cervical skin in an HC (A) and PD (C); in A, the dotted white line shows the border between epidermis and dermis: IENFD is calculated as the number of nerve fibers (arrows) crossing the border per mm. Dermal nerve fibers around SG are shown in an HC (B) and PD (D). The pictures show skin denervation in PD more evident at the level of autonomic nerve fibers of the SG. Scale bar 50 µm.

Figure 5. Cervical skin denervation correlates to disease duration and significantly increases at 12 months of follow-up.

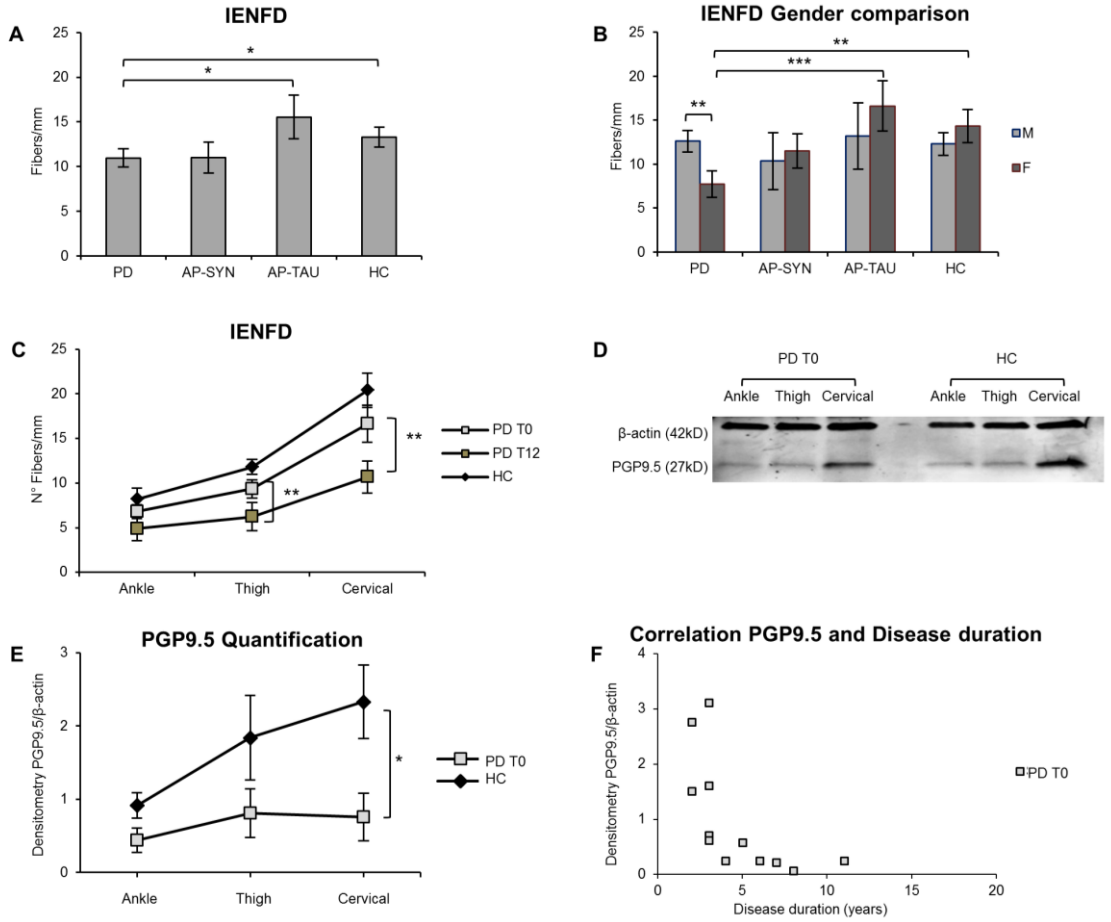

IENFD is lower in PD T0 patients compared to AP-Tau and HC subjects ($P < 0.03$) but not compared with AP-Syn (A). Total IENFD is significantly reduced in PD females versus PD males ($P = 0.012$), in PD females versus HC females ($P = 0.002$) and versus AP-Tau ($P < 0.001$) (B). In PD after 12 months IENFD is significantly lower at the thigh ($P = 0.002$) and at the cervical site ($P = 0.001$) (C). Western blot of skin lysates (an example) (D). Densitometry of PGP9.5 and b-actin bands measured by LICOR software (n = 12 PD, n = 8 HC) PGP9.5 values normalized to b-actin, show a major denervation at cervical site ($P < 0.05$) (E). PGP9.5 quantification negatively correlates to disease duration at the cervical site in PD at T0 (F).

Table 2. IENFD analysis in PD, AP, and HC subjects.

Variable	Sum Sq	Mean Sq	NumDF	DenDF	*F*	*P*
Site	2281.66	1140.83	2	74.568	37.040	<0.001
Group	300.81	100.27	3	38.540	3.256	0.032
Gender	26.35	26.35	1	40.352	0.855	0.361
Age	0.12	0.12	1	38.251	0.004	0.951
Site*Group	284.70	47.45	6	73.050	1.541	0.177
Site*Gender	38.61	19.31	2	74.550	0.627	0.537
Group*Gender	355.36	118.45	3	38.928	3.846	0.017
Site*Group*Gender	249.64	41.61	6	73.035	1.351	0.246

Results of mixed-model analysis of IENFD in relation to anatomical site, patient group, gender, age, and to the two- and three-way interactions among the anatomical site and patient group and gender. Patient identity was included as a random grouping factor. Age was included as a covariate.

Figure 6. Cervical skin denervation in PD differs according to disease gravity.

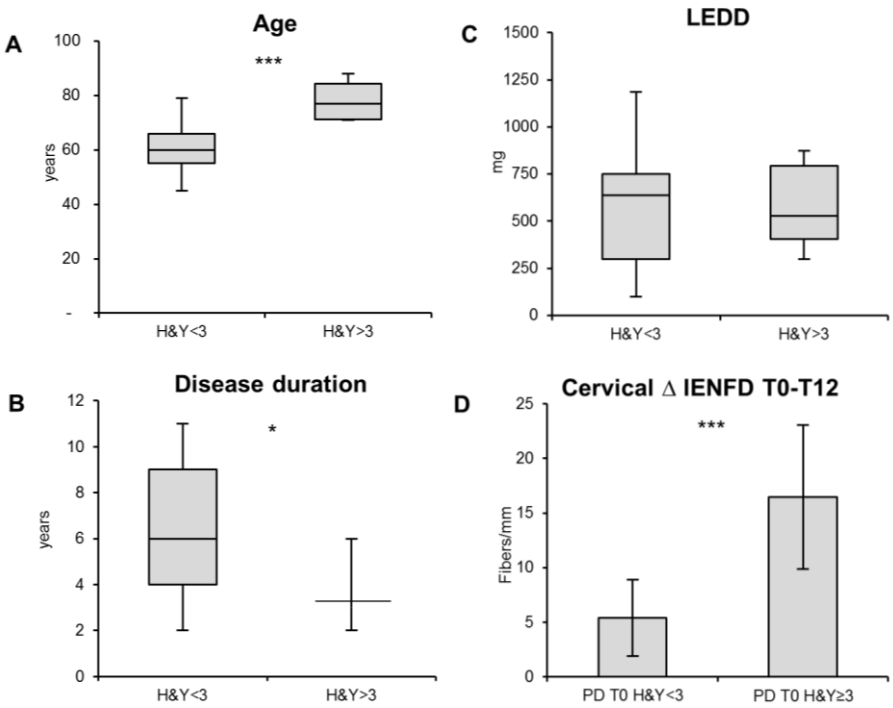

PD patients were divided into two groups based on H&Y severity. The group with H&Y ≥ 3 is significant older (P = 0.005) (A), with a lower disease duration (P = 0.036) (B), and no difference in LEDD (C). After 12 months, IENFD denervation is greater in more disabled patients at the cervical site (P = 0.019) (D).

4. αSyn oligomers and small nerve fiber pathology in skin biopsy are biomarkers of PD

Given the encouraging results obtained with the 5G4 antibody, we decided to move forward by exploiting the proximity ligation assay (PLA), a new highly sensitive and specific technique for oligomeric αSyn detection (αSyn-PLA).

This technique was previously applied in post-mortem PD [93] and MSA [94] brain, in *in-vivo* gastrointestinal tissues [95], and very recently in skin biopsies of PD patients [58]. In this last work, αSyn-PLA was described within synaptic terminals of cutaneous autonomic fibers, especially in PD patients compared to HC [58]. However, PLA was not used in skin biopsies to differentiate PD from AP and not in a longitudinal study.

In this study, we analyzed αSyn-PLA in ankle and cervical skin biopsies of patients with PD, MSA, AP-Tau, and HC, demonstrating that αSyn oligomers were significantly more expressed in PD and MSA patients than in HC and AP-Tau and yield a high diagnostic performance for synucleinopathies.

Moreover, major issues in using skin biopsy as a definitive diagnostic tool for PD are the discrepancies of reported specificity and sensitivity, the various sites of skin biopsy, and the lack of standardized protocols. Thus, we compared the diagnostic accuracy for PD of αSyn-PLA *vs*. P-αSyn and *vs*. 5G4 antibody according to the anatomical site, finding that both the choice of pathological αSyn marker and the anatomical site significantly influences the diagnostic performance. Indeed, αSyn-PLA displays the best accuracy when considering both locations or the cervical site alone, while P-αSyn and 5G4 performed better when considering the ankle site alone.

Furthermore, we documented significant denervation in both cervical and ankle sites occurs after two years of follow-up in PD patients. More importantly, we showed that denervation progresses significantly with disease duration even in a relatively short period (two years) while no significant changes in clinical scales or pathological αSyn amounts were detectable. Epidermal denervation was associated with the progression of cognitive and motor impairments.

The paper obtained with this data has been accepted by the journal “npj Parkinson’s Disease (November 2021).

Methods

Patients' recruitments

Thirty patients with idiopathic PD, 22 age and sex-matched HC, and 23 AP were prospectively recruited from the movement disorders outpatient clinic at the Neurocenter of Southern Switzerland in Lugano, from July 2015 to January 2021 as part of the NSIPD001 study [50]. Inclusion criteria for PD were a clinical diagnosis according to the UK Brain Bank diagnostic criteria [16], disease duration of at least two years, no family history, and no significant cognitive impairment or major autonomic dysfunction symptoms in the history. HC subjects were recruited among patients' partners and hospital staff without any known pathology. The AP group included 12 patients with probable MSA and 11 patients with possible AP-Tau, eight with probable PSP, and three with possible CBD. AP's inclusion criteria were based on published diagnostic criteria for MSA [79], PSP [82], and CBD [81]. Exclusion criteria were co-morbidities causing peripheral polyneuropathies (diabetes, renal failure, thyroid pathology, vitamin B12 deficiency, HIV and HCV infection, Lyme disease, syphilis, acute or chronic inflammatory diseases) and tumors. After 2 years (T24) PD and AP patients underwent a follow-up clinical evaluation and a second skin biopsy (Fig.1).

The Cantonal Ethics Committee approved the study protocol, and all enrolled subjects gave written informed consent to the study.

Clinical assessment

Disease severity was determined by the H&Y [83] and the MDS-UPDRS [96] scales. Cognitive impairment was assessed with MMSE [84] and MoCA [85] scales. Symptoms of autonomic dysfunction were rated with the Composite Autonomic Symptom Score 31 (COMPASS-31) [97]. Mood disorders were screened with BDI-II [98] questionnaire, while REM sleep Behavior Disorder with the RBD Screening Questionnaire [99]; olfactory function was tested with the Sniffin' Sticks Smell test (Burghart Messtechnik GmbH, Wedel, Germany). The LEDD was calculated for all PD and AP patients [100].

Skin biopsy

A 3-mm punch skin biopsy was performed on the clinically more affected side, as previously described [50,57]. Each subject underwent skin collection at two anatomical sites, namely at the C8 dermatomal level (cervical) and at the distal leg, about 10 cm above the lateral malleolus (ankle). Skin samples were fixed overnight at 4°C in Paraformaldehyde-Lysine-Periodate 2% fixative. The day after, skin samples were frozen and cut with a cryotome to obtain 50 µm-thin tissue sections for free-floating immunofluorescence analysis [50,90]. All the immunofluorescence staining were manually performed by an operator blind to the clinical diagnosis

Intraepidermal Nerve Fiber Density

Three non-consecutive 50 µm-thin tissue sections per localization per patient were stained with the antibody against PGP9.5 (Abcam, Cambridge UK, 1:1000) [57]. Cell nuclei were counterstained with 4′,6-diamidino-2-phenylindole (DAPI, Sigma-Aldric h, Saint Louis USA, 1:5000). According to published standard protocols [90,92], PGP9.5 positive nerve fibers crossing the dermal-epidermal junction were counted to determine the linear IENFD. The length of the section was measured, and IENFD was obtained by dividing the number of fibers by the length of the section and expressed as "number of fibers/mm". IENFD was determined at both ankle and cervical sites, and total IENFD was calculated as the mean of nerve densities at both localizations.

Direct proximity ligation assay

Direct PLA was performed with the Duolink PLA kit (Duolink Kit Sigma-Aldrich, Saint Louis, USA). Following the manufacturer's instructions, the oligonucleotides probes MINUS and PLUS were separately conjugated to the mouse monoclonal αSyn antibody with blocking activity (anti-αSyn 211, 1mg/mL, Abcam, Cambridge, UK) [93]. Three non-consecutive 50µm thin tissue sections per localization per patient were washed in TBS and then incubated for 2 hours at room temperature in a freshly made blocking solution (4% normal goat serum, 1% Triton in TBS). Sections were incubated with αSyn-PLUS and αSyn-MINUS probes (1:100 in PLA diluent) and rabbit anti-PGP9.5 antibody (Abcam, Cambridge, UK, 1:1000) for 1h at 37°C and then overnight at room temperature.

The day after, the amplification reaction was performed by serial incubation with: 1) ligase enzyme diluted 1:40 in ligation buffer (Duolink kit, Sigma Aldrich, Saint Louis USA) for 1 hour at 37°C; 2) polymerase enzyme diluted 1:80 in the Amplification buffer (Duolink kit, Sigma Aldrich, Saint Louis USA) and secondary antibodies AlexaFluor488 goat anti-rabbit (ThermoFisher Scientific, Waltham USA, 1:700) for 2 hours at 37°C. Finally, cell nuclei were counterstained with DAPI (1:5000 in PBS for 4 minutes), and section slides were mounted with Vectashield (Vector Laboratories, Burlingame, USA).

The assay's specificity for αSyn-PLA was first assessed in paraffined brain sections from PD and HC (Fig. 2). Serial negative controls without oligonucleotide probes and amplification reaction enzymes were also conducted (Fig. 2).

Confocal microscope analysis of αSyn-PLA

To increase the specificity of the analysis, we considered only αSyn-PLA signal within the nerves which colocalized with the axonal marker PGP9.5 (colocalization signal) or which was located in proximity to degenerated nerve fibers, defined by axonal swellings and fragmentations or interposed between nerve fiber breakpoints (dotted signal) (Fig. 3).

Skin sections were first rated under an inverted fluorescence microscope (Nikon Eclipse Ti-E, Tokyo, Japan). For each section, both somatosensory and autonomic innervation were screened: intraepidermal nerve fibers, dermal nerve bundles, and autonomic structures (SG, MAP, and vessels). All SG and MAP were

analyzed by a Nikon confocal microscope using the NIS Elements 4.11.01 imaging software. Serial pictures, every 2µm on the Z-axis, were taken using a 20X magnification. To avoid missing small amounts of signal within dermal nerve bundles, we also analyzed at least three nerve bundles that were randomly chosen at each anatomical site by confocal microscope**.** Two independent examiners analyzed every stack of the obtained pictures with ImageJ software, blinded to the clinical diagnosis. For each image, we reported the presence/absence of signal. Structures were defined as "positive" if showing αSyn-PLA. Anatomical sites were defined as "positive" when at least one positive structure was present. The subjects were defined as "positive" when they showed at least one positive site. Negative subjects did not present PLA signals at any site. To assess the anatomical distribution of PLA signal in each group, we also considered ankle and cervical sites separately.

Quantification of αSyn-PLA

The percentage of positive SG and MAP structures was calculated for each patient. For each structure, the number of colocalization points was counted and, if one subject showed signal in multiple structures and sites, the sum of the points was considered. Finally, we calculated the area occupied by αSyn-PLA signal normalized for the area of innervation. First, the stacks on the Z-axis were merged, then the area of the structure (DAPI), the area of innervation (PGP9.5), and the area of αSyn-PLA within nerves were measured with the "freehand selection" tool. The area of innervation was normalized for the area of the structure, and then the percentage of the innervation area occupied by αSyn-PLA signal was measured.

Phosphorylated αSyn and 5G4 immunofluorescence

Three non-consecutive 50µm-thin tissue sections per localization per patient were incubated overnight with antibodies against PGP9.5 (1.1000, Abcam, Cambridge, UK), P-αSyn at Serine 129 (1.1000, Wako Chemicals, Neuss, Germany) or 5G4 (1.400, Analytik Jena Life Science, Jena, Germany) [57]. The day after, sections were incubated with secondary antibody AlexaFluor488 and AlexaFluor594 (ThermoFisher Scientific, Waltham USA, 1:700) and counterstained with DAPI. All sections were analyzed at a fluorescence microscope by two independent raters blinded to the diagnosis. Colocalization of P-αSyn/5G4 and PGP9.5 was considered as positive signal as previously described [50].

Statistical analysis

Statistical analyses were performed with IBM SPSS Statistics 26.0 (IBM Corp. Released 2019. IBM SPSS Statistics for Windows, Version 26.0. Armonk, NY: IBM Corp). Variable distribution was assessed by the Kolmogorov-Smirnov test. One-way ANOVA test with posthoc Bonferroni's test for multiple comparisons was used for normally distributed variables expressed as mean ± standard deviation. Kruskal-Wallis' test was applied to non-normally distributed variables expressed as medians and interquartile range. $\chi 2$ or Fisher's exact tests were used for categorical variables expressed as percentages (%). Odds ratios (OR) were assessed by univariate logistic regression analysis, while the AUC and the diagnostic performances of

selected variables were obtained with ROC curves analysis. For matched analysis (T0 vs. T24), non-normally distributed variables were analyzed by Wilcoxon pairs signed-rank test and categorical variables by McNemar test. Associations between IEFND (cervical, ankle, and total) at T0 and worsening of clinical characteristics (MoCA, MMSE, MDS-UPDRS-III) at T24 were tested using logistic regression models adjusted by age and LEDD, with OR and 95% confidence intervals calculation (95% CI).

The linear discriminant analysis model was used to classify patients. Canonical components 1 and 2 were calculated from weighted linear combinations of variables (αSyn-PLA, P-αSyn, αSyn-5G4, and IENFD) to maximize the separation between groups.

Results

Demographics and clinical data

Demographic characteristics and clinical assessments of the study groups are summarized in Table 1. As expected, AP patients showed a more severe disease than PD, measured by H&Y and MDS-UPDRS, and a higher cognitive impairment, measured by MMSE and MoCA. AP-Tau subjects were significantly older than HC and more depressed than PD. MSA showed a greater autonomic dysfunction measured by COMPASS-31.

After 24 months, six patients died (1 PD, 2 MSA, 3 AP-Tau), 18 patients dropped out of the study (5 PD, 5 MSA, 8 AP-Tau). Twenty-four of the 30 PD patients underwent a 24-month follow-up analysis (T24) (Fig. 1). The 6 PD patients who did not perform the T24 assessment were significantly more affected than the other PD subjects (H&Y, *P*=0.050; MDS-UPDRS-III, *P*=0.031) (Table 2). Since few subjects with MSA and none with AP-Tau performed the T24 evaluation, we did not perform statistical analysis at T24 in these groups.

PD and MSA display a small nerve fiber pathology

PD and MSA showed a significant reduction of total and ankle IENFD compared to HC (Table 1). A tendency towards a reduced IENFD at the cervical site was present in PD, even if not significant, possibly due to a higher variability.

PD and MSA show high positivity for αSyn-PLA

The co-localization signal, defined as an αSyn-PLA signal within the PGP9.5 positive nerves (Fig. 3), was the most frequent, while the dotted one, defined as the signal located in proximity to degenerated nerve fibers or interposed between nerve fiber breakpoints (Fig. 3), was observed exclusively in PD and MSA, not in AP-Tau or HC (Fig. 4a). In the MSA group, the dotted signal was always kept in association with the co-localization signal, while in the PD group, 3,3% of patients showed a dotted signal only.

The percentage of patients showing αSyn-PLA was significantly higher in PD and MSA groups than HC and AP-Tau (Fig. 4a-c). Considering the two anatomical sites separately, the cervical area differentiated between PD and HC and AP-Tau (Fig. 3b). No differences were observed between groups at the ankle site

(Fig. 4c). MSA showed a higher positivity at the ankle than at the cervical area (Fig. 4c). A double positivity at both anatomical sites was observed only in PD and MSA groups (16.7% and 11.1%, respectively).
The majority of αSyn-PLA was detected in nerve fibers surrounding autonomic structures. In 2 out of 30 PD patients, the signal was observed in dermal nerve bundles. Most of the signal was evident in SG innervation (Fig. 4d): PD and MSA group displayed a greater positivity than HC and AP-Tau, considering both localization and the cervical site alone (Fig. 4e). No differences between groups in PLA signal were observed in MAP.
MSA displayed a greater area of αSyn-PLA signal within nerves than PD (Fig. 4h-j), especially at the cervical site. No differences were observed in the number of αSyn-PLA signals.
Finally, the presence of αSyn-PLA was associated with the diagnosis of PD and MSA by univariate logistic regression analysis (Table 3). PD showed higher odds ratios than MSA, except for αSyn-PLA in SG. Moreover, an association with PD diagnosis was observed considering αSyn-PLA signal at cervical site only.

αSyn-PLA showed higher diagnostic accuracy for PD and MSA than P-αSyn and αSyn-5G4

In addition to αSyn-PLA, subjects were investigated for P-αSyn and αSyn-5G4. All markers were more expressed in PD than HC and AP-Tau, but αSyn-PLA displayed higher sensitivity when considering both locations and the cervical area (Fig. 5 a-c). Within groups, no differences were revealed between the three markers (Fig. 5 d-f). The ROC curve analysis demonstrated that αSyn-PLA had the highest AUC when considering both locations or the cervical site (5 g-h-j-k). Nevertheless, at the ankle, only P-αSyn and αSyn-5G4 could discriminate between groups (Fig. 5 i-l), even if with a lower AUC than αSyn-PLA in the cervical area. Finally, only αSyn-PLA allowed the discrimination between MSA and HC, considering both anatomical sites together (Fig. 5 m).

PD patients present a progression of denervation not of pathological αSyn at T24

The comparison between subjects with PD at time point 0 (T0) and after 24 months (T24) showed a significant reduction in total IENFD, ankle IENFD and cervical IENFD (Fig. 6 a-c). No differences in the percentage of patients positive for αSyn-PLA, P-αSyn, and αSyn-5G4 were detected (Fig. 6 d-f), but a slight reduction for all markers at the cervical site and an increase of αSyn-PLA signal in the ankle were noted. No significant changes in clinical scales and LEDD were detected.

IENFD is a progression marker for PD

Comparisons of skin biopsy parameters at T0 according to the clinical state at T24 demonstrated that: 1) lower cervical IENFD was measured in those presenting a progression of cognitive decline at the MMSE scale and 2) lower ankle IENFD was observed in the group presenting a progression of motor impairment at the MDS-UPDRS-III scale (Fig. 6 g-h). These results were confirmed by logistic regression, showing that low cervical IENFD was associated with an increased risk of developing a cognitive decline, while low ankle IENFD was associated with an increased risk of developing motor impairment at T24, after adjusting for age and LEDD (Fig. 6 i-k).

A skin biopsy-derived compound marker stratified subjects according to the clinical diagnosis

A linear discriminant analysis model based on the IENFD and the expression of αSyn-PLA, P-αSyn, and αSyn-5G4 at both sites at T0, allowed the separation of subjects according to their clinical diagnosis (Fig. 7 a). Patients were discriminated with 77.8% of accuracy: 26 out of 30 PD and 5 out of 9 MSA were correctly diagnosed, while the discrimination between HC and AP-Tau was more challenging (Fig. 7 b). Subsequently, pairwise comparisons were performed (Fig. 7 c-h), showing high sensitivity (77.7%-93.3%) and specificity (66.6% - 100.0%) in the discrimination between two groups at the time.

Figures and Tables

Figure 1. Flowchart of the study population

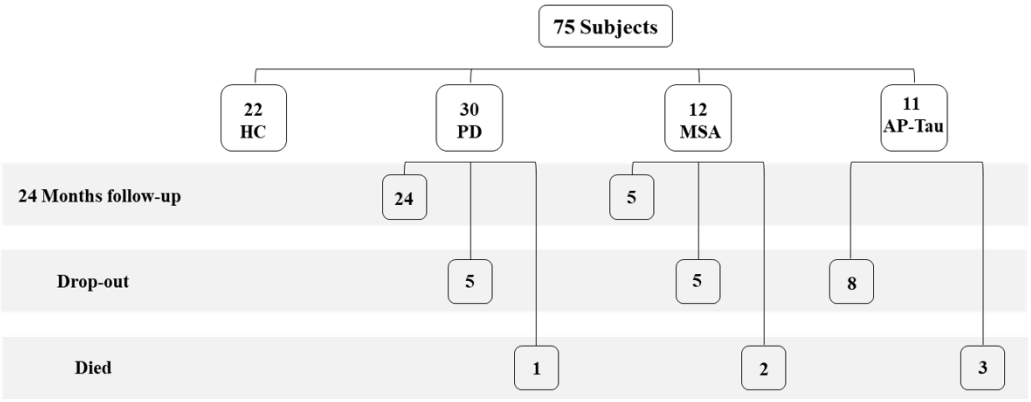

Figure 2. αSyn-PLA technical controls

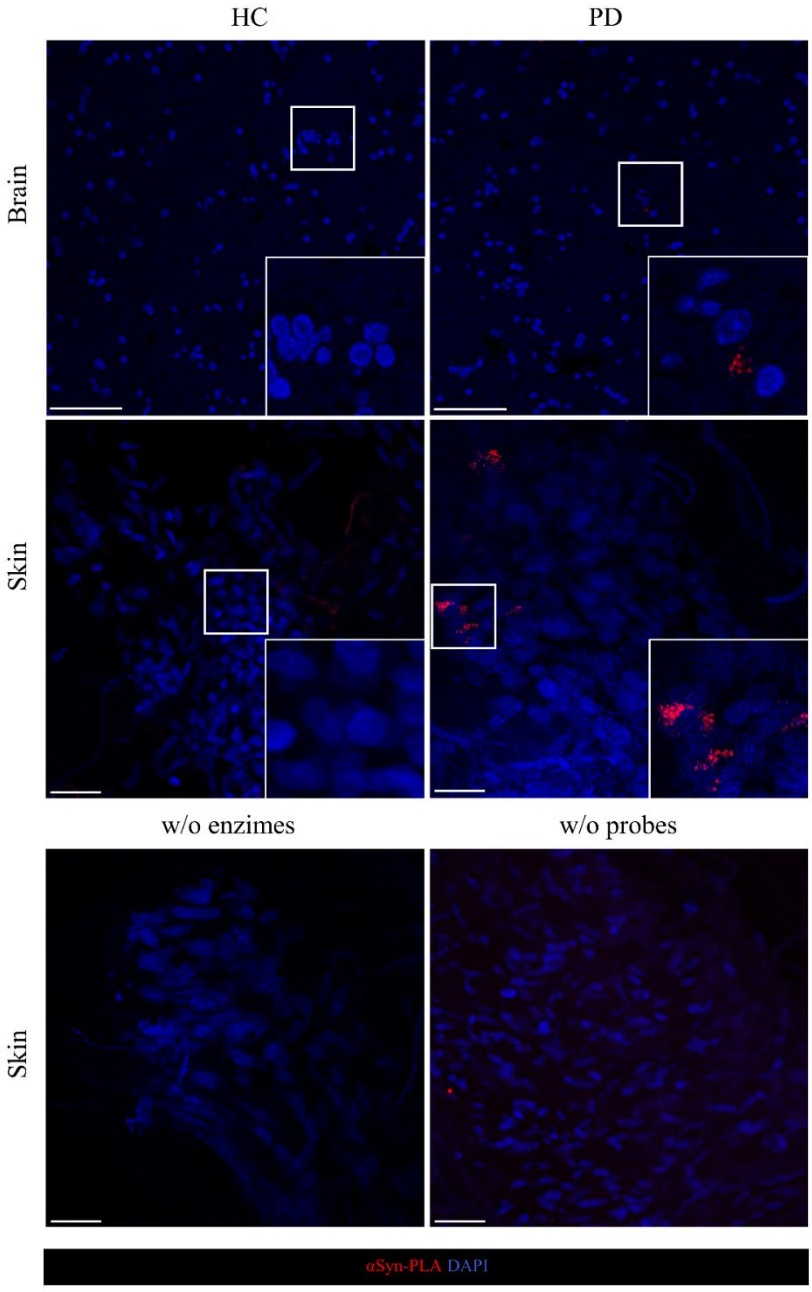

αSyn-PLA staining in basal ganglia and mid-brain region obtained from post-mortem human brains of HC and PD patients respectively, compared to the signal obtained in cervical skin. In the bottom panel, negative controls are shown without amplification reaction enzymes or oligonucleotide probes.

Table 1 Demographic data and clinical scores

						Pairwise Comparisons					
	HC [n=22]	**PD** [n=30]	**MSA** [n=12]	**AP-Tau** [n=11]	**Overall** ***P*-value**	PD vs. HC	MSA vs. HC	AP-Tau vs. HC	PD vs. MSA	PD vs. AP-Tau	MSA vs. AP-Tau
Age (years)	60 ± 11	67 ± 11	66 ± 10	73 ± 9	**0.021**	0.072	0.127	**0.001**	1.000	0.131	0.151
Sex (ref. male)	54.4%	60.0%	41.7%	45.5%	0.521	-	-	-	-	-	-
Disease duration (years)	-	4.0 (2.8-8.3)	5.0 (1.3-6.8)	4.0 (3.0-5.0)	0.465	-	-	-	-	-	-
H&Y	-	2.0 (1.0-3.0)	4.0 (3.0-5.0)	4.0 (3.0-4.0)	**<0.000**	-	-	-	**<0.000**	**<0.000**	0.608
MDS-UPDRS-I	-	4.0 (2.0-6.0)	8.0 (7.5-10.5)	12.0 (6.5-18.5)	**0.006**	-	-	-	**0.009**	**0.016**	0.310
MDS-UPDRS-II	-	5.0 (2.5-9.8)	15.0 (9.5-21.0)	24.0 (13.5-34.0)	**0.002**	-	-	-	**0.022**	**0.001**	0.322
MDS-UPDRS-III	-	17.0 (11.3-22.3)	30.0 (23.0-46.5)	39.0 (25.5-59.0)	**<0.000**	-	-	-	**0.001**	**<0.000**	0.573
MDS-UPDRS-Total	-	26.5 (15.3-36.0)	53.0 (36.5-67.0)	90.0 (44.0-112.5)	**0.001**	-	-	-	**0.013**	**0.001**	0.310
COMPASS-31 OH	-	8.0 (0.0-16.0)	24.0 (16.0-30.0)	8.0 (0.0-28.0)	**0.030**	-	-	-	**0.007**	0.674	0.131
COMPASS-31 VM	-	0.0 (0.0-0.0)	0.0 (0.0-0.0)	0.0 (0.0-0.0)	0.353	-	-	-	-	-	-
COMPASS-31 SM	-	0.0 (0.0-4.2)	2.1 (0.0-2.1)	0.0 (0.0-2.1)	0.519	-	-	-	-	-	-
COMPASS-31 GI	-	0.9 (0.0-6.5)	5.4 (3.6-6.7)	0.0 (0.0-6.3)	0.065	-	-	-	-	-	-
COMPASS-31 BL	-	0.0 (0.0-0.0)	1.1 (1.1-2.2)	0.0 (0.0-0.0)	**0.000**	-	-	-	**0.000**	0.805	**0.000**
COMPASS-31 PM	-	0.0 (0.0-0.0)	0.0 (0.0-0.0)	0.0 (0.0-0.0)	1.000	-	-	-	-	-	-
COMPASS-31 Total	-	14.2 (0.0-24.8)	32.3 (22.2-38.2)	12.0 (4.2-28.0)	**0.026**	-	-	-	**0.010**	0.942	**0.020**
BDI-II	-	6.0 (3.0-8.5)	6.0 (3.0-14.0)	14.5 (10.8-17.0)	**0.002**		-	-	0.423	**<0.000**	**0.029**
MMSE	-	30.0 (29.0-30.0)	29.0 (25.0-30.0)	28.0 (23.0-28.0)	**<0.000**	-	-	-	**0.029**	**<0.000**	0.131

MoCA	-	27.0 (24.0-29.0)	25.0 (19.5-26.7)	20.0 (16.0-24.0)	**0.004**	-	-	-	0.095	**0.001**	0.109
Olfactory test	-	6.0 (4.0-8.3)	9.0 (7.5-10.3)	7.0 (4.5-8.5)	0.073	-	-	-	-	-	-
RBD questionnaire	-	3.0 (1.0-5.0)	4.0 (1.0-5.8)	2.0 (0.0-4.0)	0.547	-	-	-	-	-	-
LEDD (mg)	-	495.0 (202.5-737.5)	312.0 (143.0-468.8)	250.0 (125.0-452.0)	0.486	-	-	-	-	-	-
IENFD total (Fibers/mm)	14.5 (10.8-17.1)	11.2 (9.5-14.7)	11.6 (10.0- 12.7)	15.2 (9.2-18.7)	**0.029**	**0.017**	**0.013**	0.947	0.522	0.103	0.079
IENFD cervical (Fibers/mm)	20.8 (15.6-26.4)	16.7 (12.3-23.1)	18.1 (13.5-21.3)	21.5 (15.2-24.7)	0.194	-	-	-	-	-	-
IENFD ankle (Fibers/mm)	8.6 (6.8-10.9)	5.4 (4.3-9.7)	5.9 (3.7-7.3)	7.5 (4.8-10.7)	**0.033**	**0.017**	**0.005**	0.298	0.589	0.417	0.387

Clinical and skin innervation assessment of HC and patients with PD, MSA, and AP-Tau. Abbreviations: COMPASS-31: OH: orthostatic hypotension, VM: vasomotor, SM: sudomotor, GI: gastrointestinal, BL: bladder, PM: pupillomotor. P-values < 0.05 were considered significant and shown in bold.

Table 2. Comparison of drop-out *vs.* not drop-out PD patients at T24

Variable	Drop-out [n=6]	Not drop-out [n=24]	Overall *P*-value
Age (years)	74 ± 4	65 ± 12	0.158
Sex (ref. male)	33.3%	66.7%	0.153
Disease duration (years)	8.5 (3.8-20.5)	4.0 (2.8-7.3)	0.078
H&Y	3.0 (2.0-3.0)	2.0 (1.0-2.8)	**0.050**
MDS-UPDRS-I	6.0 (3.5-18.0)	3.5 (2.0-6.0)	0.113
MDS-UPDRS-II	6.0 (2.0-24.0)	5.5 (2.0-9.3)	0.739
MDS-UPDRS-III	22.0 (18.5-33.3)	14.0 (8.0-20.0)	**0.031**
MDS-UPDRS Total	32.0 (26.0-80.5)	23.0 (12.0-33.0)	0.086
COMPASS-31 Total	10.8 (5.8-33.8)	17.8 (0.0-24.1)	0.494
BDI-II	6.0 (3.0-7.0)	5.0 (3.0-9.0)	0.862
MMSE	29.0 (26.0-29.5)	30.0 (29.0-30.0)	0.082
MoCA	27.0 (18.0-29.5)	28.0 (25.0-29.0)	0.684
Olfactory test	5.0 (4.0-6.0)	7.0 (4.0-9.0)	0.469
RBD questionnaire	4.0 (1.0-6.5)	3.0 (1.0-5.0)	0.581
LEDD (mg)	682.5 (235.0-940.5)	375.0 (180.0-688.0)	0.302
IENFD total (N°fibers/mm)	10.2 (5.4-10.8)	12.5 (9.8-15.5)	**0.038**
IENFD cervical (N°fibers/mm)	15.9 (10.4-17.5)	16.8 (11.5-23.4)	0.127
IENFD ankle (N°fibers/mm)	4.5 (3.9-5.7)	6.9 (4.3-10.2)	0.594

P-values < 0.05 were considered significant and shown in bold.

Figure 3. αSyn-PLA signal detection

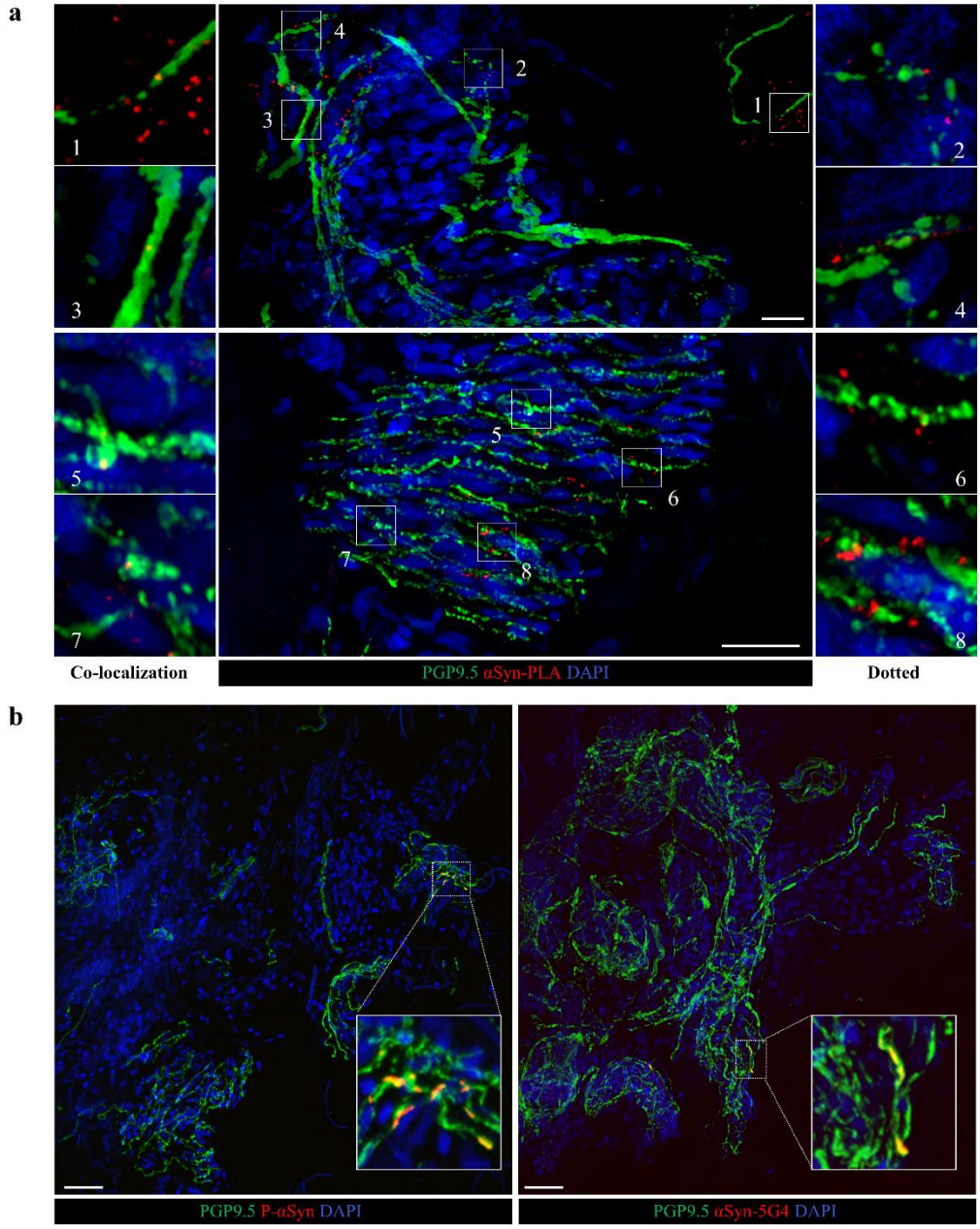

(a) Confocal images of a SG (top) and MAP (bottom) in skin biopsy at the cervical site of a PD patient: in green the panaxonal marker PGP9.5, in red αSyn oligomers detected by PLA technique. The Co-localization signal of αSyn-PLA and nerve fibers (magnification on the left) was defined by a yellow signal. The dotted signal (magnification on the right) was defined by an αSyn-PLA signal in the proximity of degenerating nerve fibers, characterized by swelling and fragmentations, or interposed between nerve fiber breakpoints. Scale bar 50 µm. (b) Confocal images of SG in cervical skin biopsy of a PD patient. In red, on the left phosphorylated αSyn, and on the right, aggregated αSyn detected by 5G4 antibodies. Co-localization of P-αSyn/PGP9.5 and αSyn-5G4/PGP9.5 is shown in yellow. Scale bar 50µm.

Figure 4. αSyn-PLA signal is significantly more expressed in PD and MSA

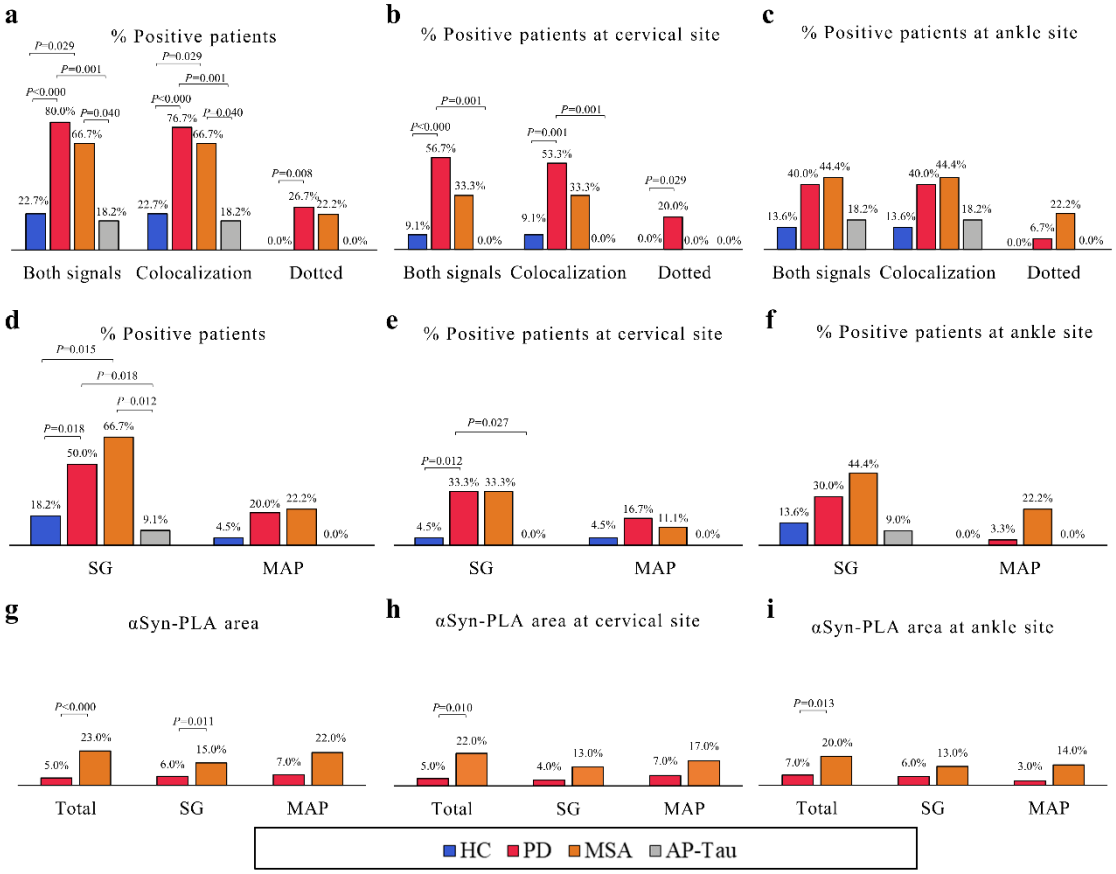

(a-c) αSyn-PLA signal is higher in PD and MSA. (d-f) The signal is observed mainly in the autonomic fibers surrounding SG and to a lesser extent MAP, independently from the anatomical site. (g-i) The area of intra-nervous oligomeric αSyn is significantly higher in MSA patients than PD at both locations.

Table 3. Univariate logistic regression analysis

PD *vs*. HC		*P*-value	Odd ratio	95% CI
Both Localizations	All structures	**0.000**	13.60	3.56-51.92
	SG	**0.023**	4.500	1.23-16.49
Cervical	All structures	**0.002**	13.08	2.58-66.28
	SG	**0.032**	10.5	1.23-89.68
PD *vs*. AP-Tau		***P*-value**	**Odd ratio**	**95% CI**
Both Localizations	All structures	**0.001**	18.00	3.05-106.12
	SG	**0.038**	10.000	1.134-88.167
MSA *vs*. HC		***P*-value**	**Odd ratio**	**95% CI**
Both Localizations	All structures	**0.028**	6.800	1.223-37.497
	SG	**0.014**	9.000	1.550-52.266
MSA *vs*. AP-Tau		***P*-value**	**Odd ratio**	**95% CI**
Both Localizations	All structures	**0.037**	9.000	1.140-71.038
	SG	**0.018**	20.000	1.676-238.630

Univariate logistic regression analysis shows the association between αSyn-PLA detection and clinical diagnosis according to anatomical locations and autonomic structures. The P-value, the odd ratio, and 95% confidence intervals (95% CI) are reported for each comparison. *P*-values < 0.05 are showed in bold.

Figure 5. Comparative analysis and diagnostic performance of αSyn-PLA, P-αSyn, and 5G4

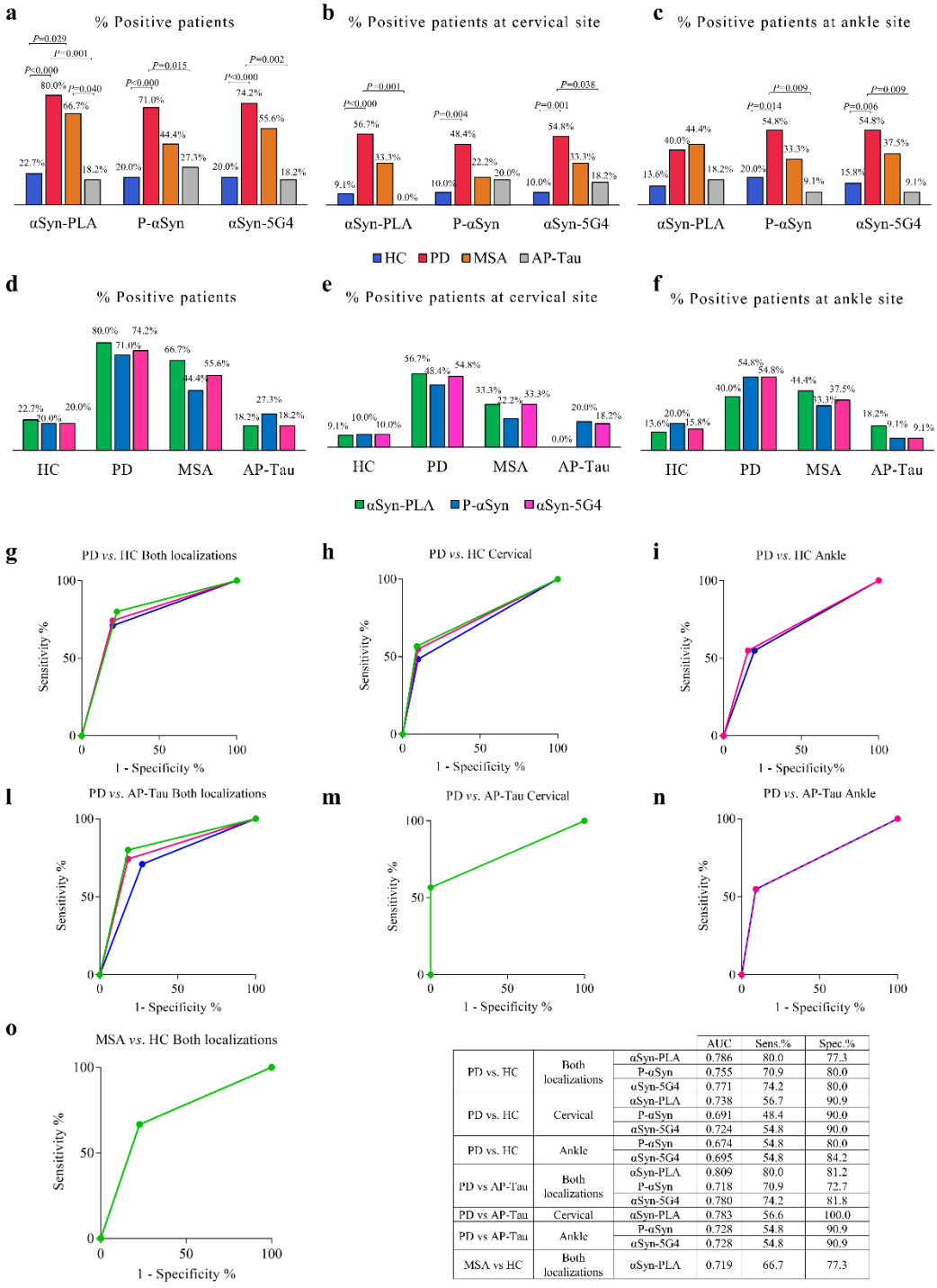

			AUC	Sens.%	Spec.%
PD vs. HC	Both localizations	αSyn-PLA	0.786	80.0	77.3
		P-αSyn	0.755	70.9	80.0
		αSyn-5G4	0.771	74.2	80.0
PD vs. HC	Cervical	αSyn-PLA	0.738	56.7	90.9
		P-αSyn	0.691	48.4	90.0
		αSyn-5G4	0.724	54.8	90.0
PD vs. HC	Ankle	P-αSyn	0.674	54.8	80.0
		αSyn-5G4	0.695	54.8	84.2
PD vs AP-Tau	Both localizations	αSyn-PLA	0.809	80.0	81.2
		P-αSyn	0.718	70.9	72.7
		αSyn-5G4	0.780	74.2	81.8
PD vs AP-Tau	Cervical	αSyn-PLA	0.783	56.6	100.0
PD vs AP-Tau	Ankle	P-αSyn	0.728	54.8	90.9
		αSyn-5G4	0.728	54.8	90.9
MSA vs HC	Both localizations	αSyn-PLA	0.719	66.7	77.3

αSyn-PLA presented the highest sensitivity for PD and MSA at both locations and allowed the differentiation from HC and AP-Tau (a). At the cervical site, αSyn-PLA and αSyn-5G4 showed higher sensitivity than P-αSyn for PD (b). In the ankle, P-αSyn and αSyn-5G4 were more sensitive for PD than αSyn -PLA (c). Within groups, no differences were observed between markers, but αSyn-PLA showed a higher sensitivity for MSA than P-αSyn and αSyn-5G4 (d-f). ROC curve analysis of PD *vs*. HC (g-i), PD *vs*. AP-Tau (j-l), MSA *vs*. HC (m). The area under the curve (AUC), sensitivity, and specificity for each marker and location are reported.

Figure 6. PD patients present a progression of denervation not of pathological αSyn at T24 and IENFD predicts cognitive and motor decline

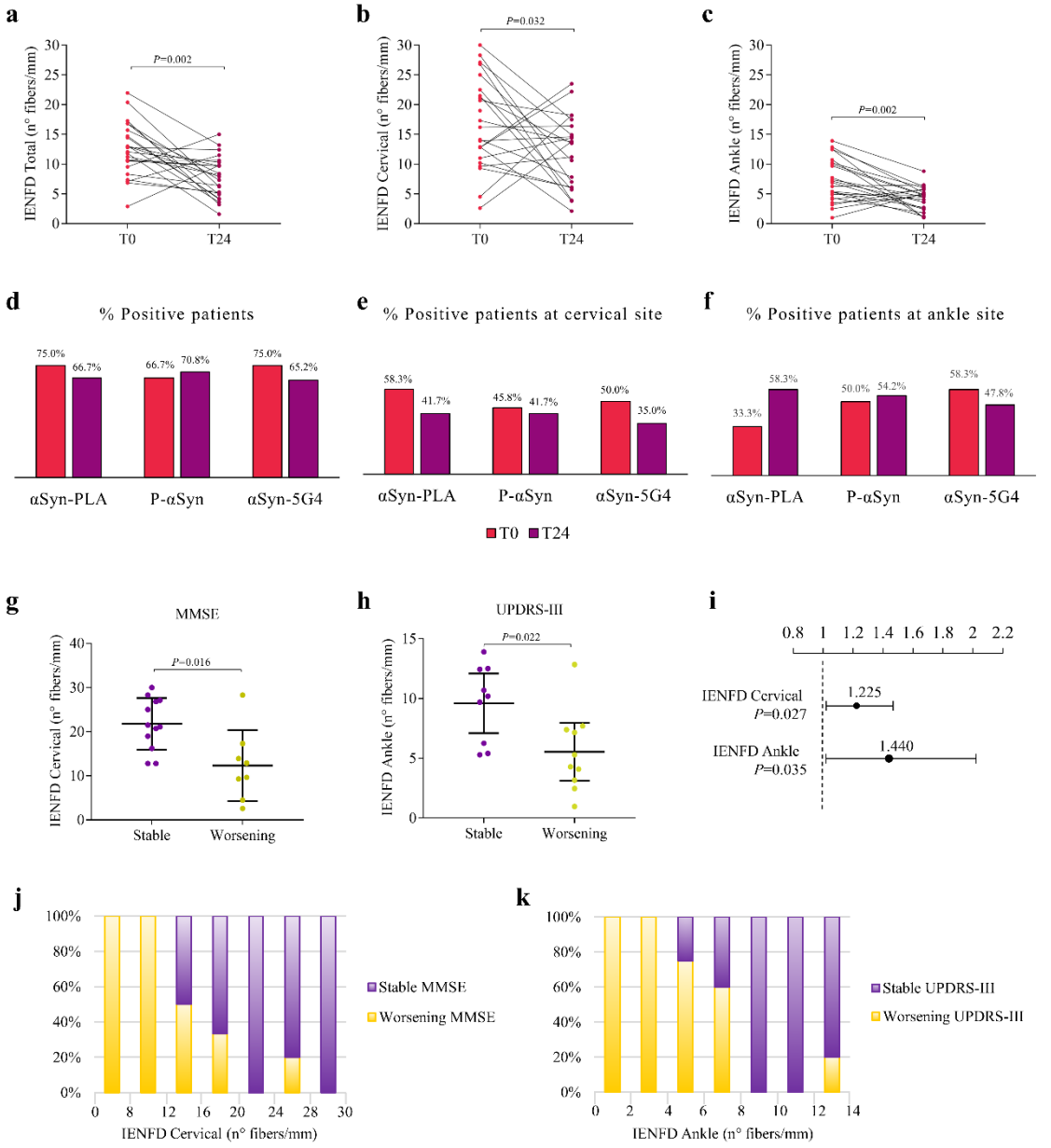

After 24 months, PD patients showed a significant progression of intraepidermal denervation (a) at both anatomical sites (b-c). No significant differences were observed in the percentage of positivity for αSyn-PLA, P-αSyn, and αSyn-5G4 (d-f) but a slight reduction for all markers at the cervical site and an increase of αSyn-PLA in the ankle are noted. Patients with a worsening MMSE scale at T24 showed a lower cervical IENFD at T0 (g), while a lower ankle IENFD was present at T0 in patients with a progressive motor impairment at the MDS-UPDRS-III scale (h). Univariate logistic regression analysis showed an association between cervical IENFD and MMSE, and between ankle IENFD and MDS-UPDRS-III; ODD ratio and P-value are reported (i). Percentage of patients with cognitive (j) and motor (k) progression at T24 are represented according to respectively cervical and ankle IENFD at T0.

Figure 7. Skin biopsy-derived compound marker allows stratification of patients according to the diagnosis

a

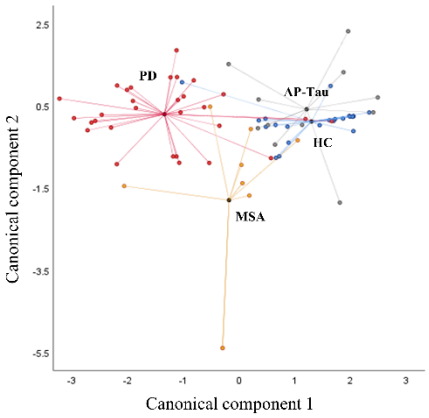

b

		Predicted			
		HC	PD	MSA	AP-Tau
Real	HC	17	1	0	4
	PD	2	26	1	1
	MSA	1	2	5	1
	AP-Tau	3	0	0	8
				Accuracy	77.8%
				Leave-one-out validation	44.4%

c

		Predicted	
		HC	PD
Real	HC	21	1
	PD	3	27
		Accuracy	92.3%
		Leave-one-out validation	86.5%
		Sensitivity	90.0%
		Specificity	95.5%

d

		Predicted	
		HC	MSA
Real	HC	21	1
	MSA	1	8
		Accuracy	93.5%
		Leave-one-out validation	80.6%
		Sensitivity	88.8%
		Specificity	95.5%

e

		Predicted	
		HC	AP-Tau
Real	HC	17	5
	AP-Tau	2	9
		Accuracy	78.8%
		Leave-one-out validation	51.5%
		Sensitivity	81.8%
		Specificity	77.2%

f

		Predicted	
		PD	MSA
Real	PD	27	3
	MSA	3	6
		Accuracy	84.6%
		Leave-one-out validation	59.0%
		Sensitivity	90.0%
		Specificity	66.6%

g

		Predicted	
		PD	AP-Tau
Real	PD	28	2
	AP-Tau	0	11
		Accuracy	95.1%
		Leave-one-out validation	75.6%
		Sensitivity	93.3%
		Specificity	100.0%

h

		Predicted	
		MSA	AP-Tau
Real	MSA	7	2
	AP-Tau	0	11
		Accuracy	90.0%
		Leave-one-out validation	35.0%
		Sensitivity	77.7%
		Specificity	100.0%

Canonical plot showing patients according to the diagnosis. The model was built considering the presence/absence of αSyn-PLA, P-αSyn, αSyn-5G4, and intraepidermal nerve fiber density (IENFD) at both anatomical sites. The axes of the plot (canonical components 1 and 2) were calculated from weighted linear combinations of variables to maximize the separation between the four groups. Each subject is represented by a point (a). Confusion matrix reporting real and predicted diagnosis, accuracy, internal validation by the leave-one-out algorithm, sensitivity, and specificity are reported for all groups and pairwise comparisons (b-h).

5. Immune profiling of plasma-derived EVs identifies PD

In the last few years, many studies have raised a great interest in EVs, their molecular profile and content, and their diagnostic potentials. So far, most of the studies on EVs in neurodegenerative diseases focused on their possible role in the transmission of pathologic misfolded proteins and fewer on their functions in cell-to-cell signaling in neuroinflammation. Indeed, the immune system is involved in PD, as demonstrated by neuroinflammatory changes in brain histopathology and elevated immune markers in peripheral blood, suggesting that the immune system may play a primary pathogenic role in PD [101,102]. Therefore, we hypothesized that circulating EVs carry important information on brain inflammatory immune response and that their characterization can be exploited for diagnostic purposes.

Plasma-derived EV were isolated from PD, matched HC, MSA, and AP-Tau subjects. The expression levels of 37 EV surface markers related to inflammatory and immune cells were measured by flow cytometry. We found that distinctive pools of EV markers stratified patients according to the clinical diagnosis. PD and MSA displayed overexpression of immune markers compared to AP-Tau, suggesting a different immune dysregulation. Moreover, via supervised machine learning algorithms, we built a diagnostic model based on EV surface markers expression that correctly classified 88.9% of patients, with reliable diagnostic performance after internal and external validations.

This study has been carried out in close collaboration with several research centers. Dr. Lucio Barile, Dr. Jacopo Burrello, and Ms. Sara Bolis, from Laboratory for Cardiovascular Theranostics, Cardiocentro Ticino Foundation, Lugano, Switzerland, have significant expertise in EVs and helped us with EVs characterization and flow cytometry. Dr. Pierluigi Mauri and Mr. Dario DiSilvestre from Proteomic and Metabolomic Laboratory, Institute for Biomedical Technologies–National Research Council (ITB-CNR), Segrate, Italy, performed the proteomic analysis. Biomedical Engineer Alessio Burrello from the Department of Electrical, Electronic and Information Engineering “Guglielmo Marconi” (DEI), University of Bologna, Italy, supported us in developing the diagnostic models. Dr. Cinthia Farina, from the Immunobiology of Neurological Disorders Lab, Institute of Experimental Neurology (INSpe) and Division of Neuroscience, IRCCS San Raffaele Scientific Institute, Milan, Italy, have major expertise in the immunobiology of neurological disorders and supported us in the correct interpretation of the data. The results of this study have been published in the journal “Neurology: Neuroimmunology and Neuroinflammation” (Doi: 10.1212/NXI.0000000000000866).

Methods

Study Design

This was a cross-sectional, case-control study aiming to: 1) characterize distinctive EV subpopulations in plasma of PD, MSA, AP-Tau, and HC by immunophenotyping 37 different membrane proteins using an innovative flow cytometry multiplex bead-based platform [103]; 2) to correlate the differential expression of EV-surface antigens to clinical scales of gravity; 3) to build diagnostic models based on distinctive EV-surface proteins through supervised machine learning algorithms. Finally, since EVs are taken up by surrounding and distant cells, we performed a functional evaluation of their protein interactors to highlight protein targets, biological pathways, and molecular functions potentially affected in PD, MSA, and AP-Tau.

Subjects

Twenty-seven patients with idiopathic PD, 8 with probable MSA, 9 with probable AP-Tau, and 19 age-matched HC for the PD group were consecutively enrolled from July 2015 to January 2019. These subjects served as training cohort for the diagnostic model.

Patients were recruited from the movement disorders outpatient clinic at Neurocenter of Southern Switzerland in Lugano; HC were recruited among patients' partners. Inclusion criteria for PD were: 1) a definite clinical diagnosis according to the UK Parkinson's Disease Society Brain Bank criteria for diagnosis [16]; 2) no family history and no significant cognitive impairment or major dysautonomic symptoms in the history. AP's inclusion criteria were based on published diagnostic criteria for MSA [79], PSP [82], and CBD [81]. Each subject underwent blood collection and clinical evaluation. Disease gravity was assessed by H&Y [83] and MDS-UPDRS [26] scales during the off-stage; cognitive profile by MMSE [84] and MoCA [85]; mood disorder by BDI-II [86] scale; REM sleep Behavior Disorder by RBD screening questionnaire [87]; olfactory function by Burghart Messtechnik GmbH (olfactory test). LEDD was calculated for PD and AP patients [88].

Exclusion criteria were significant co-morbidities: diabetes, renal failure, thyroid pathology, vitamin B12 deficiency, HIV infection, syphilis, coagulopathy, fever, acute or chronic inflammatory diseases, and tumors.

A separate cohort of 40 subjects (20 HC, 10 PD, 5 MSA, 5 AP-Tau) served as a validation cohort for the diagnostic model (see below the paragraph "Diagnostic modeling and validation in an external cohort").

Standard Protocol Approvals, Registrations, and Patient Consents

Subjects were consecutively included in the NSIPD001 study, according to the study protocol that the Cantonal Ethics committee approved. All enrolled subjects gave written informed consent to the study following the declaration of Helsinki.

Blood collection and plasma preparation

Ten ml of blood was collected into anticoagulant-EDTA tubes after four hours-fasting. The following protocol was performed to obtain plasma enriched in EVs 15: fresh whole blood was centrifuged for 15 minutes at 1600g at 10 °C to eliminate cellular components. To further deplete platelets and cellular debris, the supernatant was centrifuged 15 minutes at 3000g at 4ºC; then, two consecutive centrifuges were

performed at 10000g for 15 minutes and 20000g for 30 minutes at 4ºC, allowing the elimination of apoptotic bodies and larger EVs (Fig. 1A). The obtained plasma was aliquoted and stored at -80°C. The storage period varied among samples according to the consecutive enrollment of subjects in the study, between 2015-07 to 2019-01.

Nanoparticle Tracking Analysis (NTA)

Nanoparticle concentration and diameter were measured by NanoSight LM10 (Malvern Instruments, UK) equipped with a 405 nm laser and Nanoparticle Tracking Analysis NTA 2.3 software. One µl of plasma was diluted 1:1000 in particle-free PBS. Three consequent videos of 60 seconds each were acquired. Minimum expected particle size, minimum track length, and blur setting were set to automatic, and the detection threshold was set to 4 to reveal all particles, as previously described [104]. The particle concentration and the particle size distribution graph were determined per each sample by averaging the results from the analysis of 3 independent videos.

MACSPlex Exosome Assay and flow cytometry analysis

The screening approach (MACSPlex human Exosome Kit, Miltenyi, Bergisch Gladbach, Germany) was previously described [103]. Briefly, it is based on 4.8 µm diameter polystyrene beads, labeled with different amounts of 2 dyes (phycoerythrin [PE] and fluorescein isothiocyanate [FITC]), to generate 39 different bead-subsets discriminable by flow cytometry analysis. Each bead subset is conjugated with a different capture antibody that recognizes EVs carrying the respective antigen (37 EV surface epitopes plus two isotype controls). The list of 37 antigens is reported in Table 1. After beads + sample overnight incubation, EVs bound to beads are detected by allophycocyanin [APC]-conjugated anti-CD9, anti-CD63, and anti-CD81 antibodies (Fig. 1A). Plasma samples (60 µL) diluted 1:2 in buffer solution were analyzed with MACSQuant Analyzer-10 flow cytometer (Miltenyi, Bergisch Gladbach, Germany). Triggers for the side and forward scatter were selected to confine the measurement on the multiplex beads. A blank control composed only by MACSPlex Buffer and incubated with beads and detection antibodies was used to measure the background signal. Each EV marker's median fluorescence intensity (MFI) was normalized to the mean MFI for specific EV markers (CD9, CD63, and CD81), obtaining normalized MFI (nMFI). All analyses were based on nMFI values. Samples were analyzed blindly to the clinical diagnosis.

To test the reliability/specificity of MACSPlex human Exosome Kit for EVs, we compared the procedure described above with and without EV enrichment by ultracentrifugation. We found no differences between procedures (Fig. 2). Therefore, plasma samples were directly processed without EV enrichment by ultracentrifugation. The assay's technical consistency and reproducibility were confirmed by repeatedly analyzing the same sample and assessing plasma from the same subject at different time points (Fig.3).

Western Blot analysis

Western Blot analysis was performed on 100 µl of plasma samples incubated overnight with 5µl of MACSPlex detection beads at 10°C at 800 rpm. The next day, the unbounded fraction was discarded, and

samples were lysed with RIPA buffer. Total proteins were separated on a gradient SDS Page 4-12% gel and transferred onto the PVDF membrane. The blot was incubated with the following primary antibodies: anti-Alix (rabbit polyclonal, Abcam, Cambridge UK, 1:1000); anti-tumor susceptibility gene 101 (TSG101) (rabbit polyclonal, Abcam, Cambridge UK, 1:1000); anti-CD81 (mouse monoclonal, ThermoFisher Scientific, Waltham USA, 1:300); anti-apolipoprotein A1 (APOA1) (rabbit polyclonal, Abcam, Cambridge UK, 1:300); anti-GRP94 (rabbit polyclonal, Abcam, Cambridge UK, 1:500).

Network analysis of EV-surface markers' protein interactors

Protein interactors of differentially expressed EV-surface markers were retrieved by Cytoscape PESCA plugin [105], and a global Homo sapiens protein-protein interaction (PPI) network of 1588 nodes and 36984 edges was reconstructed. For each quantitative comparison (PD vs. HC, MSA vs. HC, AP-Tau vs. HC), a specific PPI sub-network was built considering the first neighbors of each EV-surface protein. Each sub-network was analyzed at the topological level by Cytoscape Centiscape plugin [106]: to select putative hubs and bottlenecks, we took into account the network size, and only nodes with all Betweenness, Bridging and Centroid values above the average calculated on the whole corresponding network were retained as previously reported [107,108]. At the same time, nodes belonging to each sub-network were evaluated at the functional level by DAVID [109] and the most enriched Kyoto Encyclopedia of Genes and Genomes pathways (KEGG) databases. Molecular functions were extracted; specifically, Homo sapiens set as background, count >5 and $P< 0.001$, corrected by Bonferroni's test.

Statistical analysis

Statistical analyses were performed with IBM SPSS Statistics 22.0, PYTHON 2.7, and GraphPad PRISM 7.0a. Variable distribution was assessed by the Kolmogorov-Smirnov test. Normally distributed variables (age) were expressed as mean ± SD and analyzed by 1-way ANOVA test with posthoc Bonferroni's test for multiple comparisons. Non-normally distributed variables (disease duration, H&Y, MDS-UPDRS, BDI-II, MMSE, MoCA, Olfactory test, RBD, LEDD, NTA, MACSPlex analysis) were expressed as medians and interquartile range and analyzed using Kruskal-Wallis' test. Categorical variables (sex) were expressed as absolute number and percentage (%) and analyzed by χ^2 or Fisher's exact tests. Univariate logistic regression analysis was performed to assess the OR. ROC curves analysis was used to evaluate the AUC and to compare diagnostic performances of selected variables. Younden index (J = Sensitivity + Specificity -1) was calculated to determine the cut-off with greater accuracy. Correlations were evaluated by Pearson's R test and regression curve analysis; correlations were considered strong for R between |1.0| and |0.5|, moderate between |0.5| and |0.3|, weak between |0.3 and |0.1|. A P-value lower than 0.05 was considered significant.

Diagnostic modeling and validation

In clinical practice, machine learning supervised algorithms are exploited to formulate predictions of selected outcomes based on a given set of labeled paired input-output training sample data [110,111]. A linear

discriminant analysis was used as a feature reduction strategy to the 3D canonical plot (Fig. 4B); canonical components 1, 2, and 3 were calculated from weighted linear combinations of variables to maximize separation between the four groups (HC, PD, MSA, AP-Tau); in the plot, each patient is represented by a point, the center of the spheres indicates the mean of (canonical 1; canonical 2; canonical 3) for each diagnosis, spheres include patients with a linear combination coefficient that falls within the mean ± SD (canonical 1± SD; canonical 2 ± SD; canonical 3 ± SD). A diagnostic model was built through a random forest (RF) classification algorithm on the training cohort (n=63); the algorithm created 20 different classification trees with a maximum number of 8 splits for each tree. The diagnosis derives from the outcome of each classification tree of the RF: for example, if at least 11 of 20 trees predict PD, the patient will be classified as PD. The model was validated by a leave-one-out algorithm (internal validation) and in a different cohort (n=40, external validation). The leave-one-out validation was used to exclude overfitting bias and evaluate the model's generalizability; briefly, the algorithm is trained on n-1 patients (where "n" is the total number of patients), and the remaining patient is used to test the model. The test patient is then changed and accordingly the training subgroup. The process is repeated a total of n-times, with the test patient rotating at each round and the remaining subset used for model training. The external validation was performed with the same RF model trained on the training cohort.

Results

Demographic and clinical characteristics of study groups

Demographic data and clinical assessments for each group are summarized in Table 2. MSA group included 4 MSA-C and 4 MSA-P; AP-Tau group included six patients with probable PSP and 3 with possible CBD. AP-Tau subjects were significantly older than HC. Sex ratio and disease duration did not differ across groups. It is known that AP are characterized by a more aggressive disease course than PD. Indeed, MSA and AP-Tau had a more severe disease gravity measured by H&Y and MDS-UPDRS; they also displayed a higher cognitive impairment measured by MMSE and MoCA. Finally, AP-Tau subjects were more depressed than PD as measured by BDI-II. LEDD was not different between groups of patients.

PD group shows an increased number of EVs

NTA showed that the PD group had the highest number of nanoparticles/ml compared to HC and AP-Tau (P=0.001), not to MSA, whereas no differences in diameter were found between groups (Fig. 1B). Since NTA is not specific for EVs, we used the MFI of CD9/CD63/CD81 (specific markers of EVs) by flow cytometry analysis as a measure of EV concentration. Mean MFI of CD9/CD63/CD81 was significantly higher in PD compared to HC (P=0.023) and AP-Tau (P=0.037), not to MSA (Fig. 1C). Importantly mean MFI for CD9/CD63/CD81 correlated with nanoparticle concentration obtained with NTA analysis (Fig. 1D).

EVs were furtherly characterized according to current standard guidelines 3. After EV immuno-capture by MACSPlex kit capture beads, we performed a western blot analysis showing the presence of EV specific luminal markers (TSG101, Alix), EV specific tetraspanin (CD81), and the absence of contaminants (APOA1

and GPR94) (Fig. 1E). These results confirm the presence of EVs and the lack of relevant contamination in samples analyzed by flow cytometry.

EV-surface antigens expression differs between groups

Among the 37 EV-surface markers, 17 resulted differentially expressed between groups. Sixteen markers differed between PD and HC: T cell (CD4), B cell (CD19), Leukocyte (CD45), Antigen Presenting Cell (CD1c) related markers, 8 involved in cell adhesion (CD2, CD11c, CD31, CD41, CD42a, CD62, CD146, MCSP), 3 in immune cell activation (CD25, CD40, CD209), and the molecules of major histocompatibility complex class I (HLA-ABC).

Twelve markers were different between MSA and HC: T cell-related (CD4), B cell-related (CD19), involved in cell adhesion (CD29, CD2, CD11c, CD31, CD42a, CD62, CD146, CD209), immune cell activation (CD40) and HLA-ABC. AP-Tau and HC groups differ for only four markers: CD25, CD31, CD40, and CD42a. No significant difference was found between PD and MSA groups, while CD2 differed between PD and AP-Tau. CD2 and CD19 discriminated between MSA and AP-Tau patients.

The heat map (Fig. 4A) built on the differentially expressed EV markers highlighted HC as a homogenous group with relatively low expression of EV markers, in analogy to the AP-Tau group, while higher levels of expression characterized PD and MSA.

Further, a linear discriminant analysis model based on differential expression of all EV markers allowed the separation of subjects according to their diagnosis, as shown in the canonical plot (Fig. 4B).

Protein network hubs and functional pathways analysis of EV-surface antigens

PPI network topological analysis selected the most relevant interactors of differentially expressed EV markers in terms of hubs. Hubs refer to proteins with more connections within the cell or occupying crucial network positions, suggesting a critical role in controlling information flow over the network [108,111]. Analysis of hubs accounts for network size, and only nodes with values above the average normalization for the level of connections in the total network are selected [107,108]. Hubs for PD vs. HC and MSA vs. HC comparisons were coincident (SP1, MSN, ITGB2, EZR, C1QBP, CARL), while the network on AP-Tau vs. HC showed a different set of proteins (FLNA, FN1, GP1BB, HSPA4, NFKB1, STAT3, VIM, VWF, YWHAZ) (Fig. 5A-C). Similarities between PD and MSA were also observed in terms of pathways and molecular functions (Fig. 5D). Most represented KEGG categories included the immune system, signal transduction, endocrine system, and signaling molecules and interaction. Except for the endocrine system, they were more enriched in PD and MSA, suggesting potential more robust activation of immune response in these groups. Of note, the FoxO signaling pathway was higher in AP-Tau.

EV-surface antigens correlate to cognitive impairment and disease gravity in PD and MSA

In PD, CD25 inversely correlated with cognitive impairment measured by MMSE and MoCA, CD146 inversely correlated with MMSE, while CD62P directly correlated with BDI-II (Fig. 6A-D). No significant correlations were found between EV antigen's expression and LEDD in PD and AP groups. In the MSA group,

mean MFI for CD9, CD63, and CD81 inversely correlated with MoCA, while nanoparticles concentration directly correlated to disease duration and CD31 inversely correlated with H&Y (Fig. 6E-G). No correlations were observed in the AP-Tau group. No significant correlations were found between EV antigen's expression and LEDD in PD and AP groups.

Differential EV-surface antigens expression and diagnostic outcome

Univariate logistic regression analysis, allowing the assessment of associations between each EV marker and the diagnosis, confirmed 11 EV-surface antigens as potential discriminants for PD diagnosis, 6 for MSA, and 3 for AP-Tau (Fig. 7). Among markers significantly associated with the different diagnoses, CD1c, CD11c, CD19, CD41b, CD45, and CD146 were exclusive of the PD group; CD29 was exclusive for the MSA group. CD2 displayed the strongest association with the diagnosis of PD (OR=1.191) and MSA (OR=1.256), whereas CD40 with AP-Tau (OR=1.131).

ROC curve analysis of EV-surface antigens shows the best performance for MSA and PD

ROC curve analysis for all pathological groups (PD, MSA, AP-Tau) vs. HC confirmed a reliable diagnostic performance of each single differentially expressed EV marker (Fig. 8). The linear weighted combination of the three markers with the highest AUC showed better diagnostic performance than single markers in all groups. The combination of all EV-surface markers in one single compound marker showed a further diagnostic improvement in PD and MSA groups.

Random Forest model discriminates the different groups

A RF diagnostic model was built using the 17 surface antigens differentially expressed in plasma-derived EVs. The forest was composed of 20 different classification trees (a representative tree is reported in Fig. 9A). The model discriminated patients of the four groups (HC, PD, MSA, AP-Tau) with high accuracy (88.9%). All PD subjects were correctly diagnosed, one MSA and one HC were respectively misdiagnosed as HC and PD, whereas among nine AP-Tau, two were predicted as HC and three as PD (Fig. 9B). Subsequently, pairwise comparisons were performed (Fig. 9C-H). The RF model was validated by a leave-one-out algorithm, which confirmed the model's generalizability and excluded overfitting bias (accuracy of internal validation 63.8%, with a 72.2-91.5% range for pairwise comparisons). Finally, we validated our model in an external cohort of 40 subjects: the overall accuracy was 77.5%, resulting in the correct diagnosis of 31 out of 40 subjects (Fig. 9I-J). The accuracy after external validation was consistent with the one resulting from the internal validation, supporting the reliability of the diagnostic model. Demographic data of the external cohort were similar to those of the training cohort and are shown in Table 3.

Figures and Tables

Figure 1. EV enrichment, MACSPlex exosome assay, and EV characterization

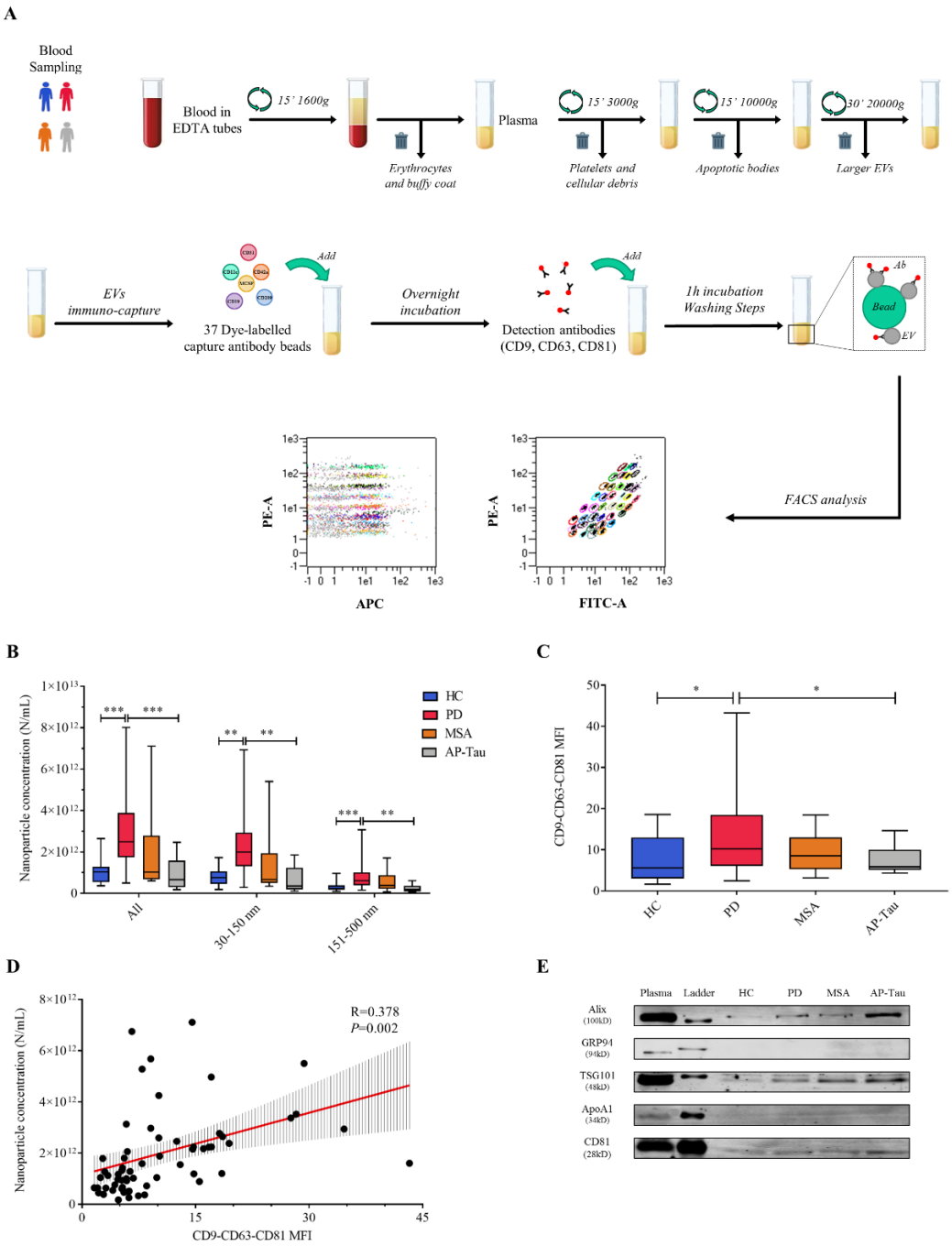

(A) Protocol for EV enrichment and MACSPlex exosome assay. (B) Nanoparticle concentration (N/mL plasma) by NTA, stratified for diameter (smaller nanoparticles, 30–150 nm; larger nanoparticles 151–500 nm). (C) MFI for CD9, CD63, and CD81 at flow cytometry analysis. (D) Correlation between mean MFI of CD9−CD63−CD81 and N/mL by NTA: the regression line is reported in red, with 95% CI. (E) Western blot of samples from HC, PD, MSA, and AP-Tau subjects after immunocapturing compared with whole plasma (dilution 1:100), showing the presence of specific EV markers (CD81, Alix, tumor susceptibility gene 101) and the absence of plasma contaminants (apolipoprotein A1, GRP94). Data are expressed as median and interquartile range; p-values < 0.05 were considered significant (*p < 0.05, **p < 0.01, ***p < 0.001).

Table 1. List of 37 EV-surface antigens

EV-surface marker description		Role
CD1c	APC cells surface glycoprotein	Antigen-presenting protein
CD2	T and NK cell surface antigen	Mediator of adhesion between T-cells and other cell types
CD3	T cells surface glycoprotein	Mediator of signal transduction
CD4	T cells transmembrane glycoprotein	Co-receptor for MHC class II molecule
CD8	T cells transmembrane glycoprotein	Co-receptor for MHC class I molecule
CD9	Tetraspanin super-family	Regulator of cell adhesion
CD11c	Integrin alpha-X	Receptor for fibrinogen
CD14	Monocyte differentiation antigen	Co-receptor for bacterial lipopolysaccharide
CD19	B-lymphocyte antigen	Co-receptor for the B-cell antigen receptor complex (BCR)
CD20	B-lymphocyte antigen	Regulation of cellular calcium influx necessary for the development, differentiation, and activation of B cells
CD24	Signal Transducer	Modulator of B-cell activation responses
CD25	Interleukin-2 receptor subunit alpha	Marker for immune cell activation
CD29	Integrin beta-1	Extracellular matrix component
CD31	Platelet endothelial cell adhesion molecule	Regulator of leukocyte transendothelial migration (TEM)
CD40	Costimulatory surface molecule	Co-stimulator of T and B cells
CD41b	Integrin alpha-IIb	Receptor for fibronectin, fibrinogen, plasminogen, prothrombin, thrombospondin, and vitronectin
CD42a	Platelet glycoprotein 9	Mediator of platelet adhesion to blood vessels
CD44	Cell-surface receptor	Regulator of activation, recirculation, and homing of T cells
CD45	Receptor-type tyrosine-protein phosphatase C	Positive regulator of T-cell coactivation
CD49e	Integrin alpha-5	Receptor for fibronectin and fibrinogen
CD56	Neural Cell Adhesion Molecule 1	Cell adhesion molecule involved in neuron-neuron adhesion, neurite fasciculation, outgrowth of neurites
CD62P	P-selectin	Mediator of interaction between activated endothelial cells or platelets with leukocytes
CD63	Tetraspanin super-family	Modulator of signal transduction
CD69	Early activation antigen	Signal transmitting receptor in lymphocytes, natural killer cells, and platelets
CD81	Tetraspanin super-family	Modulator of signal transduction
CD86	T-lymphocyte activation antigen	Co-stimulator of T cells proliferation and interleukin-2 production
CD105	Endoglin	Vascular endothelium glycoprotein that regulates angiogenesis

CD133/1	Prominin-1	Regulator of cell differentiation, proliferation, and apoptosis
CD142	Tissue factor	Coagulation regulator
CD146	Melanoma Cell Adhesion Molecule	Cell adhesion molecule
CD209	C-type lectin receptor	Pathogen-recognition receptor
CD326	Epithelial cell adhesion molecule	Cell adhesion regulator
HLA-ABC	Major Histocompatibility Complex class I	Immune response regulator
HLA-DRDPDQ	Major Histocompatibility Complex class II	Immune response regulator
MCSP	Melanoma-associated Chondroitin Sulfate Proteoglycan	Regulator of cell proliferation and migration
ROR1	Neurotrophic Tyrosine Kinase, receptor-related 1	Neurite growth modulation in central nervous system
SSEA-4	Stage-Specific Embryonic Antigen-4	Marker of bone-marrow-derived very small embryonic-like stem cells

Description and role for each EV-surface marker included in flow cytometry multiplex analysis

Figure 2. MACSPlex Exosome Assay: with and without ultracentrifugation

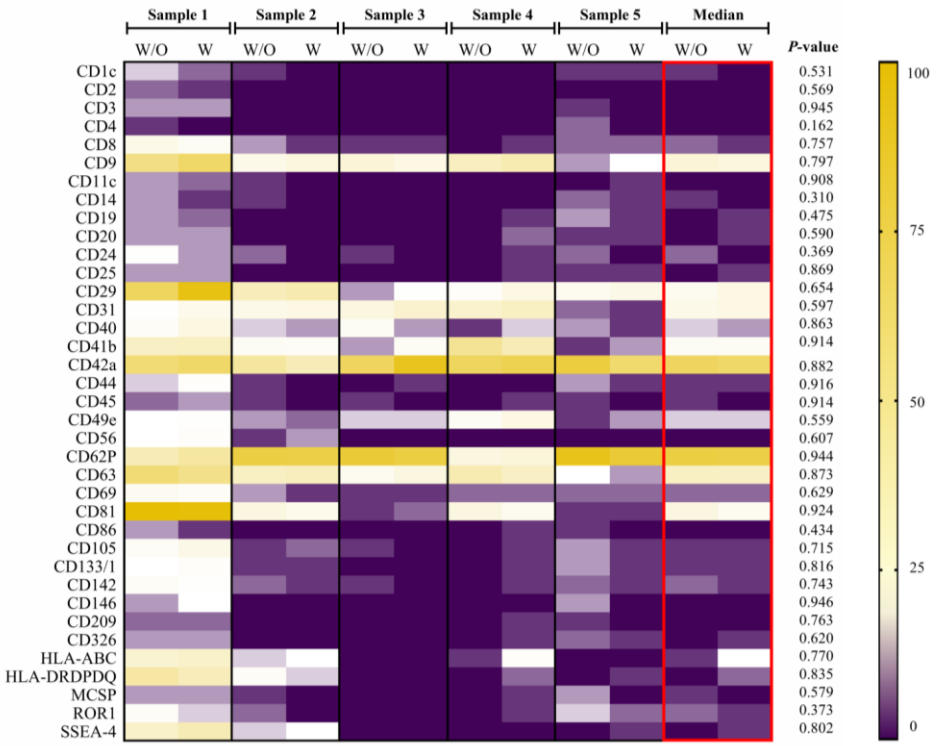

Comparison between samples (n=5) with EV enrichment (W) by ultracentrifugation vs. without EV enrichment (W/O). The heatmap reports the nMFI (purple = low nMFI; yellow = high nMFI) for the 37 EV-surface markers evaluated by flow cytometry and median values for the two protocols.

Figure 3. Technical validation of the MACSPlex Exosome Assay

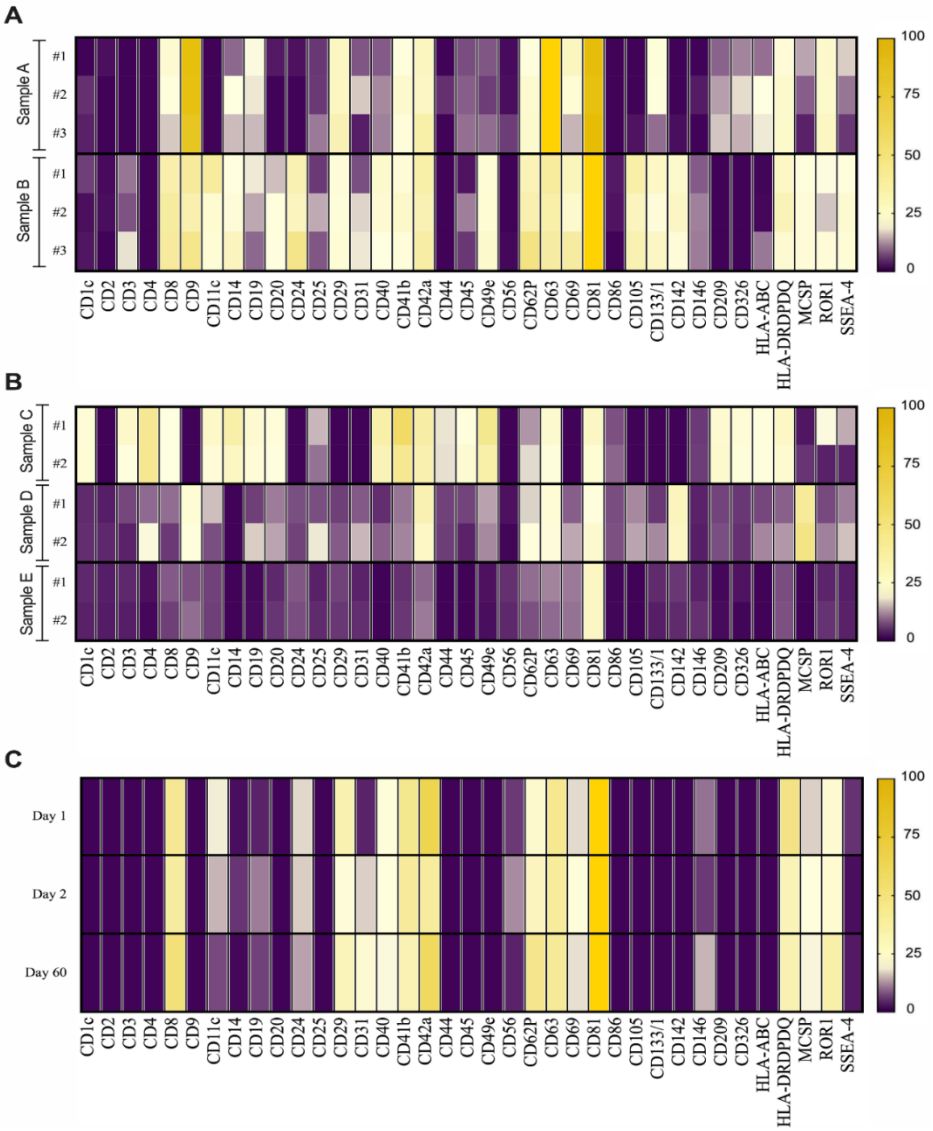

(A) Comparison of triplicates of sample A vs. sample B analyzed the same day (delta mean:0.4; st.dev.:4.5); (B) Comparison of duplicates of sample C, D, and E analyzed in 2 consecutive days (delta mean:0.5; st.dev.:1.9). (C) Comparison of samples from the same patient taken at day 1, day 2, and day 60 (delta mean:0.7; st.dev.:5.6). The heatmap reports the nMFI (purple = low nMFI; yellow = high nMFI) for the 37 EV-surface markers evaluated by flow cytometry.

Table 2. Demographic data and clinical scores

			AP			Pairwise comparisons					
Variable	**HC [n = 19]**	**PD [n = 27]**	**MSA [n = 8]**	**AP-Tau [n = 9]**	**Overall *p* value**	**HC vs PD**	**HC vs MSA**	**HC vs AP-Tau**	**PD vs MSA**	**PD vs AP-Tau**	**MSA vs AP-Tau**
Age (y)	61 ± 8.2	66 ± 11.8	68 ± 8.6	74 ± 5.2	**0.013**	0.556	0.729	**0.008**	1.000	0.184	0.924
Sex (ref. male)	10 (52.6%)	17 (63.0%)	2 (25.0%)	4 (44.4%)	0.279	—	—	—	—	—	—
Disease duration (y)	—	4.0 [2.0–8.0]	5.5 [1.3–7.8]	4.0 [2.5–5.5]	0.863	—	—	—	—	—	—
H&Y	—	2.0 [1.0–3.0]	5.0 [4.0–5.0]	4.0 [3.0–5.5]	**<0.001**	—	—	—	**<0.001**	**0.001**	1.000
MDS-UPDRS	—	23.0 [13.0–34.5]	42.5 [38.0–43.0]	40.5 [28.8–81.5]	**0.043**	—	—	—	0.509	0.277	1.000
BDI-II	—	5.0 [3.0–8.5]	8.0 [2.8–15.8]	14.5 [11.8–19.0]	**0.008**	—	—	—	1.000	**0.012**	0.682
MMSE	—	30.0 [29.0–30.0]	26.0 [24.0–29.0]	26.0 [22.0–28.0]	**<0.001**	—	—	—	**0.049**	**0.002**	1.000
MoCA	—	27.0 [23.8–29.0]	24.5 [17.3–27.0]	20.0 [14.5–23.0]	**0.016**	—	—	—	0.955	**0.041**	1.000
Olfactory test	—	7.0 [4.0–9.0]	9.0 [7.5–10.3]	7.0 [4.8–8.8]	0.131	—	—	—	—	—	—
RBD	—	3.0 [1.8–5.0]	3.0 [1.0–5.8]	3.0 [0.5–4.5]	0.875	—	—	—	—	—	—
LEDD	—	562.5 [202.5–737.5]	375.0 [108.0–375.0]	250.0 [100.0–452.0]	0.448	—	—	—	—	—	—

Clinical characteristics of patients with PD, MSA, and AP-Tau compared with HCs. P-values <0.05 were considered significant and shown in bold.

Figure 4. Differential expression of EV-surface markers

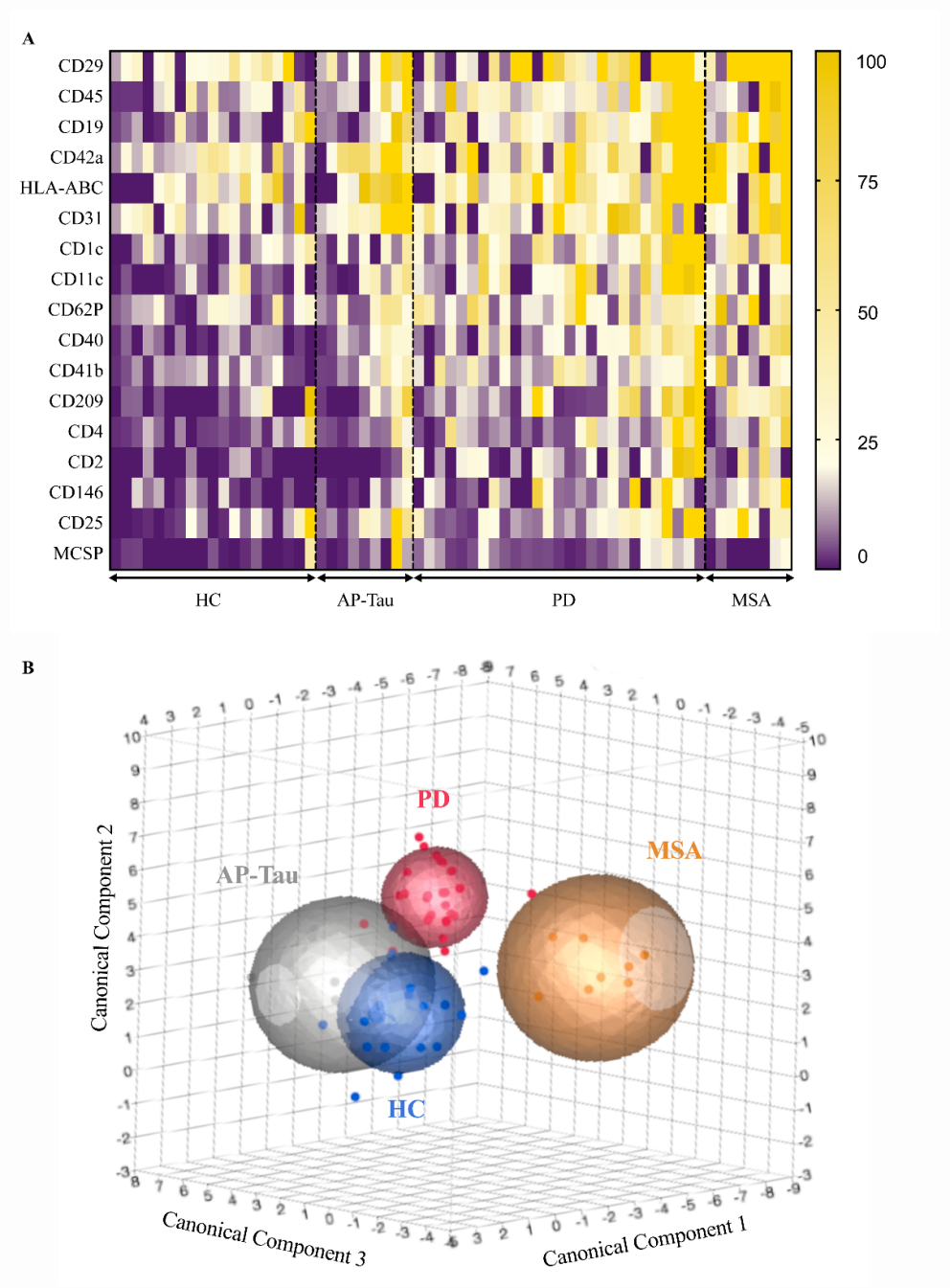

Patients' stratification for diagnosis and EV surface marker expression (expressed as normalized median fluorescence intensity [nMFI]). (A) Heatmap representation of the 17 EV surface markers differentially expressed between patients with PD, MSA, and AP-Tau and HCs (purple = low nMFI, yellow = high nMFI). (B) Canonical plot showing patients according to the diagnosis: PD, red vs. MSA, orange vs. AP-Tau, gray vs. HC, blue; the model was built considering the 37 EV surface markers analyzed by flow cytometry. The plot's axes (canonical 1, canonical 2, and canonical 3) were calculated from weighted linear combinations of variables to maximize separation between the four groups. Each subject is represented by a point, and spheres include patients with a linear combination coefficient that falls within the mean ± SD (canonical 1 ± SD; canonical 2 ± SD; canonical ± SD).

Figure 5. EV surface proteins upregulated in PD, MSA, and AP-Tau and functional evaluation of their protein interactors

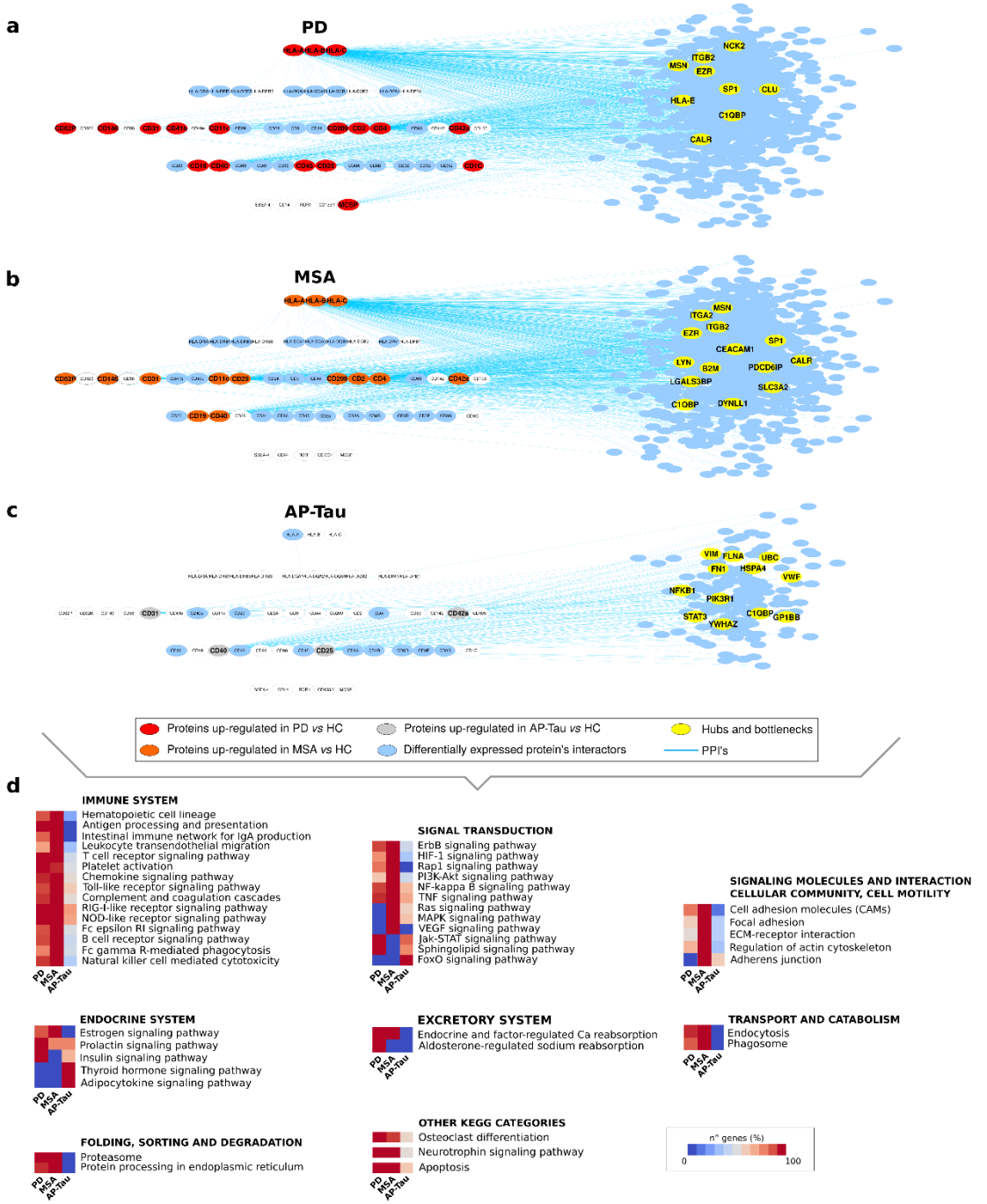

Protein-protein interaction network showing the first neighbors of each differentially expressed EV surface marker in (A) PD, (B) MSA, and (C) AP-Tau *vs.* HC. (D) Kyoto Encyclopedia of Genes and Genomes pathways enriched by considering the first neighbors of each EV surface protein in PD, MSA, and AP-Tau vs. HC; DAVID database background: Homo sapiens, gene count >5 and $p < 0.001$.

Figure 6. Correlations between clinical scales and EV surface marker expression

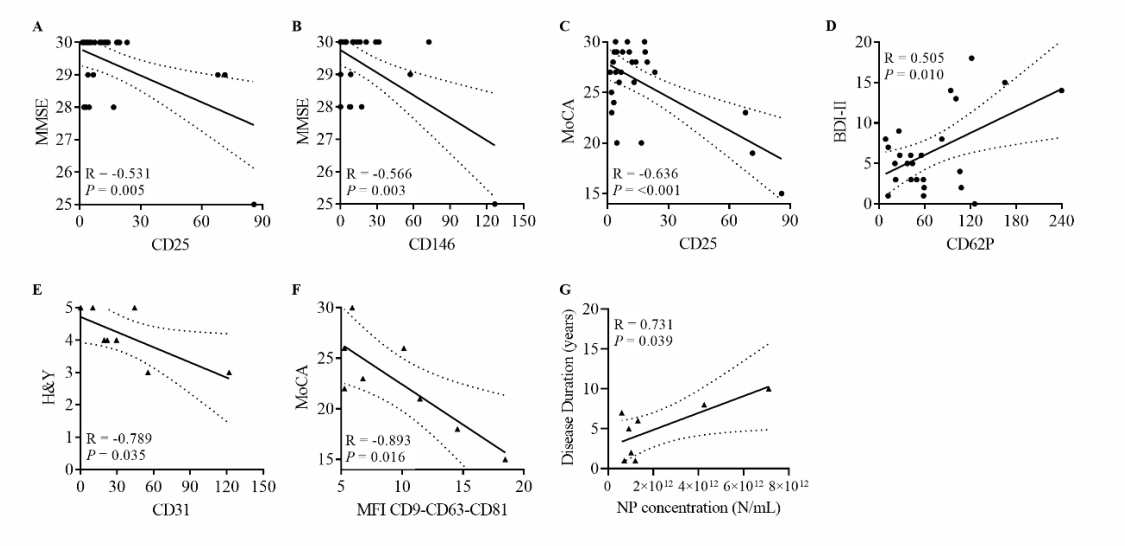

Correlations between EV surface markers normalized MFI, nanoparticle concentration (N/mL plasma), and clinical parameters in patients with PD (circles; A-D) and MSA (E-G). The regression line is reported together with its 95% CI (dashed line).

Figure 7. Univariate analysis of EV-surface markers

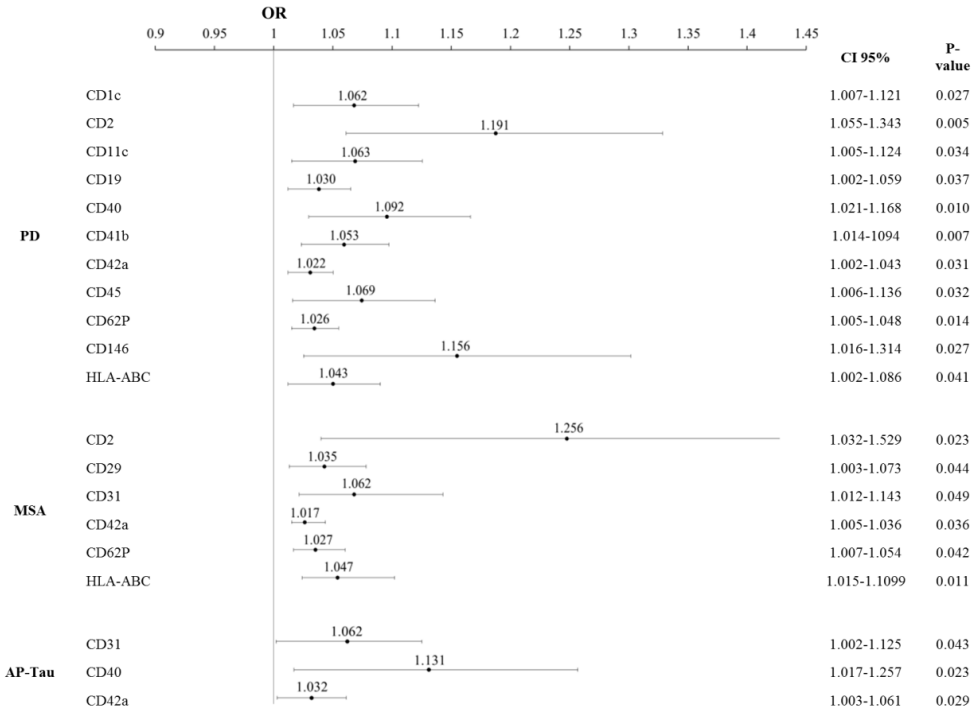

Logistic regression analysis was performed to assess the OR and 95% CI for EV-surface markers differentially expressed between HC and each pathological group (PD; MSA; AP-Tau). An OR greater than 1 indicates an increased likelihood of diagnosis (PD, MSA, AP-Tau); *P*-values < 0.05 were considered significant. No significant associations were not reported.

Figure 8. ROC curve analysis of EV-surface markers

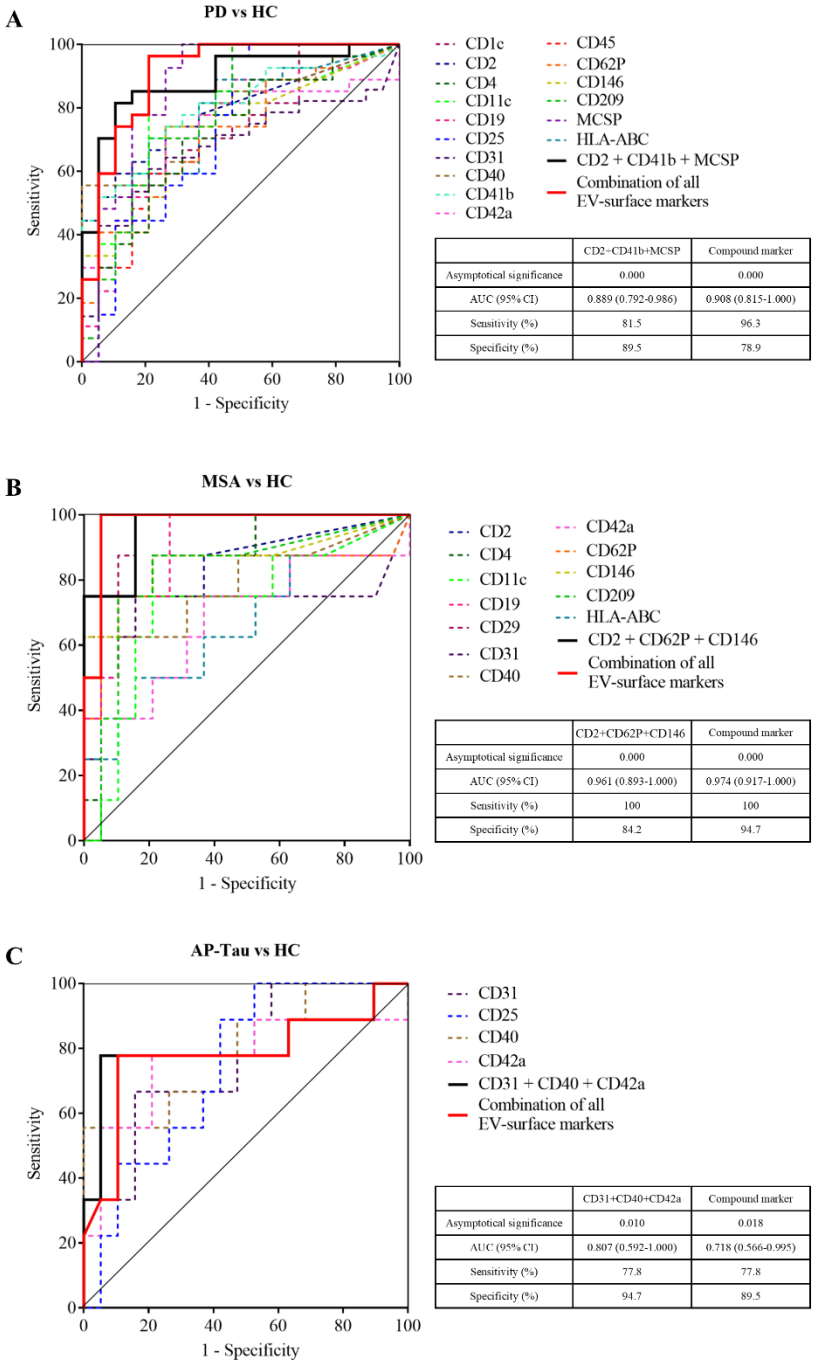

	CD2+CD41b+MCSP	Compound marker
Asymptotical significance	0.000	0.000
AUC (95% CI)	0.889 (0.792-0.986)	0.908 (0.815-1.000)
Sensitivity (%)	81.5	96.3
Specificity (%)	89.5	78.9

	CD2+CD62P+CD146	Compound marker
Asymptotical significance	0.000	0.000
AUC (95% CI)	0.961 (0.893-1.000)	0.974 (0.917-1.000)
Sensitivity (%)	100	100
Specificity (%)	84.2	94.7

	CD31+CD40+CD42a	Compound marker
Asymptotical significance	0.010	0.018
AUC (95% CI)	0.807 (0.592-1.000)	0.718 (0.566-0.995)
Sensitivity (%)	77.8	77.8
Specificity (%)	94.7	89.5

ROC curves identifying the best cutoff for each EV surface marker, discriminating pathologic groups from HC. The referral line is reported in gray. (A) PD vs HC; (B) MSA vs HC; (C) AP-Tau vs HC. In each plot, ROC curves for the combination of the 3 EV surface markers with the highest AUCs and a compound EV marker (linear weighted combination of all EV surface markers differentially expressed for each comparison) are shown (black and red lines, respectively). The tables provide asymptotic significance AUC with 95% CI, sensitivity, and specificity on the compound EV markers. P-Values < 0.05 were considered significant.

Figure 9. RF modeling to predict diagnosis and its validation in an external cohort of subjects

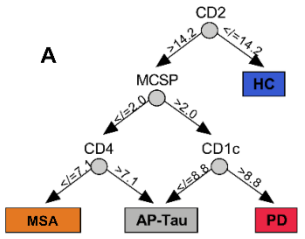

B

		Predicted			
		HC	PD	MSA	AP-Tau
Real	HC	**18**	1	0	0
	PD	0	**27**	0	0
	MSA	1	0	**7**	0
	AP-Tau	2	3	0	**4**
		Model Accuracy		88.9%	
		Leave-one out validation		63.8%	

C

		Predicted	
		HC	PD
Real	HC	**18**	1
	PD	0	**27**
Model Accuracy		97.8%	
Leave-one out validation		87.0%	
Sensitivity		100%	
Specificity		94.7%	

D

		Predicted	
		HC	MSA
Real	HC	**19**	0
	MSA	0	**8**
Model Accuracy		100%	
Leave-one out validation		91.5%	
Sensitivity		100%	
Specificity		100%	

E

		Predicted	
		HC	AP-Tau
Real	HC	**19**	0
	AP-Tau	4	**5**
Model Accuracy		85.7%	
Leave-one out validation		82.1%	
Sensitivity		55.6%	
Specificity		100%	

F

		Predicted	
		PD	MSA
Real	PD	**27**	0
	MSA	4	**4**
Model Accuracy		88.6%	
Leave-one out validation		76.1%	
Sensitivity		50.0%	
Specificity		100%	

G

		Predicted	
		PD	AP-Tau
Real	PD	**27**	0
	AP-Tau	4	**5**
Model Accuracy		88.9%	
Leave-one out validation		72.2%	
Sensitivity		55.6%	
Specificity		100%	

H

		Predicted	
		MSA	AP-Tau
Real	MSA	**7**	1
	AP-Tau	2	**7**
Model Accuracy		82.4%	
Leave-one out validation		72.7%	
Sensitivity		77.8%	
Specificity		87.5%	

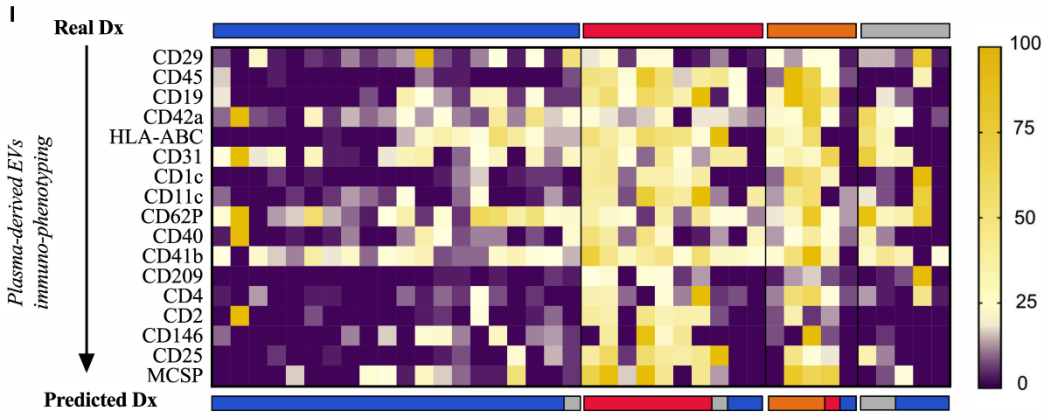

J

		Predicted			
		HC	PD	MSA	AP-Tau
Real	HC	**19**	0	0	1
	PD	2	**7**	0	1
	MSA	1	1	**3**	0
	AP-Tau	3	0	0	**2**
		Model Accuracy		77.5%	

RF modeling to diagnose patients based on the combination of the 17 differentially expressed extracellular vesicle surface markers. (A) Representation of 1 of the 20 different classification trees created by the algorithm to predict the diagnosis PD vs MSA vs AP-Tau vs HC (B–H). Confusion matrix reporting real and predicted diagnosis, accuracy, sensitivity, specificity, and internal validation by the leave-one-out algorithm for each comparison (see Methods). (I) External validation of the RF model; 40 patients were included in the analysis (20 HC, blue; 10 PD, red; 5 MSA, orange; 5 AP-Tau, gray.

Table 3. Table 3. Demographic data and clinical scores of the validation cohort

Variable	HC [n=20]	PD [n=10]	AP		Overall *P*-value	*Pairwise Comparisons*					
			MSA [n=5]	AP-Tau [n=5]		HC vs. PD	HC vs. MSA	HC vs. AP-Tau	PD vs. MSA	PD vs. AP-Tau	MSA vs. AP-Tau
Age (years)	61 ± 9.9	67 ± 9.3	65 ± 6.4	72 ± 13.0	0.108	-	-	-	-	-	-
Sex (ref. male)	8 (40.0%)	5 (50.0%)	2 (40.0%)	2 (40.0%)	0.959	-	-	-	-	-	-
Disease duration (years)	-	5.5 [4.0-10.0]	7.0 [3.5-8.5]	5.0 [3.5-7.0]	0.545	-	-	-	-	-	-
H&Y	-	2.0 [2.0-3.0]	5.0 [3.0-5.0]	4.0 [2.5-4.8]	**0.004**	-	-	-	**0.010**	0.112	1.000
MDS-UPDRS	-	25.00 [14.5-29.0]	26.5 [24.0-28.0]	30.5 [19.8-81.5]	0.227	-	-	-	-	-	-
BDI-II	-	5.5 [4.0-10.5]	10.0 [3.5-16.5]	16.0 [11.8-19.0]	0.258	-	-	-	-	-	-
MMSE	-	30.0 [29.0-30.0]	29.0 [28.0-29.5]	27.0 [16.3-28.0]	**0.012**	-	-	-	0.668	**0.016**	0.845
MoCA	-	26.0 [20.0-28.3]	26.0 [22.5-26.5]	19.0 [7.8-22.8]	0.083	-	-	-	-	-	-
Olfactory test	-	7.5 [4.8-9.3]	9.0 [5.5-10.5]	5.0 [4.8-5.0]	0.565	-	-	-	-	-	-
RBD	-	5.0 [2.8-6.5]	1.0 [0.0-3.5]	1.5 [0.3-6.5]	0.072	-	-	-	-	-	-
LEDD	-	481.3 [100.0-1009.3]	123.0 [0.0-187.5]	100.0 [93.8-162.5]	0.087	-	-	-	-	-	-

Demographic and clinical characteristics of patients enrolled in the validation cohort: 20 HC, 10 patients with PD, 5 with MSA, and 5 with AP-Tau.

6. Profiling Inflammatory EVs in Plasma and Cerebrospinal Fluid: An Optimized Diagnostic Model for PD

The immunophenotyping of multiple plasma-derived EV surface markers allows us to build a diagnostic model to stratify patients according to their clinical diagnosis with 88.9% accuracy. However, most plasma-derived EVs come from hematopoietic cells, particularly platelets, B cells, and T cells [70], and probably only a small percentage have a neuronal origin. Thus, to increase the sensitivity and specificity of our model for neurodegenerative diseases, we analyzed matched samples of CSF and plasma in a subgroup of patients, assuming that EV surface markers, expressed both in plasma and CSF, may have higher relevance for the respective neurodegenerative disease. Indeed, CSF permeates the cerebral cortex, spinal cord, cerebral ventricles, and medullary canal, receiving EVs mainly from the CNS.

In this pilot study, we recalibrate the previous diagnostic model on EV surface markers expressed both in plasma and CSF in each diagnostic group obtaining and improving a diagnostic system that remains based on EV profiling in plasma. In particular, we built three different two-level integrated diagnostic models, for PD, for MSA, and for AP-Tau, which displayed an overall diagnostic accuracy of 92.6%.

This study has been carried out closely with the Laboratory for Cardiovascular Theranostics, Cardiocentro Ticino Foundation, Lugano, Switzerland. In particular, Dr. Lucio Barile, Dr. Jacopo Burrello, and Ms. Sara Bolis helped us with EV characterization and flow cytometry. Biomedical engineer Alessio Burrello from the Department of Electrical, Electronic and Information Engineering “Guglielmo Marconi” (DEI), University of Bologna, Italy, supported us in developing the diagnostic models. The results of this study have been published in the journal “Biomedicines” (Doi: 10.3390/biomedicines9030230).

Methods

Subjects

A total of 16 patients, for which matched plasma and CSF samples were analyzed in the current study, made up the optimization cohort: 4 idiopathic PD, four probable MSA, and four probable AP-Tau, among which three had probable PSP, and one had possible CBD (Table 1). The plasma discovery cohort included 84 subjects (Table 2) [64]. Subjects were recruited from the movement disorder outpatient clinic at Neurocenter of Southern Switzerland in Lugano. Inclusion criteria for MSA, PSP, and CBD were based on published diagnostic criteria [79,81,82]. Each subject under-went blood sampling and clinical evaluation, and a subgroup also underwent CSF sampling. Disease gravity was assessed by H&Y [83] and MDS-UPDRS scales [26]; cognitive profile by MMSE [84] and MoCA [85]; mood disorder by BDI-II scale [86]; REM sleep Behavior Disorder by RBD screening questionnaire [87]; olfactory function by olfactory test (Burghart Messtechnik GmbH, Wedel, Germany). LEDD was calculated for PD and AP [88]. Patients were excluded from the analysis in case of significant comorbidities: diabetes, renal failure, thyroid pathology, vitamin B12 deficiency, HIV infection, syphilis, coagulopathy, fever, acute or chronic inflammatory diseases, and tumors. Finally, four subjects who underwent CSF collection in the emergency room for acute headache were included in the study as HC, after CSF analysis showed normal parameters and other pathologies were excluded. The 16 patients for which matched plasma and CSF samples were analyzed in the current study made up the optimization cohort, whereas 84 patients from our previous study [112] made up the plasma discovery cohort and were used to test basic and integrated diagnostic models.

Plasma and CSF Preparation

In total, 10 mL of blood was collected into anticoagulant-EDTA tubes after at least 4 h fasting. The following protocol was performed to obtain EV enriched plasma [113] (Fig. 1a): samples were centrifuged for 15 min at 1600× g at 10 °C, to eliminate cellular components; then, three consecutive centrifuges were performed to further purify the plasma, eliminating apoptotic bodies and larger EVs (15 min at 3000× g, 15 min at 10,000× g and 30 min at 20,000× g at 4 °C). We previously demonstrated no significant change in flowcytometric analysis by MACSPlex assay of plasma samples with and without EV enrichment by ultracentrifugation [112]. Samples were aliquoted and stored at −80 °C.

Five mL of CSF was collected into 15 mL polypropylene tubes and immediately frozen (Fig. 1a). After thawing, 500 µL of CSF samples underwent serial centrifuges as plasma samples plus further ultracentrifugation to maximize EV enrichment (18 h at 100,000× g at 4 °C). Pellets were resuspended in 30 µL of particle-free PBS. The storage period varied among samples according to the consecutive enrollment of subjects in the study, between 2015-07 and 2020-10.

Nanoparticle Tracking Analysis

Nanoparticle concentrations and diameters were measured by NanoSight LM10 (Malvern Panalytical, Malvern, UK) equipped with a 405 nm laser and Nanoparticle Tracking Analysis NTA 2.3 software (Malvern Panalytical, Malvern, UK). Only for NTA analysis, to rule out a confounding effect of ultracentrifugation on

EV amount and diameter, plasma samples (100 µL) were centrifuged akin to CSF samples for 18 h at 100,000× g at 4 °C. The obtained pellet was resuspended in 100 µL of particle-free PBS. A total of 1 µL of ultraconcentrated plasma or CSF was diluted in particle-free PBS—1:500 and 1:250, respectively. NTA analyses were performed as previously described [112].

MACSPlex Exosome Assay and Flow Cytometry Analysis

The screening approach (MACSPlex human Exosome Kit, Miltenyi, Bergisch Gladbach, Germany) was previously described [103,114] and is summarized in Fig. 1a. The complete list of the 37 EV surface markers analyzed is represented in Fig.1b. In total, 60 µL of plasma and 30 µL of ultracentrifuged CSF were added to the MACSPlex Buffer solution (final volume 120 µL) and analyzed with MACSQuant Analyzer flow cytometer (Miltenyi, Bergisch Gladbach, Germany). As a blank control, we used MACSPlex Buffer incubated with beads and detection antibodies. Median fluorescence intensity (MFI) for each EV surface marker was normalized by the mean MFI for specific EV markers (CD9, CD63, and CD81). All analyses were based on normalized MFI (nMFI) values. Samples were analyzed blind to the clinical diagnosis. Tests for the reliability/specificity of MACSPlex human Exosome Kit for EVs and the technical consistency and reproducibility of the assay were performed in our previous work [112].

Statistical Analysis

Statistics were performed using IBM SPSS Statistics 22.0 (IBM SPSS, Armonk, New York, USA), PYTHON 2.7 (Python Software Foundation, DE, USA), and GraphPad PRISM 7.0a (GraphPad Software, San Diego, CA, USA). A Kolmogorov–Smirnov test was applied to evaluate variables distribution. Non-normally distributed variables (disease duration, H&Y, MDS-UPDRS, BDI-II, MMSE, MoCA, Olfactory test, RBD, LEDD, NTA, MACSPlex analysis) were expressed as medians (interquartile range) and analyzed by Kruskal–Wallis' test. Normally distributed variables (age) were expressed as mean ± standard deviation (SD) and analyzed by 1-way ANOVA test with Bonferroni's correction for multiple comparisons. Categorical variables (sex) were expressed as absolute number and percentage (%) and analyzed by χ^2 (when applicable) or Fisher's tests. Matched measurements (plasma vs. CSF), variables were analyzed by Wilcoxon pairs signed-rank test.

4.6. Diagnostic Modelling

Supervised learning algorithms were used to combine levels of expression of single EV surface markers in a specific EV surface marker signature and discriminate patients according to clinical diagnosis. Linear discriminant analysis was used as a feature re-duction strategy to build the 3D canonical plots; canonical components were calculated from the weighted linear combination of expression levels for the 37 EV markers to maximize the separation between the four groups (HC, PD, MSA, AP-Tau); each point represents a patient and spheres include patients with a linear combination coefficient that falls within the mean of canonical components 1, 2, and 3 ± SD. The diagnostic models were built exploiting a RF classification algorithm, as previously reported [112]. Briefly, each forest is composed of 20 classification trees with a maximum number of 8 splits for each tree; the diagnosis derives from the outcome of each tree of the RF

(i.e., if at least 11 of 20 trees of the RF predict PD, the patient will be classified as PD). The basic RF models were built on the expression of 17 EV surface markers (CD29, CD45, CD19, CD42a, HLA-I, CD31, CD1x, CD11c, CD62P, CD40, CD41b, CD209, CD4, CD2, CD146, CD25, MCSP), which were demonstrated to be differentially expressed in plasma samples in HC, PD, MSA, and AP-Tau in our previous study [112].

The integrated version of RF models was built selecting only markers expressed in CSF- and plasma-derived EVs from patients with PD (8 EV markers: CD4, CD19, CD2, CD1c, HLA-I, CD41b, CD29, and CD45), MSA (10 EV markers: CD4, CD19, CD2, CD1c, HLA-I, MCSP, CD146, CD41b, CD29, and CD45), or AP-Tau (6 EV markers: CD4, CD2, CD1c, HLA-I, CD41b, and CD45). Integrated models were directly validated on the original discovery cohort. A representative classification tree was shown for each model, and a confusion matrix reported accuracy, sensitivity, specificity, positive and negative predictive values.

Results

Demographic and Clinical Characteristics

The optimization cohort included 16 patients: 4 PD, 4 MSA, 4 AP-Tau (3 PSP, 1 CBD), and 4 HC. These subjects underwent plasma and CSF collection for paired flow cytometry analysis. Clinical characteristics are summarized in Table 1. No differences were observed between groups ($p > 0.05$ for all comparisons). The plasma discovery cohort included 84 patients from our previous study [14] and was used to test both the basic and integrated diagnostic models (Table 2). In Fig. 2, a flowchart of the study is represented.

PD Group Shows an Increased Number of CSF-Derived EVs

NTA revealed higher concentration of CSF-derived nanoparticles/mL in PD compared to HC ($p = 0.048$, Fig. 3a); this difference was mainly due to larger vesicles (151–500nm; $p = 0.045$). A trend towards a higher amount of EVs was also observed in MSA and AP-Tau. Although EV diameter was 1.4/1.5-fold higher in PD and AP patients than HC, the difference was not significant (Fig. 3b).

CSF-Derived EV Immunophenotyping Stratifies Patients According to the Clinical Diagnosis

The immunophenotyping of 37 surface markers on CSF-derived EVs by MACSPlex assay did not identify statistically significant differences between the four groups when each EV marker was considered individually (Fig. 3c). However, several antigens, related to T cells (CD2, CD3, CD8, CD14, CD86), B cells (CD20), endothelial cells (CD105), and the major histocompatibility complex class I human leukocyte antigen-ABC (HLA-ABC), displayed higher expressions in PD, MSA, AP-Tau then HC. Nevertheless, the linear weighted combination of all EV markers in a single specific signature by supervised learning (linear discriminant analysis, see methods) allowed the discrimination of patients according to their diagnosis, as shown in the canonical plots (Fig. 3d,e).

Different Surface Marker Expressions

We compared the same subjects' plasma- and CSF-derived EVs in pathological groups (PD, MSA, and AP-Tau; n = 12). Plasma samples showed higher numbers of nanoparticles/ mL compared to CSF, even after

stratification for EV diameter ($p < 0.001$ for all comparisons; Fig. 4a). Moreover, CSF-derived nanoparticles were significantly larger ($p = 0.005$; Fig. 4b). We quantified MFI of tetraspanins CD9, CD63, and CD81 (specific markers of EVs) by flow cytometry as an alternative measure of EV concentration. Plasmatic samples had a higher level of CD81-MFI and of average MFI for CD9, CD63, and CD81 ($p < 0.001$) compared to CSF (Fig. 4c). Consistently, nanoparticle concentration by NTA directly correlated to mean MFI for CD9-CD63-CD81 ($R = 0.552$; $p = 0.005$). Among the 37 EV surface markers analyzed in paired plasma vs. CSF samples, five markers were differentially expressed in the PD group, 11 in MSA, and 8 in AP-Tau. All these markers were more highly expressed in plasma than CSF except for CD9 in the MSA group (Fig. 5 and 6).

The Integrated Random Forest Model Demonstrates Higher Diagnostic Accuracy

In our previous work, 17 plasmatic EV surface markers were differentially expressed in 29 idiopathic PD, nine probable MSA, ten probable AP-Tau patients, compared to 36 HC (plasma discovery cohort). A RF model (we will refer to this model as "basic" throughout the present manuscript) was built combining levels of expression of these EV markers [14]. Among the 17 EV surface markers differentially expressed in the plasma discovery cohort, we selected those also expressed in CSF (nMFI different from 0) for each diagnostic group. Eight were expressed both in plasma and CSF-derived EVs in patients with PD (CD4, CD19, CD2, CD1c, HLA-I, CD41b, CD29, and CD45), 10 in patients with MSA (CD4, CD19, CD2, CD1c, HLA-I, MCSP, CD146, CD41b, CD29, and CD45), and 6 in patients with AP-Tau (CD4, CD2, CD1c, HLA-I, CD41b, and CD45) (Fig. 7). Assuming that EV surface markers expressed both in plasma and CSF may have higher relevance for the respective neurodegenerative disease, we built an "integrated" version of our basic diagnostic model based on plasma EV expression. In particular, we built one model for each type of disease (PD, MSA, AP-Tau). Integrated versions of RF models were subsequently validated in the original plasma discovery cohort (Fig. 2).

The level 1 RF basic model[112] (built on the 17 EV surface markers differentially expressed in plasma) was applied to the discovery cohort ($n = 84$; Table 2) to differentiate subjects with neurodegenerative diseases from HC (Fig. 2). The model correctly diagnosed all patients (sensitivity 100.0%), whereas 6 of 36 HC were misclassified (specificity 83.3%). With an overall accuracy of 92.9% (Fig. 8a), 54 patients (48 patients and 6 HC) were introduced to level 2 analysis, aiming at the selective recognition of PD, MSA, or AP-Tau. The level 2 RF integrated model discriminated PD from non-PD patients (Fig. 8b) with higher sensitivity than the RF basic model (96.6% vs. 93.1%, respectively) and increased accuracy (92.6% vs. 90.7%, respectively). Similarly, the diagnostic performance was higher in the integrated version for discriminating MSA from non-MSA patients (Fig. 8c), with an accuracy of 92.6% and a sensitivity of 55.6%, while the RF basic model displayed accuracy and sensitivity of 88.9% and 33.3%. Finally, the advanced RF model discriminating AP-Tau from non-AP-Tau patients (Fig. 8d) correctly predicted 50 of 54 patients (92.6% accuracy) with increased sensitivity (70.0%) and specificity comparable to the basic model (97.7%). Overall, the integrated version of the RF model allowed an increased sensitivity in discriminating specific diseases, with higher negative predictive values for all patients.

Figures and Tables

Table 1. Clinical characteristics of the cerebrospinal fluid (CSF) optimization cohort

Variable	HC [n=4]	PD [n=4]	AP		*P*-value
			MSA [n=4]	AP-Tau [n=4]	
Age (years)	59 ± 20.3	67 ± 12.9	60 ± 4.6	66 ± 12.5	0.794
Sex (ref. male)	1 (25.0)	2 (50.0)	1 (25.0)	2 (50.0)	0.785
Disease duration (years)	-	4.0 [0.8-6.5]	3.0 [1.0-5.8]	3.5 [3.0-8.5]	0.859
H&Y	-	1.5 [1.0-2.8]	3.5 [2.3-4.8]	4.0 [2.0-4.0]	0.129
MDS-UPDRS	-	34.5 [17.0-51.3]	34.8 [26.5-34.8]	67.0 [29.0-67.0]	0.511
BDI-II	-	7.0 [2.3-14.0]	5.5 [3.5-9.0]	16.0 [11.0-16.0]	0.094
MMSE	-	30.0 [30.0-30.0]	28.0 [24.5-30.0]	24.0 [22.0-24.0]	0.051
MOCA	-	28.0 [26.3-29.8]	23.0 [16.3-29.0]	19.0 [16.0-19.0]	0.114
Olfactory test	-	6.0 [3.0-6.0]	9.0 [4.5-10.5]	7.0 [5.0-7.0]	0.722
RBD	-	7.0 [3.0-8.8]	4.0 [2.5-4.8]	2.0 [1.0-2.0]	0.139
LEDD	-	238 [100-750]	-	-	-

Clinical characteristics of HC compared to patients diagnosed with PD, MSA, AP-Tau. Variables are reported as mean ± SD, median (interquartile range), and absolute number (percentage), as appropriate.

Table 2. Characteristics of patients in plasma discovery cohort

Variable	HC [n=36]	PD [n=29]	AP		Overall *P*-value	*Pairwise Comparisons*					
			MSA [n=9]	AP-Tau [n=10]		HC vs. PD	HC vs. MSA	HC vs. AP-Tau	PD vs. MSA	PD vs. AP-Tau	MSA vs. AP-Tau
Age (years)	62 ± 8.6	67 ± 11.6	66 ± 8.7	72 ± 8.6	**0.025**	0.341	1.000	**0.027**	1.000	0.774	1.000
Sex (ref. male)	18 (50.0)	18 (62.1)	3 (33.3)	5 (50.0)	0.474	-	-	-	-	-	-
Disease duration (years)	-	4.0 [2.5-8.5]	5.0 [1.0-7.5]	3.5 [2.8-5.3]	0.682	-	-	-	-	-	-
H&Y	-	2.0 [1.0-3.0]	4.5 [3.3-5.0]	4.0 [3.0-5.0]	**<0.001**	-	-	-	**0.001**	**0.001**	1.000
MDS-UPDRS	-	24.0 [13.5-37.3]	42.0 [26.5-42.0]	47.0 [30.5-99.0]	**0.029**	-	-	-	0.568	**0.041**	1.000
BDI-II	-	5.0 [3.0-8.0]	6.0 [3.0-14.0]	15.0 [12.5-18.0]	**0.003**	-	-	-	1.000	**0.002**	0.151
MMSE	-	30.0 [29.0-30.0]	27.5 [24.3-29.8]	27.0 [22.5-28.0]	**<0.001**	-	-	-	0.061	**0.001**	0.699
MOCA	-	27.0 [23.3-29.0]	23.0 [18.0-26.0]	19.5 [14.5-22.5]	**0.006**	-	-	-	0.292	**0.008**	0.726
Olfactory test	-	7.0 [4.0-8.6]	9.0 [6.0-10.0]	7.0 [4.5-8.5]	0.305	-	-	-	-	-	-
RBD	-	3.0 [2.0-5.0]	4.0 [1.0-5.5]	2.5 [0.8-4.3]	0.678	-	-	-	-	-	-
LEDD	-	563 [180-750]	-	-	-	-	-	-	-	-	-

Clinical characteristics of patients from the plasma discovery cohort (n=84): HC are compared to patients with PD, MSA, AP-Tau. Variables are reported as mean ± SD, median [interquartile range], absolute number (percentage), as appropriate. A P<0.05 was considered significant and shown in bold.

Figure 1. Plasma and CSF preparation for MACSPlex human Exosome assay.

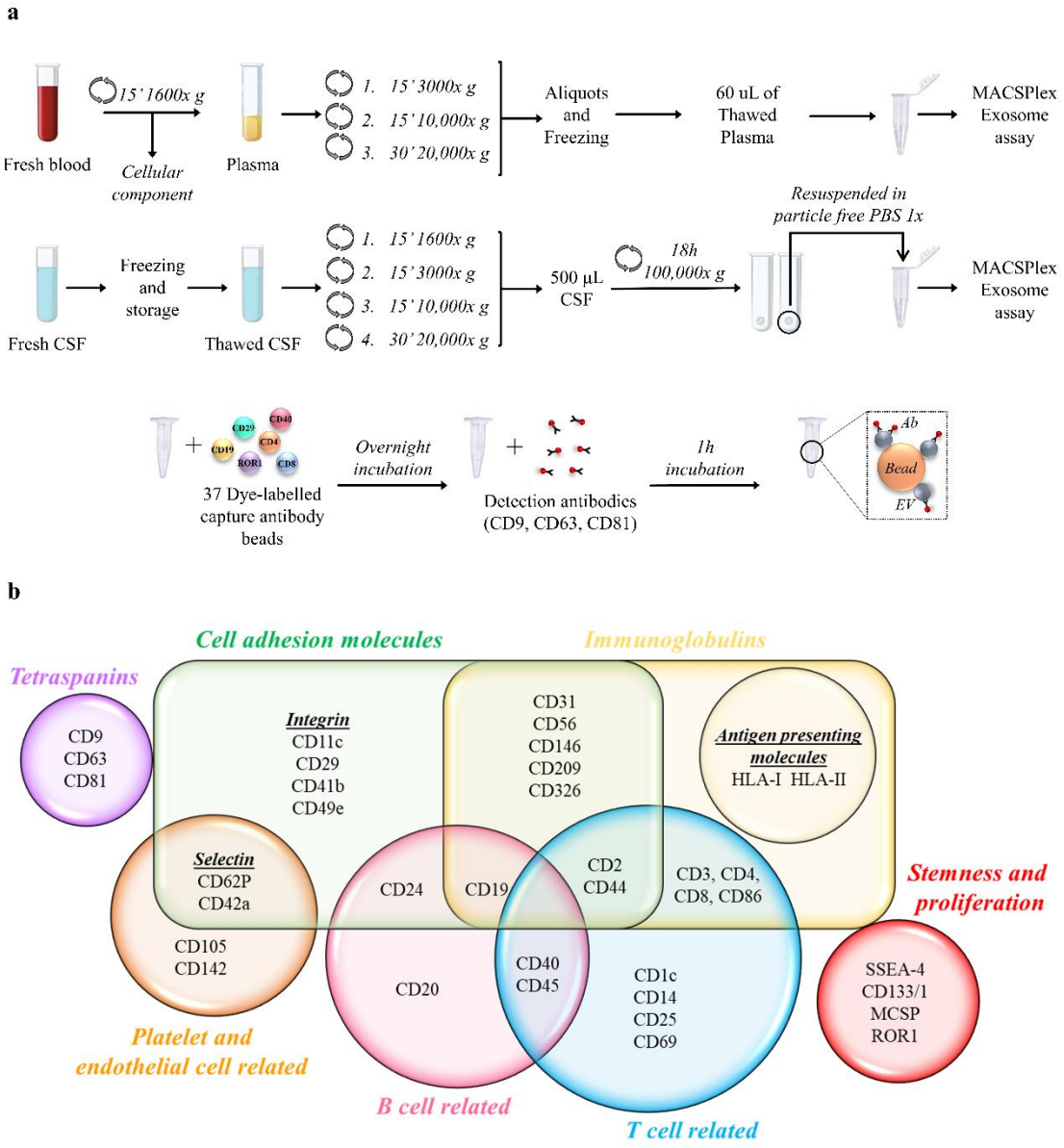

(a) Protocol EV enrichment and characterization by MACSPlex Exosome Assay. Blood and cerebrospinal fluid (CSF) underwent serial centrifugation to eliminate cellular components and larger EVs. Samples were incubated overnight with PE- and FITC-labeled capture beads, coated with antibodies against 37 different EV surface markers. APC-conjugated detection antibodies against CD9, CD63, and CD81 were added and incubated for 1 h. After washing steps, samples were analyzed by flow cytometry. (b) Schematic representation of the 37 EV surface markers analyzed by MACSPlex human Exosome assay.

Figure 2. Study flowchart

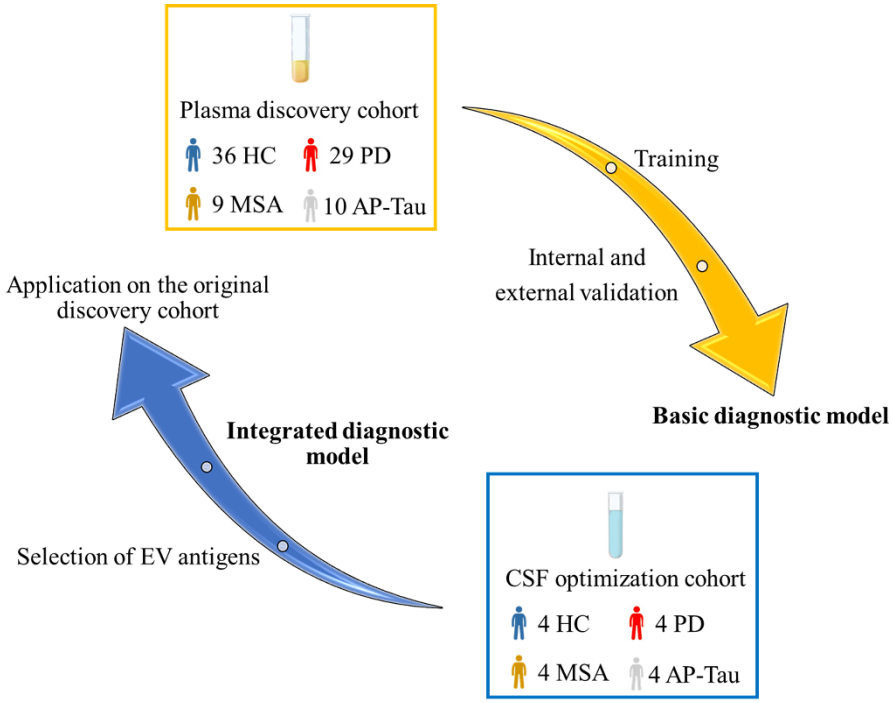

The plasma discovery cohort was used to train and validate the basic diagnostic model based on plasma-derived EV profiling. The CSF-derived EV profiling in an optimization cohort was used to generate an integrated model subsequently tested in the discovery cohort.

Figure 3. CSF-derived EVs characterization.

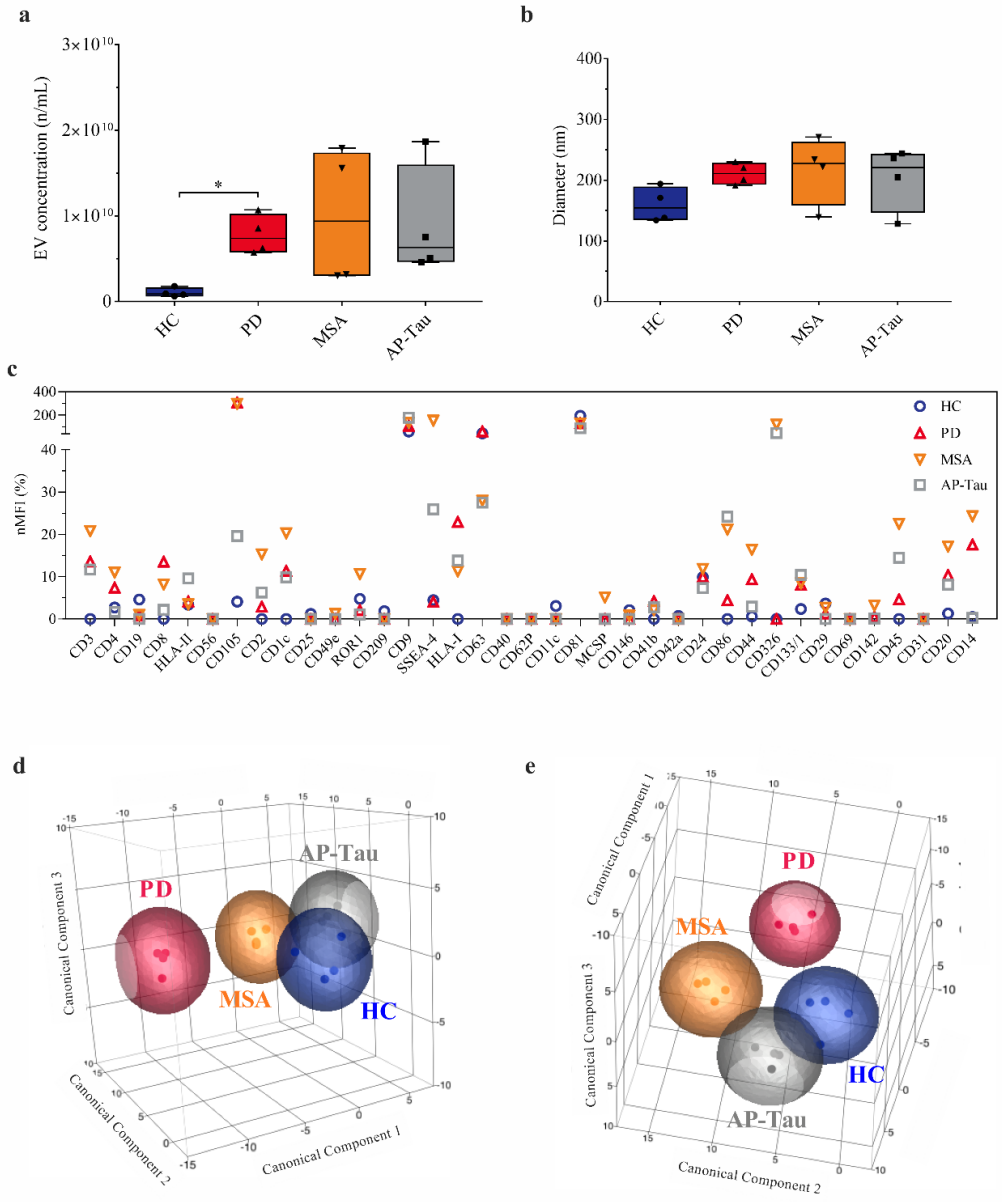

Characterization of CSF-derived EVs by NTA and MACSPlex human exosome assay flow cytometry. HC were compared with PD, MSA, or AP-Tau patients. (a) EV concentration (n/mL CSF) at NTA. (b) EV diameter (nm) at NTA. Boxplots show median and interquartile range; bars show minimum and maximum values (* $p < 0.05$). (c) Normalized median fluorescence intensity (nMFI; %) for 37 EV surface markers. (d–e) Different perspectives of 3D-canonical plot reporting patient discrimination according to EV surface marker expression (each patient is indicated by a point, and diagnoses are represented by colors: HC, blue; PD, red; MSA, orange; AP-Tau, grey). Canonical axes of the plot (canonical components 1, 2, and 3) are defined by linear discrimination analysis from weighted linear combinations of the 37 EV markers analyzed by flow cytometry. Spheres include patients with linear combination coefficients that fall within the mean ± SD (canonicals 1, 2, and 3 ± SD).

Figure 4. EV quantitative analysis: plasma vs. CSF.

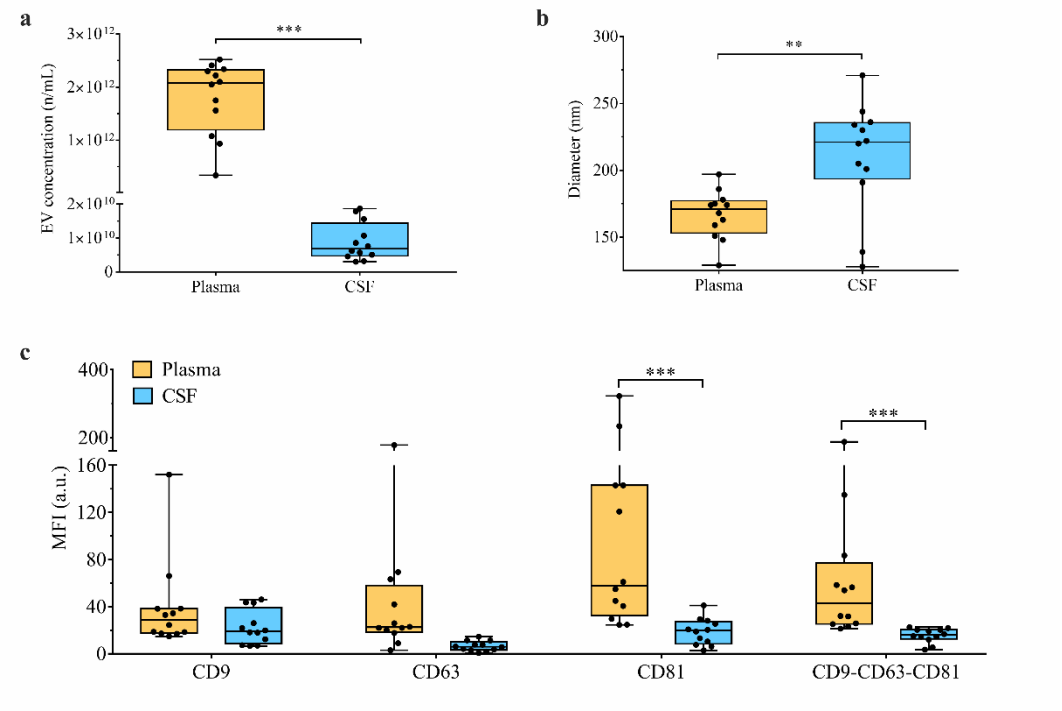

Quantitative analysis of EVs by nanoparticle tracking analysis and MACSPlex assay flow cytometry; plasma samples were compared to paired CSF samples in patients with PD (n = 4), MSA (n = 4) and AP-Tau (n = 4). (a) EV concentration (n/mL plasma or CSF) at NTA. (b) EV diameter (nm) at NTA. (c) MFI (expressed as arbitrary unity; a.u.) for CD9, CD63, CD81 and CD9-CD63-CD81 at flow cytometry. Boxplots show median and interquartile range; bars show minimum and maximum values (**$p < 0.05$; *** $p < 0.001$).

Figure 5. EV surface markers expression in plasma and CSF

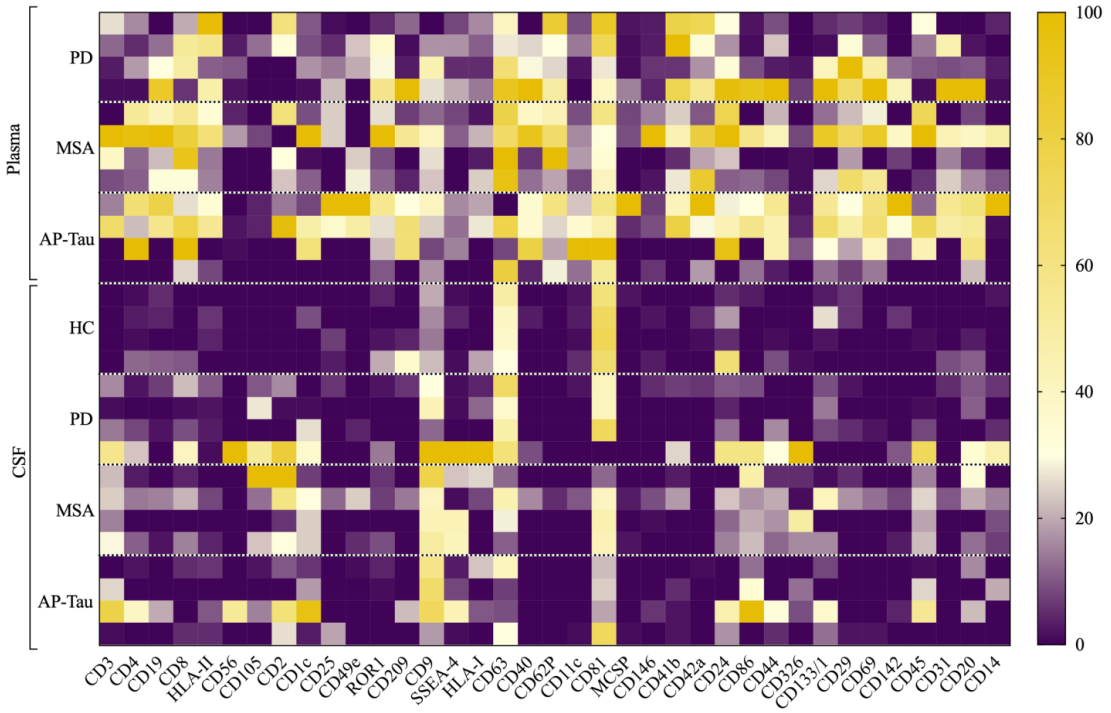

Stratification of patients for diagnosis and expression of EV-surface antigens in plasma and CSF. The heat map shows normalized median fluorescence intensity (purple = low nMFI; yellow = high nMFI) for the 28 analyzed samples: 12 plasma samples from patients with PD, MSA, and AP-Tau (n=4 per group) were compared to the respective CSF sample, plus 4 CSF samples from HC.

Figure 6. Evaluation of EV surface antigens in pathological groups

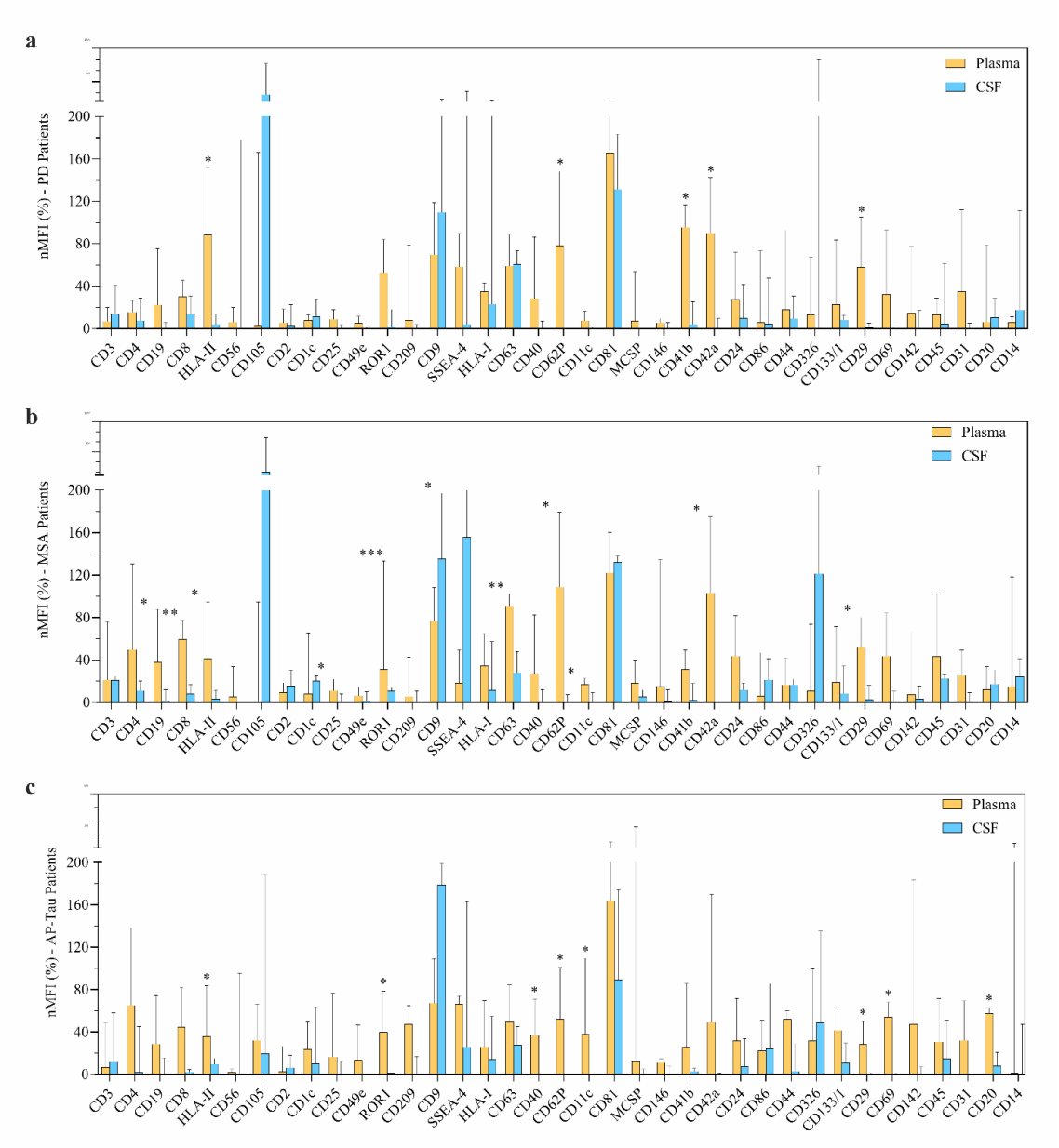

The expression of 37 EV surface antigens was assessed by flow cytometry and expressed as normalized median fluorescence intensity (nMFI; %); 12 plasma samples (yellow; n=4 per group) from patients with PD (a), MSA (b), and AP-Tau (c) were compared to the respective CSF (light blue) samples. Bars show median and inter-quartile range (*P<0.05; **P<0.01; **P<0.001).

Figure 7. EV surface marker selection.

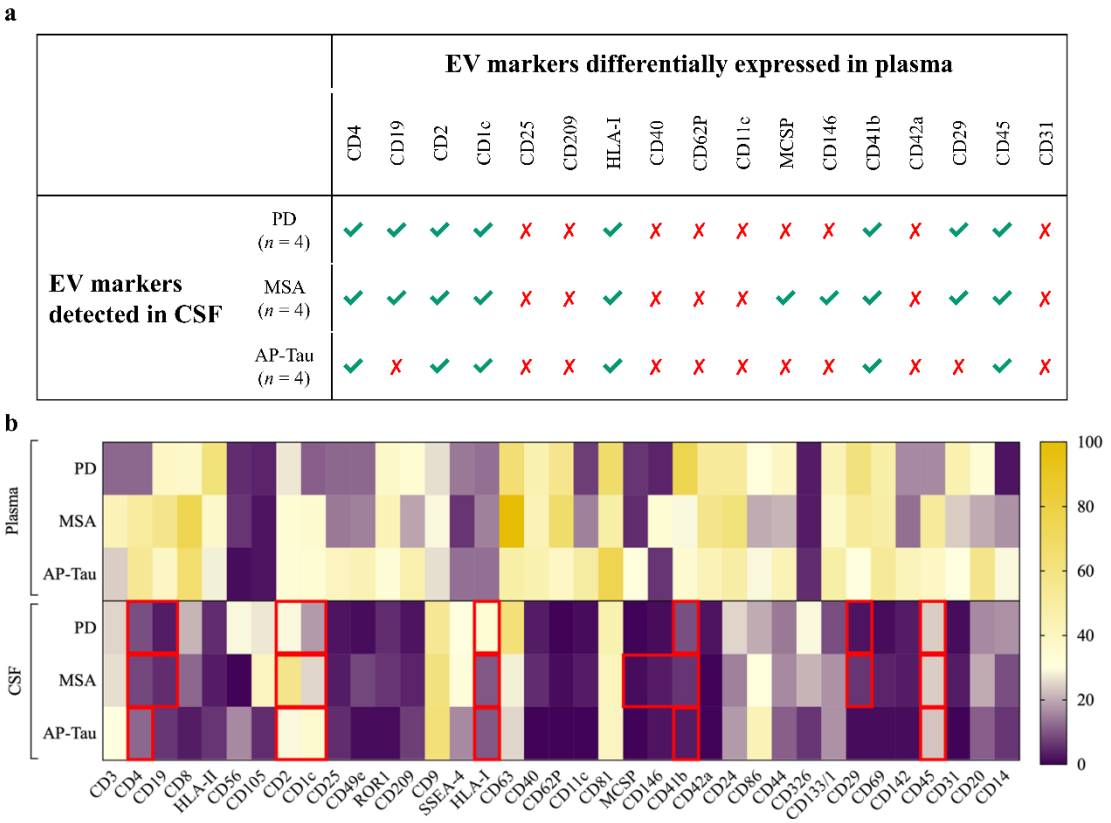

Selection of EV surface markers for the 2-level random forest diagnostic model: (a) EV surface markers differentially expressed in plasma and detected in CSF of PD, MSA, or AP-Tau. (b) Heatmap representation of the 37 EV surface markers in plasma and CSF of matched subjects with PD, MSA, and AP-Tau. The selected markers in each diagnostic category were highlighted with red boxes.

Figure 6. Diagnostic modeling.

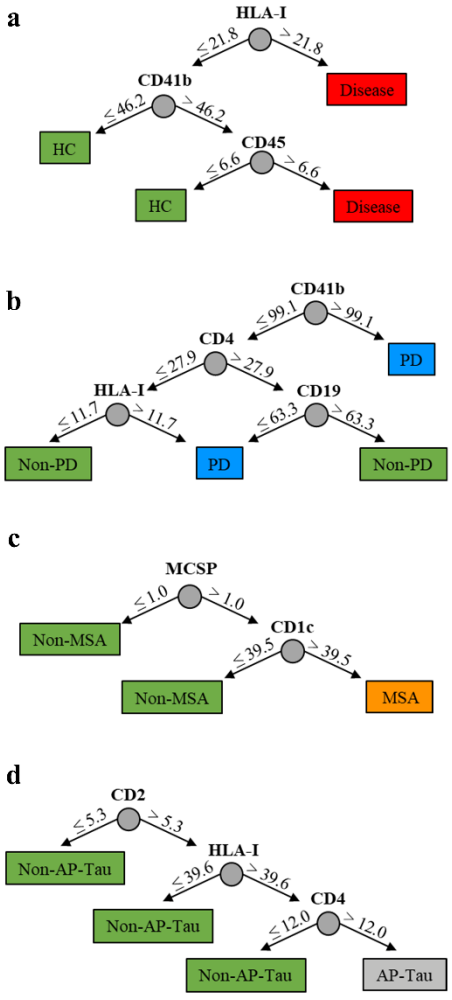

Basic		PREDICTED	
		Disease	HC
REAL	Disease	48	0
	HC	6	30
Model Accuracy			92.9%
Sensitivity			100.0%
Specificity			83.3%
Positive Predictive Value			88.9%
Negative Predictive Value			100.0%

Level 1
(Disease *vs* . HC)

Level 2
(PD vs. Non-PD;
MSA vs. Non-MSA;
AP-Tau vs. Non-AP-Tau)

Basic		PREDICTED	
		PD	Non-PD
REAL	PD	27	2
	Non-PD	3	22
Model Accuracy			90.7%
Sensitivity			93.1%
Specificity			88.0%
Positive Predictive Value			90.0%
Negative Predictive Value			91.7%

Integrated		PREDICTED	
		PD	Non-PD
REAL	PD	28	1
	Non-PD	3	22
Model Accuracy			92.6%
Sensitivity			96.6%
Specificity			88.0%
Positive Predictive Value			90.3%
Negative Predictive Value			95.7%

Basic		PREDICTED	
		MSA	Non-MSA
REAL	MSA	3	6
	Non-MSA	0	45
Model Accuracy			88.9%
Sensitivity			33.3%
Specificity			100.0%
Positive Predictive Value			100.0%
Negative Predictive Value			88.2%

Integrated		PREDICTED	
		MSA	Non-MSA
REAL	MSA	5	4
	Non-MSA	0	45
Model Accuracy			92.6%
Sensitivity			55.6%
Specificity			100.0%
Positive Predictive Value			100.0%
Negative Predictive Value			91.8%

Basic		PREDICTED	
		AP-Tau	Non-AP-Tau
REAL	AP-Tau	5	5
	Non-AP-Tau	0	44
Model Accuracy			90.7%
Sensitivity			50.0%
Specificity			100.0%
Positive Predictive Value			100.0%
Negative Predictive Value			89.8%

Integrated		PREDICTED	
		AP-Tau	Non-AP-Tau
REAL	AP-Tau	7	3
	Non-AP-Tau	1	43
Model Accuracy			92.6%
Sensitivity			70.0%
Specificity			97.7%
Positive Predictive Value			87.5%
Negative Predictive Value			93.5%

Development of a 2-level integrated RF model to discriminate patients with PD, MSA, or AP-Tau in the plasma discovery cohort (n = 84). (a) Level 1 of RF model, discriminating subjects with neurodegenerative diseases from HC. Patients classified as "disease" at level 1 were introduced to level 2. (b) Two-level RF model, discriminating PD from non-PD patients. (c) Two-level RF model, discriminating MSA from non-MSA patients. (d) Two-level RF model, discriminating AP-Tau from non-AP-Tau patients. A confusion matrix (basic vs. integrated version) and a representative classification tree are shown for each RF model. In bold marks are represented the numbers of correctly predicted diagnoses and the overall accuracy of the model.

7. Discussion

The first part of this thesis investigated the diagnostic potential of aggregated and oligomeric αSyn in skin biopsies taken from different anatomic areas. We found that these two pathological forms of the protein have a higher expression in patients with PD and AP-Syn, namely in MSA, compared to HC and AP-Tau, and yield a high diagnostic performance for PD.

Since most of the previous works on skin biopsy in PD focused on detection of P-αSyn [115], we began by evaluating P-αSyn in our cohort of patients and found that P-αSyn was detected mainly in dermal nerve fascicles innervating autonomic structures (SG, MAP, and arterioles) and was significantly more expressed in the PD group than in the others.

In parallel to P-αSyn, we evaluated by immunofluorescence other disease-associated αSyn forms, particularly oligomers and small aggregates. The reasons are mainly two: 1) phosphorylation is a physiological cellular process for protein function regulations, and higher phosphorylation at Serine 129 could be the response to a generic stress cellular stress or insult [19,78], thus the identification of more specific pathological form of αSyn could lead to the development of a diagnostic tool with higher sensitivity and specificity; 2) oligomers and small aggregates are supposedly involved at early phases of pathology, preceding the formation of insoluble aggregates in the brain, while P-αSyn could be a later event in disease progression [116], thus the study of early αSyn pathological species could help in the diagnosis of early PD.

We first evaluated aggregated αSyn with 5G4 antibody, which binds with higher affinity aggregates than monomers of αSyn, and then we targeted specifically αSyn oligomers with PLA technique. As for P-αSyn, both were detected primarily in autonomic fibers and expressed mainly in PD and MSA subjects. For PD diagnosis, αSyn-5G4 and αSyn-PLA resulted as sensitive and specific as P-αSyn; indeed, the comparative analysis of the diagnostic performance of P-αSyn vs. αSyn-5G4 and vs. αSyn-PLA showed similar AUCs. However, in discriminating PD from HC and AP-Tau, αSyn-PLA displayed the best accuracy, especially considering both locations or the cervical site alone. P-αSyn and 5G4, possible markers of later stages, were the only ones able to discriminate the groups at the ankle site. Thus, the choice of pathological αSyn marker and skin biopsy site influences the diagnostic performance and can help better understand the temporal dynamics of αSyn seeding and spreading in the peripheral nervous system in the course of the disease. In addition, the information that the immunofluorescence of αSyn-5G4 and αSyn-PLA for cervical site only is just as effective in PD diagnosis as the immunofluorescence of both anatomical sites is an important finding for simplifying the procedure of sampling skin biopsies toward an effective and less invasive biomarker search. Moreover, the higher sensitivity of αSyn-5G4 and αSyn-PLA vs. P-αSyn in cervical skin biopsies, if replicated in other studies, especially in early and premotor PD, may represent an essential step toward the detection of an early biomarker of PD disease.

Of note, in our analysis, αSyn-PLA was the only technique yielding discrimination between MSA and HC. These are remarkable results for αSyn-PLA considering that a very recent study has shown that P-

αSyn detection in the skin has a higher diagnostic accuracy for synucleinopathies than real-time quaking-induced conversion (RT-QuIC) in the skin, a sensible and accurate technology to measure prion-like self-aggregation of pathological αSyn [117]. However, limitations of our analysis are that we focused on patients with well-established clinical diagnoses and long disease duration to avoid confounding data in cases of uncertain diagnosis, particularly in the early phases. Furtherly, the results may be partially influenced by methodological issues since αSyn-PLA signal was analyzed by confocal microscopy while P-αSyn and αSyn-5G4 were analyzed by fluorescence microscopy so that a better resolution was guaranteed in the first condition.

PD and MSA are challenging to distinguish by skin biopsy. In the brain, larger αSyn cytoplasmatic inclusions are mainly detected in PD neurons and MSA glial cells. Nevertheless, in MSA patients, oligomers/small aggregates were also seen in neurons as well as in oligodendrocytes by PLA[94]. In line with these observations, we found overexpression of αSyn oligomers in peripheral nerves of both groups. In PD, pathological proteins were mainly at the cervical site, in MSA at ankle; this is in line with previous observations of a distal-to-proximal gradient of αSyn aggregates in MSA [118], possibly consequent of a different spreading of αSyn oligomers, or because different αSyn strains have been postulated in MSA versus PD [119]. In MSA, we also observed larger colocalization areas of PLA signal within nerves than in PD, suggesting a larger amount of oligomeric αSyn. Despite these differences, we could not discriminate the two groups based only on a single marker detection in skin biopsy. In MSA, we found pathological αSyn, especially in autonomic fibers, although the distribution of P-αSyn in autonomic or somatosensory nerve fibers in this group is debated in the literature, and some authors have shown a predominance of P-αSyn in somatosensory nerve fibers instead of autonomic ones [74]. However, while αSyn oligomers are small aggregates preceding the formation of fibrils in the early stages of pathology, P-αSyn accumulates in Lewy bodies, and yet it is still debated whether phosphorylation at Serine 129 enhances or suppresses αSyn aggregation and toxicity [120], as this could be a later event in disease progression. Thus, αSyn-PLA and P-αSyn are probably markers of different stages of the disease. A recent study focused on αSyn content in MAP found that patients with Lewy-body neurogenic orthostatic hypotension displayed higher content of αSyn in sympathetic noradrenergic nerves than MSA [121]. Thus, skin biopsy analysis can distinguish between PD and MSA by selecting multiple protein targets and anatomical sites.

Even if to a significantly lesser extent, P- αSyn, αSyn-5G4, and αSyn-PLA were found in HC, mainly at ankle site, within nerves and never associated with degenerated axons. From a biological point of view, this result is not completely surprising. Indeed, the presence of incidental αSyn pathology has been detected in brain autopsies of 10-20% of subjects > 70 years, without neurological diseases [122]. Roberts et al. described a diffuse kind of αSyn-PLA signal in HC too, mainly located in the neuropil around neurons and less frequently in the white matter of brain areas usually affected by PD pathology [93]. The neuropil is primarily composed of unmyelinated axons, dendrites, and synapsis, which are very similar to the composition of small fiber nerves, either unmyelinated C fiber or small myelinated Aδ, present in the skin. Indeed, aggregates of αSyn, are preferentially formed in projection neurons with very long,

thin unmyelinated axons, which are more susceptible to axonal transport deficit, energetic/metabolic stress, mitochondrial failure, and lack the trophic support of glial cells [123]. Aggregated αSyn has been observed in the gastrointestinal mucosa of HC [95,124], and also Mazzetti et al. detected a non-significant quote of αSyn oligomers in autonomic nerves of HC [58]. Thus, pathological αSyn oligomers in HC may represent aberrant oligomerization of αSyn at the synapses or/and axonal transport of pathological species as a very early subclinical event that may become more relevant with aging and/or external toxic events in a susceptible population. However, our study cohort comprises established PD with a long disease duration, and more extensive studies, including prodromal phases of disease using αSyn-PLA technology in skin biopsies, are warranted.

Furthermore, in both studies on skin biopsy, we confirmed the presence of a small fiber neuropathy in PD and MSA that is not related to levodopa therapy or vitamin B12 deficiency, and it is very likely secondary to the neurodegeneration process. In the first study, we documented significant cutaneous denervation in the PD group at the cervical site, associated with the advance of the disease and independent by αSyn deposits, suggesting cervical denervation as a potential biomarker of neurodegeneration and disease progression. In the second, we showed that denervation progresses significantly with disease duration even in a relatively short period (two years), while no significant changes in clinical scales or pathological αSyn amounts were detectable in this study. Furthermore, we demonstrated that a lower ankle IENFD at T0 was associated with a progression of motor impairment at the MDS-UPDRS-III scale and that a lower cervical IENFD was associated with a progression of cognitive decline at MMSE, independently from age and LEDD. These findings confirm brain pathology studies showing that clinical symptoms in PD align with neuronal degeneration rather than with the αSyn aggregation burden [125]. Thus, the relevance of IENFD as a progression marker in PD is worthy of further investigations in more extensive studies because if the clinical significance of IENFD changes is confirmed, skin denervation could be considered as a proxy measure of neurodegenerative events occurring in the brain and possibly an ancillary biomarker in clinical trials. Moreover, the measure of IENFD by skin biopsy bears the advantage of being easily and rapidly performed at low cost and being extensively studied and standardized in the last twenty years to diagnose small fiber neuropathy [90,91]. Nevertheless, a significant limitation of our studies is that the most severely affected patients of the cohort were lost at follow-up, thus potentially limiting the ability to evaluate more aggressive forms of the disease with a high rate of progression.

However, it remains interesting to understand if there is a link between the accumulation of pathological αSyn and cutaneous nerve fibers degeneration. It has been shown that αSyn preferentially aggregates in neurons with long, hyper branching, thin, and unmyelinated axons, such as the axons of the nigrostriatal projection, the cardiac sympathetic system, the vagal intestinal autonomic system [14,78,123], and the skin. Orimo et al. [14] showed that αSyn deposits in cardiac sympathetic distal axons precede neuronal cell accumulation and heralds centripetal axonal degeneration. Since we measured intraepidermal somatic sensory axons density while aggregated αSyn were found mainly in autonomic nerve structures, quantifying autonomic nerves is mandatory to verify this theory in the skin.

Moreover, we saw robust denervation in PD patients at all skin sites, but especially at the neck, with a proximal-to-distal gradient, the opposite of what is classically observed in dying-back, length-dependent peripheral neuropathy. This supports a possible centrifugal spread of neurodegeneration from the cell bodies toward the periphery.

Regarding the spreading of the pathological protein, studies on the diffusion of misfolded αSyn in animal models have shown the spreading from the peripheral gastrointestinal system through the vagus nerve by retrograde axonal transport to the medulla oblongata [78]. A multi-hit hypothesis has been proposed suggesting that αSyn deposition is not monofocally initiated but may be induced by multiple independent factors (e.g., infective agents or viruses) outside the central nervous system through the nasal cavity or the digestive tract [78]. In addition, more recently, to better explain the considerable heterogeneity within PD, Borghammer et al. hypothesized the classification of PD subjects into PNS-first and CNS-first subtypes [45]. These two subtypes show differential clinical features at the beginning of the disease: PNS-first patients are RBD-positive with a marked autonomic disfunction, while the CNS-first are RBD-negative with mainly dopaminergic dysfunction. This could be related to the initial αSyn deposit: in the PNS and enteric nervous system or the brainstem and limbic system, respectively.

Of note, we observed that epidermal denervation was more severe in women with synucleinopathies. These data are consistent with the evidence of sex differences in the prevalence, clinical course, and motor and cognitive manifestations of PD [126]. In addition, it is known that gender influences epidermal nerve fibers density in healthy subjects [92], and females are more prone to develop idiopathic small fiber neuropathy [127]. Thus, even if these results are hard to explain in the light of current knowledge, they highlight the need to take account of sex in the design of clinical trials and biomarkers search studies.

Finally, a compound marker based on all three markers for pathological αSyn (αSyn-PLA, αSyn-5G4, P-αSyn) and IENFD was able to stratify patients with high accuracy according to the diagnosis and discriminate between PD and MSA (84.6%), which is a significant challenge in clinical practice. Therefore, this first part of the thesis highlights how skin biopsy represents a minimally invasive, easily accessible, and repeatable source of biomarkers for PD in vivo. Multiple target epitopes of proteins involved in the disease's pathogenesis are detectable. It allows the quantification of small fiber neuropathy through IENFD, which represents a promising prognostic marker. A thorough evaluation of multiple markers bearing complementary information and small-fiber pathology by skin biopsy is advisable for diagnosing PD in routine clinical practice and for the future development of more adequate biomarkers as surrogate endpoints in pharmacological clinical trials for PD.

In the second part of this thesis, we characterized plasma- and CSF-derived EV subpopulations and set up a diagnostic model for the stratification of PD and AP patients. To develop a non-invasive diagnostic tool, we started our study analyzing plasma samples. We first demonstrated that plasma EV concentration was higher in PD patients compared to other groups. Previous reports have shown that

the total number and size of EVs were not augmented in PD serum [128], while a more recent study demonstrated an increased number of plasmatic brain-derived EVs in PD [129]. For sure, methodological factors such as isolation/extraction and quantification of EVs explain these differences. However, at the molecular level, it is recognized that the endosome/lysosomes pathway is a common defective pathway in sporadic and genetic PD [130], and EVs are generated and secreted by the endosomal compartment called multivesicular bodies by fusion with the plasma membrane. Thus, the process of EV secretion may be enhanced when there is an inhibition of fusion of multivesicular bodies with lysosomes, as expected in PD [131] so that increased production of EVs in PD is likely. No differences were instead observed in the diameter.

Usually, most EVs in blood arise from platelets and erythrocytes; however, leucocytes, endothelial cells, monocytes, neutrophils, and lymphocytes may release EVs [132]. The flow cytometry analysis demonstrated that 16 and 12 EV markers partly related to immune cells were upregulated in PD and MSA, only 4 in AP-Tau compared to HC. In particular, PD and MSA shared 11 EV-surface markers. Considering functions and roles of EV-surface markers analyzed in this study, this result favors the hypothesis of a major, or at least different, immune dysregulation in PD and MSA *vs*. AP-Tau. Despite sharing several overlapping clinical features, synucleinopathies and tauopathies are distinguished by distinctive neuropathological hallmarks: deposits of aggregated αSyn in neurons and glial cells in the former group and neurofibrillary tangles of Tau in the latter as shown by immunohistological studies [19]. Although inflammatory features have been described in patients with synucleinopathies and tauopathies by PET studies [133-135], the activated pathways are probably different. Animal studies have shown that the neurotoxic effects of beta-amyloid aggregates in a model of tauopathy (Alzheimer's disease) are mediated via Toll-like receptor 4-dependent glial cell activation, while αSyn aggregates in a model of PD, activated Toll-like receptor 2 independently from Toll-like receptor 4 [133,135]. Moreover, a recent multicenter study has shown higher levels of CSF inflammatory biomarkers in PD with dementia and MSA compared with controls and not in AP-Tau vs. HC, plus those markers correlated with motor and cognitive impairment [134]. Likewise, our analysis showed a moderate correlation between CD25, CD146 and cognitive impairment in PD suggesting a link between inflammation and a major cognitive decline: CD25 is a co-stimulatory molecule supporting immune cells activation [136], and CD146 acts as an essential regulator of pericyte–endothelial cell communication in blood–brain barrier and it has been identified as a potential key therapeutic target for cerebrovascular disorders [137]. In MSA the concentration of EVs measured by NTA and flow cytometry analysis correlated with disease duration and cognitive impairment. These findings favor the hypothesis of the perpetuation of toxic effects by circulating EVs due to chronic immune activation, even if a compensatory/neuroprotective role of EVs in response to the progressive neurodegeneration cannot be excluded.

Among EV-markers differentially expressed in PD, CD146 and MCSP (Melanoma-associated Chondroitin Sulfate Proteoglycan) are of interest because they have been associated with melanoma and used to detect circulating tumor cells [138]. Consistently, many epidemiological studies have

supported a link between PD and melanoma, showing that PD patients have a higher incidence of this tumor, even if the underlying pathogenic mechanisms are unknown [139].

The network analysis of potential interactors of EV-surface markers demonstrated that functional pathways and network hubs in PD and MSA were coincident and different from AP-Tau. Interestingly among hubs shared by PD and MSA, we found SP1, a transcription factor playing a pivotal role in regulating neuroinflammation in multiple sclerosis [140]. The most represented KEGG pathways were immune system, signal transduction, signaling molecules and folding, sorting, and degradation in alpha-synucleinopathies, while the FoxO signaling pathway and some pathways of the endocrine system were higher in AP-Tau, matching with the relationship that many authors have found between endocrine signaling, tauopathies and FoxO [141,142]. However, this exploratory network analysis should be interpreted with caution: AP-Tau had less differentially expressed EV-markers, consequently, the smaller network was a limiting factor in recovering potential pathways and functions in tauopathies. Anyhow, among the identified hubs, it has been encouraging to find some of them described in the literature: cytoplasmic protein NCK2 was recently described as a PD-associated gene [141]. Tyrosine-protein kinase Lyn (LYN), a specific hub of MSA, was related to enhanced microglial migration by αSyn [92]. Of note, the signal transducer and activator of transcription 3 (STAT3), a specific hub of AP-Tau, have been found to be a direct target of C3 and C3a receptor signaling, which functionally mediates Tau pathogenesis [116]. However, these network analyses are hypothetical, and further validation studies are required to assess their possible roles in causing PD and AP.

Finally, we systematically evaluated the diagnostic performance of differentially expressed EV-antigens, and a diagnostic model was built using supervised machine learning algorithms. The model showed an overall reliable accuracy, correctly predicting patient diagnosis, with the best performance for diagnosing PD (97.8%) and MSA (100%) *vs*. HC. These results were supported by ROC curve analysis on the compound marker, originating from the linear combination of all the differentially expressed EV markers, showing very high sensitivity and specificity for PD and MSA (AUC=0.908 and 0.974 respectively). Previous works have explored the utility of EVs as biomarkers for PD by quantifying brain-derived exosomes (AUC=0.75-0.82) [129] or by measuring specific target proteins like αSyn or DJ-1 in plasma neuronal-derived exosomes (AUC=0.654, 0.724) [143]. This is, to our knowledge, the first analysis of multiple immune surface markers of circulating EVs in PD and AP showing a higher diagnostic performance than previous studies, likely due to the advantage of simultaneously profiling several EVs subpopulations.

Despite this encouraging result obtained, to increase the sensitivity and specificity of our model for neurodegenerative diseases, we decided to analyze matched samples of CSF and plasma in a subgroup of patients. Indeed, only a small percentage of plasmatic EVs have a neuronal origin and a link with the pathology, while CSF-derived EVs are mainly produced by CNS cells. CSF is less accessible and more invasive to be obtained compared to plasma, thus based on the availability of our biological database, we decided to conduct a sub-analyze in CSF-derived EVs on a small number of patients and then recalibrate the previous diagnostic model on EV surface markers simultaneously expressed both in

plasma and CSF in each diagnostic group. We assumed that these EV surface markers might have higher relevance for the respective neurodegenerative disease, to improve a diagnostic system that remains based on EV profiling in plasma. In particular, we built a two-level integrated diagnostic model for PD, MSA, and AP-Tau, that displayed an overall diagnostic accuracy of 92.6%.

PD patients showed higher EVs in CSF than HC, as demonstrated in plasma [112]. In analogy, MSA and AP-Tau tended to have higher EV numbers and diameters than HC, but this was not statistically significant, probably due to the low sample size. This result is in line with other observations in patients with Alzheimer's disease where the amount of EVs in CSF correlated to myelin damage and neuronal loss [144] and in a mouse model of multiple sclerosis in which EVs correlated with brain inflammation, suggesting a pathological role of EVs [145]. Notably, we observed an increase in EVs in neurodegenerative diseases, typical of elderly populations, while in physiological conditions, the number of CSF-EVs tends to decrease[146]. Several human and animal studies have shown that a relevant inflammatory component characterizes neurodegenerative disorders. PD patients, for example, display neuroinflammatory changes in brain histopathology and elevated immune markers in peripheral blood [101,102], and inflammation has been correlated to the reduction in tyrosine hydroxylase dopaminergic neurons [147] and the expansion of activated microglia in the substantia nigra in animal models of the disease [148]. In an in vitro study, microglial cells activated by proinflammatory stimuli release more microvesicles than exosomes [149]; thus, the higher amount of EVs observed in CSF of PD could be related to the inflammatory component.

Patients with PD, MSA, and AP-Tau showed a tendency towards larger EVs in the CSF compared to HC, and in matched CSF and plasma samples of the same patients, CSF-derived EVs showed larger EVs compared to the plasmatic one. Thus, it could be conceivable that in disease groups, there is a different pathway of vesicle generation towards the production of microvesicles (50–1000 nm diameters), generated via outward budding of the plasma membrane, rather than exosomes (40–120 nm) produced in multivesicular bodies via endosomal pathway [62]. Indeed, recent observations suggest that microvesicles may have a role in inflammatory diseases [150], and it has been proposed that they act as a bridge between inflammation and neurodegeneration [151]. An in-depth EV characterization, with different methodologies and particular regard to markers differentially expressed by microvesicles and exosomes, is required to confirm this observation [150].

Regarding the EV immune profiling by MACSPlex human exosome assay applied to CSF-derived EVs, no statistically significant differences were observed in the 37 surface markers between groups. This is undoubtedly due to the main limitation of this explorative study: the low number of subjects analyzed in each diagnostic category. However, the simultaneous quantification of multiple EV markers increased the power of the assay and displayed different EV profiles of expression in subjects with PD and AP vs. HC, which allowed good discrimination of patients in accordance with the clinical diagnosis by linear discriminant analysis. Of interest, PD and AP patients expressed higher amounts of HLA-I, CD8, CD2, CD3, CD14, and CD20 in CSF, while no or shallow detection was observed in HC, suggesting a CNS activation of the immune system, in particular of the T cell-mediated immunity with specific

emphasis on intracellular endogenous synthesized antigens that involves the activation of HLA class I [152,153] and are presented to CD8 T cells [154]. Indeed, recent work on human substantia nigra demonstrated that CD8 T cell infiltration is an early pathogenic event and parallels the progression of neuronal loss and αSyn aggregation in PD [155]. This is particularly relevant in diseases pathologically characterized by intracellular accumulation of misfolded proteins and confirms the crucial role of EVs in antigen-presenting immunity by spreading HLA proteins, possibly increasing the number of dendritic cells or phagocytes presenting them or directly interacting with T cells [65].

CD105 is highly expressed in CSF of PD and MSA. Even if it is used as an endothelial cell marker during angiogenesis [156], it was initially described as a marker for activated macrophages and can identify subtypes of activated microglia [157]. In fact, in the substantia nigra of PD subjects, intense CD105 staining in microglia cells was described in association with degenerating dopaminergic neurons [158]. Microglia activation is also supported by the expression of CD86 in AP-Tau and MSA, whose upregulation had consistently been associated with activated microglia [159], and to a lesser extent in neurons [160] and astrocytes [161], during inflammatory processes.

Finally, the main result of this study is the optimization of the diagnostic model for PD, MSA, and AP-Tau based on immunophenotyping of plasma-derived EVs by integrating data from CSF-derived EVs via machine learning algorithms. Our previous basic diagnostic model [112], built on 17 EV surface markers differentially expressed in plasma between groups, correctly predicted patient diagnosis in 88.9% of subjects. The new optimized two-level RF integrated diagnostic model displayed an overall improved diagnostic accuracy of 92.6%, with increased sensitivity for all three diagnostic categories concerning the basic RF model. This result is even more relevant, considering the low numbers of subjects analyzed in this pilot study, and opens up the possibility of further improving the model's accuracy by applying this strategy to larger study groups. Indeed, CSF bears the obvious advantages of being more specific for the CNS environment, but at the same time, the collecting procedure is more invasive for patients, and the protocol to enrich for EVs is more challenging. Thus, our strategy to recalibrate the model on EV surface markers expressed both in plasma and CSF in each diagnostic group allowed us to improve the diagnostic system that remains based on EV profiling in plasma. This is a novel approach to blood biomarkers by profiling EV surface markers related to inflammatory and immune cells with potential roles in inflammation associated with neurodegeneration, while most of the current studies on EVs as biomarkers are focused mainly on evaluating target proteins in neuronal-derived exosomes [71,162]. Further, the multiplexed profiling of inflammation markers allows a more personalized approach, as this biomarker-driven phenotyping might be capable of capturing the clinical heterogeneity of PD and may be used to measure the effect of potential disease-modifying drugs on peripheral inflammatory processes as a proxy for central events. Nevertheless, the direct application of EV immunocapturing and multiarray analysis by flow cytometry to biological fluids (without isolation steps by ultracentrifugation or size exclusion chromatography) has clinical relevance, as it can be achieved in hospital-based diagnostic laboratories. Given its low cost, speed, simplicity, and high sensitivity and specificity, this approach provides a potential biochemical index to support the clinical assessment of

PD and AP. Circulating plasma-derived EVs represent an even more promising tool in characterizing, monitoring, and predicting PD, avoiding time-consuming protocols and sophisticated instrumentation. As for skin biopsy, the main limitations of these two studies on EVs are: 1) the low number of subjects, especially in AP groups; 2) the inclusion of patients only with long duration of disease; 3) the lack of post-mortem diagnostic confirmation of brain histopathologic analysis. Therefore, more extensive studies, including different cohorts of patients, especially at the early stages of the disease, and the possibility to follow the patients over the years are strongly recommended. Moreover, a customized panel of EV-surface proteins, including CNS and microglia markers, would probably increase the diagnostic model.

In conclusion, in this second part of the thesis, we systematically characterized circulating EVs in plasma of patients with PD or AP. Several EV-surface antigens were differentially expressed and correlated to disease gravity and cognitive impairment, suggesting EVs as potential biomarkers of disease, also in clinical trials for disease-modifying drugs. To improve the model, we integrated information provided by CSF. To the best of our knowledge, for the first time, we proposed diagnostic models built through supervised machine learning algorithms based on EV-specific signatures, which could discriminate patients according to the clinical diagnosis with high accuracy. Furthermore, the characterization of EV surface markers bolsters the concept of a relevant involvement of inflammation in PD and underscores the importance of EVs as pathways/biomarkers for protein aggregation-related neurodegenerative diseases.

8. Conclusion

Skin biopsy is a valuable diagnostic tool for PD. The best result was obtained considering several pathological markers simultaneously: oligomers, aggregates, and phosphorylated αSyn, and IENFD. Indeed, each marker at a time allows to discriminate synucleinopathies from controls and tauopathies but not to distinguish PD and MSA. To date, few research groups are working in this field. Ideally, a task force should be organized to standardize the procedures, from the biopsy to the final interpretation of results, to produce guidelines for the use of skin biopsy for the diagnosis of PD. Based on the results of this research work, it would be appropriate to investigate two anatomical areas (cervical and ankle) and a panel of biomarkers simultaneously: IENFD, oligomeric αSyn, and another pathological protein, different from αSyn but strongly involved in neurodegenerative disorders.

Regarding the immunophenotyping of plasmatic EVs, the field is new. We obtained excellent results with immunological markers that are non-specific for neurodegenerative disorders. Thus, we need to invest in this field due to the vast diagnostic potential, expanding the panel with other markers of neurodegeneration. Therefore, information obtained by CNS-specific body fluids, like CSF, and by patients at different stages of the disease is essential.

In conclusion, the skin and the blood analysis have provided highly relevant results, potentially impacting clinical practice. Both are low-cost, minimally invasive tests for the patients and can be repeated over time to follow the disease course. As for the skin, we have reached the point that the scientific community must unite and take the last step to standardize the procedure. For plasma, we are at the beginning of a path with enormous potential.

9. Bibliography

1 Dorsey, E. R. *et al.* Projected number of people with Parkinson disease in the most populous nations, 2005 through 2030. *Neurology* **68**, 384-386, doi:10.1212/01.wnl.0000247740.47667.03 (2007).

2 Goedert, M. Alpha-synuclein and neurodegenerative diseases. *Nat Rev Neurosci* **2**, 492-501, doi:10.1038/35081564 (2001).

3 Pinter, B. *et al.* Mortality in Parkinson's disease: a 38-year follow-up study. *Mov Disord* **30**, 266-269, doi:10.1002/mds.26060 (2015).

4 Lees, A. J., Hardy, J. & Revesz, T. Parkinson's disease. *Lancet* **373**, 2055-2066, doi:10.1016/S0140-6736(09)60492-X (2009).

5 de Lau, L. M. & Breteler, M. M. Epidemiology of Parkinson's disease. *Lancet Neurol* **5**, 525-535, doi:10.1016/S1474-4422(06)70471-9 (2006).

6 Kalia, L. V. & Lang, A. E. Parkinson's disease. *Lancet* **386**, 896-912, doi:10.1016/S0140-6736(14)61393-3 (2015).

7 de Rijk, M. C. *et al.* Prevalence of Parkinson's disease in the elderly: the Rotterdam Study. *Neurology* **45**, 2143-2146, doi:10.1212/wnl.45.12.2143 (1995).

8 Bellou, V., Belbasis, L., Tzoulaki, I., Evangelou, E. & Ioannidis, J. P. Environmental risk factors and Parkinson's disease: An umbrella review of meta-analyses. *Parkinsonism Relat Disord* **23**, 1-9, doi:10.1016/j.parkreldis.2015.12.008 (2016).

9 Thomas, B. & Beal, M. F. Parkinson's disease. *Hum Mol Genet* **16 Spec No. 2**, R183-194, doi:10.1093/hmg/ddm159 (2007).

10 Schiesling, C., Kieper, N., Seidel, K. & Kruger, R. Review: Familial Parkinson's disease--genetics, clinical phenotype and neuropathology in relation to the common sporadic form of the disease. *Neuropathol Appl Neurobiol* **34**, 255-271, doi:10.1111/j.1365-2990.2008.00952.x (2008).

11 Gibb, W. R. & Lees, A. J. The relevance of the Lewy body to the pathogenesis of idiopathic Parkinson's disease. *J Neurol Neurosurg Psychiatry* **51**, 745-752, doi:10.1136/jnnp.51.6.745 (1988).

12 Cersosimo, M. G. & Benarroch, E. E. Pathological correlates of gastrointestinal dysfunction in Parkinson's disease. *Neurobiol Dis* **46**, 559-564, doi:10.1016/j.nbd.2011.10.014 (2012).

13 Jost, W. H. Autonomic Dysfunction in Parkinson's Disease: Cardiovascular Symptoms, Thermoregulation, and Urogenital Symptoms. *Int Rev Neurobiol* **134**, 771-785, doi:10.1016/bs.irn.2017.04.003 (2017).

14 Orimo, S. *et al.* Degeneration of cardiac sympathetic nerve begins in the early disease process of Parkinson's disease. *Brain Pathol* **17**, 24-30, doi:10.1111/j.1750-3639.2006.00032.x (2007).

15 Postuma, R. B. *et al.* Identifying prodromal Parkinson's disease: pre-motor disorders in Parkinson's disease. *Mov Disord* **27**, 617-626, doi:10.1002/mds.24996 (2012).

16 Hughes, A. J., Daniel, S. E., Kilford, L. & Lees, A. J. Accuracy of clinical diagnosis of idiopathic Parkinson's disease: a clinico-pathological study of 100 cases. *J Neurol Neurosurg Psychiatry* **55**, 181-184, doi:10.1136/jnnp.55.3.181 (1992).

17 Stefanova, N., Bucke, P., Duerr, S. & Wenning, G. K. Multiple system atrophy: an update. *Lancet Neurol* **8**, 1172-1178, doi:10.1016/S1474-4422(09)70288-1 (2009).

18 Ahmed, Z. *et al.* The neuropathology, pathophysiology and genetics of multiple system atrophy. *Neuropathol Appl Neurobiol* **38**, 4-24, doi:10.1111/j.1365-2990.2011.01234.x (2012).

19 Kovacs, G. G. Molecular Pathological Classification of Neurodegenerative Diseases: Turning towards Precision Medicine. *Int J Mol Sci* **17**, doi:10.3390/ijms17020189 (2016).

20 Koga, S., Sekiya, H., Kondru, N., Ross, O. A. & Dickson, D. W. Neuropathology and molecular diagnosis of Synucleinopathies. *Mol Neurodegener* **16**, 83, doi:10.1186/s13024-021-00501-z (2021).

21 Necpal, J., Borsek, M. & Jelenova, B. "Parkinson's disease" on the way to progressive supranuclear palsy: a review on PSP-parkinsonism. *Neurol Sci* **42**, 4927-4936, doi:10.1007/s10072-021-05601-8 (2021).

22 Stamelou, M. *et al.* Evolving concepts in progressive supranuclear palsy and other 4-repeat tauopathies. *Nat Rev Neurol* **17**, 601-620, doi:10.1038/s41582-021-00541-5 (2021).

23 Bluett, B. *et al.* Best Practices in the Clinical Management of Progressive Supranuclear Palsy and Corticobasal Syndrome: A Consensus Statement of the CurePSP Centers of Care. *Front Neurol* **12**, 694872, doi:10.3389/fneur.2021.694872 (2021).

24 Gelb, D. J., Oliver, E. & Gilman, S. Diagnostic criteria for Parkinson disease. *Arch Neurol* **56**, 33-39, doi:10.1001/archneur.56.1.33 (1999).

25 Bernheimer, H., Birkmayer, W., Hornykiewicz, O., Jellinger, K. & Seitelberger, F. Brain dopamine and the syndromes of Parkinson and Huntington. Clinical, morphological and neurochemical correlations. *J Neurol Sci* **20**, 415-455, doi:10.1016/0022-510x(73)90175-5 (1973).

26 Fahn, S. Description of Parkinson's disease as a clinical syndrome. *Ann N Y Acad Sci* **991**, 1-14, doi:10.1111/j.1749-6632.2003.tb07458.x (2003).

27 Ganguly, U. *et al.* Alpha-Synuclein as a Biomarker of Parkinson's Disease: Good, but Not Good Enough. *Front Aging Neurosci* **13**, 702639, doi:10.3389/fnagi.2021.702639 (2021).

28 Nussbaum, R. L. & Polymeropoulos, M. H. Genetics of Parkinson's disease. *Hum Mol Genet* **6**, 1687-1691, doi:10.1093/hmg/6.10.1687 (1997).

29 Polymeropoulos, M. H. *et al.* Mutation in the alpha-synuclein gene identified in families with Parkinson's disease. *Science* **276**, 2045-2047, doi:10.1126/science.276.5321.2045 (1997).

30 Kim, C. Y. & Alcalay, R. N. Genetic Forms of Parkinson's Disease. *Semin Neurol* **37**, 135-146, doi:10.1055/s-0037-1601567 (2017).

31 Goedert, M., Jakes, R. & Spillantini, M. G. The Synucleinopathies: Twenty Years On. *J Parkinsons Dis* **7**, S51-S69, doi:10.3233/JPD-179005 (2017).

32 Raposo, G. & Stoorvogel, W. Extracellular vesicles: exosomes, microvesicles, and friends. *J Cell Biol* **200**, 373-383, doi:10.1083/jcb.201211138 (2013).

33 Pinnell, J. R., Cui, M. & Tieu, K. Exosomes in Parkinson disease. *J Neurochem* **157**, 413-428, doi:10.1111/jnc.15288 (2021).

34 Longhena, F., Faustini, G., Spillantini, M. G. & Bellucci, A. Living in Promiscuity: The Multiple Partners of Alpha-Synuclein at the Synapse in Physiology and Pathology. *Int J Mol Sci* **20**, doi:10.3390/ijms20010141 (2019).

35 Vacchi, E., Kaelin-Lang, A. & Melli, G. Tau and Alpha Synuclein Synergistic Effect in Neurodegenerative Diseases: When the Periphery Is the Core. *Int J Mol Sci* **21**, doi:10.3390/ijms21145030 (2020).

36 Lashuel, H. A., Overk, C. R., Oueslati, A. & Masliah, E. The many faces of alpha-synuclein: from structure and toxicity to therapeutic target. *Nat Rev Neurosci* **14**, 38-48, doi:10.1038/nrn3406 (2013).

37 Mehra, S., Sahay, S. & Maji, S. K. alpha-Synuclein misfolding and aggregation: Implications in Parkinson's disease pathogenesis. *Biochim Biophys Acta Proteins Proteom* **1867**, 890-908, doi:10.1016/j.bbapap.2019.03.001 (2019).

38 Braak, H. & Del Tredici, K. Potential Pathways of Abnormal Tau and alpha-Synuclein Dissemination in Sporadic Alzheimer's and Parkinson's Diseases. *Cold Spring Harb Perspect Biol* **8**, doi:10.1101/cshperspect.a023630 (2016).

39 Braak, H. *et al.* Staging of brain pathology related to sporadic Parkinson's disease. *Neurobiol Aging* **24**, 197-211, doi:10.1016/s0197-4580(02)00065-9 (2003).

40 Del Tredici, K. & Braak, H. Spinal cord lesions in sporadic Parkinson's disease. *Acta Neuropathol* **124**, 643-664, doi:10.1007/s00401-012-1028-y (2012).

41 Hawkes, C. H., Del Tredici, K. & Braak, H. Parkinson's disease: a dual-hit hypothesis. *Neuropathol Appl Neurobiol* **33**, 599-614, doi:10.1111/j.1365-2990.2007.00874.x (2007).

42 Hilton, D. *et al.* Accumulation of alpha-synuclein in the bowel of patients in the pre-clinical phase of Parkinson's disease. *Acta Neuropathol* **127**, 235-241, doi:10.1007/s00401-013-1214-6 (2014).

43 Liu, B. *et al.* Vagotomy and Parkinson disease: A Swedish register-based matched-cohort study. *Neurology* **88**, 1996-2002, doi:10.1212/WNL.0000000000003961 (2017).

44 Van Den Berge, N. *et al.* Evidence for bidirectional and trans-synaptic parasympathetic and sympathetic propagation of alpha-synuclein in rats. *Acta Neuropathol* **138**, 535-550, doi:10.1007/s00401-019-02040-w (2019).

45 Borghammer, P. & Van Den Berge, N. Brain-First versus Gut-First Parkinson's Disease: A Hypothesis. *J Parkinsons Dis* **9**, S281-S295, doi:10.3233/JPD-191721 (2019).

46 Borghammer, P. *et al.* Neuropathological evidence of body-first vs. brain-first Lewy body disease. *Neurobiol Dis* **161**, 105557, doi:10.1016/j.nbd.2021.105557 (2021).

47 Wakabayashi, K., Mori, F., Tanji, K., Orimo, S. & Takahashi, H. Involvement of the peripheral nervous system in synucleinopathies, tauopathies and other neurodegenerative proteinopathies of the brain. *Acta Neuropathol* **120**, 1-12, doi:10.1007/s00401-010-0706-x (2010).
48 Nishie, M. *et al.* Accumulation of phosphorylated alpha-synuclein in the brain and peripheral ganglia of patients with multiple system atrophy. *Acta Neuropathol* **107**, 292-298, doi:10.1007/s00401-003-0811-1 (2004).
49 Mori, F. *et al.* Alpha-synuclein immunoreactivity in normal and neoplastic Schwann cells. *Acta Neuropathol* **103**, 145-151, doi:10.1007/s004010100443 (2002).
50 Melli, G. *et al.* Cervical skin denervation associates with alpha-synuclein aggregates in Parkinson disease. *Ann Clin Transl Neurol* **5**, 1394-1407, doi:10.1002/acn3.669 (2018).
51 Kanda, T., Tsukagoshi, H., Oda, M., Miyamoto, K. & Tanabe, H. Changes of unmyelinated nerve fibers in sural nerve in amyotrophic lateral sclerosis, Parkinson's disease and multiple system atrophy. *Acta Neuropathol* **91**, 145-154, doi:10.1007/s004010050406 (1996).
52 Orimo, S. *et al.* Axonal alpha-synuclein aggregates herald centripetal degeneration of cardiac sympathetic nerve in Parkinson's disease. *Brain* **131**, 642-650, doi:10.1093/brain/awm302 (2008).
53 Tsukita, K., Sakamaki-Tsukita, H., Tanaka, K., Suenaga, T. & Takahashi, R. Value of in vivo alpha-synuclein deposits in Parkinson's disease: A systematic review and meta-analysis. *Mov Disord* **34**, 1452-1463, doi:10.1002/mds.27794 (2019).
54 Donadio, V. *et al.* Abnormal alpha-synuclein deposits in skin nerves: intra- and inter-laboratory reproducibility. *Eur J Neurol* **26**, 1245-1251, doi:10.1111/ene.13939 (2019).
55 Antelmi, E., Donadio, V., Incensi, A., Plazzi, G. & Liguori, R. Skin nerve phosphorylated alpha-synuclein deposits in idiopathic REM sleep behavior disorder. *Neurology* **88**, 2128-2131, doi:10.1212/WNL.0000000000003989 (2017).
56 Doppler, K. *et al.* Dermal phospho-alpha-synuclein deposits confirm REM sleep behaviour disorder as prodromal Parkinson's disease. *Acta Neuropathol* **133**, 535-545, doi:10.1007/s00401-017-1684-z (2017).
57 Vacchi, E., Pinton, S., Kaelin-Lang, A. & Melli, G. Targeting Alpha Synuclein Aggregates in Cutaneous Peripheral Nerve Fibers by Free-floating Immunofluorescence Assay. *J Vis Exp*, doi:10.3791/59558 (2019).
58 Mazzetti, S. *et al.* alpha-Synuclein oligomers in skin biopsy of idiopathic and monozygotic twin patients with Parkinson's disease. *Brain* **143**, 920-931, doi:10.1093/brain/awaa008 (2020).
59 Nolano, M. *et al.* Sensory deficit in Parkinson's disease: evidence of a cutaneous denervation. *Brain* **131**, 1903-1911, doi:10.1093/brain/awn102 (2008).
60 Nolano, M. *et al.* Small fiber pathology parallels disease progression in Parkinson disease: a longitudinal study. *Acta Neuropathol* **136**, 501-503, doi:10.1007/s00401-018-1876-1 (2018).
61 Mathivanan, S., Ji, H. & Simpson, R. J. Exosomes: extracellular organelles important in intercellular communication. *J Proteomics* **73**, 1907-1920, doi:10.1016/j.jprot.2010.06.006 (2010).
62 Cocucci, E. & Meldolesi, J. Ectosomes and exosomes: shedding the confusion between extracellular vesicles. *Trends Cell Biol* **25**, 364-372, doi:10.1016/j.tcb.2015.01.004 (2015).
63 Coleman, M. L. *et al.* Membrane blebbing during apoptosis results from caspase-mediated activation of ROCK I. *Nat Cell Biol* **3**, 339-345, doi:10.1038/35070009 (2001).
64 Thery, C., Zitvogel, L. & Amigorena, S. Exosomes: composition, biogenesis and function. *Nat Rev Immunol* **2**, 569-579, doi:10.1038/nri855 (2002).
65 Bobrie, A., Colombo, M., Raposo, G. & Thery, C. Exosome secretion: molecular mechanisms and roles in immune responses. *Traffic* **12**, 1659-1668, doi:10.1111/j.1600-0854.2011.01225.x (2011).
66 Kanninen, K. M., Bister, N., Koistinaho, J. & Malm, T. Exosomes as new diagnostic tools in CNS diseases. *Biochim Biophys Acta* **1862**, 403-410, doi:10.1016/j.bbadis.2015.09.020 (2016).
67 Zhao, Y. & Yang, G. Potential of extracellular vesicles in the Parkinson's disease - Pathological mediators and biomarkers. *Neurochem Int* **144**, 104974, doi:10.1016/j.neuint.2021.104974 (2021).
68 Stuendl, A. *et al.* Induction of alpha-synuclein aggregate formation by CSF exosomes from patients with Parkinson's disease and dementia with Lewy bodies. *Brain* **139**, 481-494, doi:10.1093/brain/awv346 (2016).
69 Gui, Y., Liu, H., Zhang, L., Lv, W. & Hu, X. Altered microRNA profiles in cerebrospinal fluid exosome in Parkinson disease and Alzheimer disease. *Oncotarget* **6**, 37043-37053, doi:10.18632/oncotarget.6158 (2015).

70 Li, Y. *et al.* EV-origin: Enumerating the tissue-cellular origin of circulating extracellular vesicles using exLR profile. *Comput Struct Biotechnol J* **18**, 2851-2859, doi:10.1016/j.csbj.2020.10.002 (2020).
71 Jiang, C. *et al.* Serum neuronal exosomes predict and differentiate Parkinson's disease from atypical parkinsonism. *J Neurol Neurosurg Psychiatry* **91**, 720-729, doi:10.1136/jnnp-2019-322588 (2020).
72 Wang, N., Gibbons, C. H., Lafo, J. & Freeman, R. alpha-Synuclein in cutaneous autonomic nerves. *Neurology* **81**, 1604-1610, doi:10.1212/WNL.0b013e3182a9f449 (2013).
73 Zange, L., Noack, C., Hahn, K., Stenzel, W. & Lipp, A. Phosphorylated alpha-synuclein in skin nerve fibres differentiates Parkinson's disease from multiple system atrophy. *Brain* **138**, 2310-2321, doi:10.1093/brain/awv138 (2015).
74 Doppler, K. *et al.* Distinctive distribution of phospho-alpha-synuclein in dermal nerves in multiple system atrophy. *Mov Disord* **30**, 1688-1692, doi:10.1002/mds.26293 (2015).
75 Donadio, V. *et al.* A new potential biomarker for dementia with Lewy bodies: Skin nerve alpha-synuclein deposits. *Neurology* **89**, 318-326, doi:10.1212/WNL.0000000000004146 (2017).
76 Kovacs, G. G. *et al.* Intracellular processing of disease-associated alpha-synuclein in the human brain suggests prion-like cell-to-cell spread. *Neurobiol Dis* **69**, 76-92, doi:10.1016/j.nbd.2014.05.020 (2014).
77 Kovacs, G. G. *et al.* An antibody with high reactivity for disease-associated alpha-synuclein reveals extensive brain pathology. *Acta Neuropathol* **124**, 37-50, doi:10.1007/s00401-012-0964-x (2012).
78 Uchihara, T. & Giasson, B. I. Propagation of alpha-synuclein pathology: hypotheses, discoveries, and yet unresolved questions from experimental and human brain studies. *Acta Neuropathol* **131**, 49-73, doi:10.1007/s00401-015-1485-1 (2016).
79 Gilman, S. *et al.* Second consensus statement on the diagnosis of multiple system atrophy. *Neurology* **71**, 670-676, doi:10.1212/01.wnl.0000324625.00404.15 (2008).
80 McKeith, I. G. *et al.* Diagnosis and management of dementia with Lewy bodies: Fourth consensus report of the DLB Consortium. *Neurology* **89**, 88-100, doi:10.1212/WNL.0000000000004058 (2017).
81 Armstrong, M. J. *et al.* Criteria for the diagnosis of corticobasal degeneration. *Neurology* **80**, 496-503, doi:10.1212/WNL.0b013e31827f0fd1 (2013).
82 Hoglinger, G. U. *et al.* Clinical diagnosis of progressive supranuclear palsy: The movement disorder society criteria. *Mov Disord* **32**, 853-864, doi:10.1002/mds.26987 (2017).
83 Hoehn, M. M. & Yahr, M. D. Parkinsonism: onset, progression and mortality. *Neurology* **17**, 427-442, doi:10.1212/wnl.17.5.427 (1967).
84 Folstein, M. F., Folstein, S. E. & McHugh, P. R. "Mini-mental state". A practical method for grading the cognitive state of patients for the clinician. *J Psychiatr Res* **12**, 189-198, doi:10.1016/0022-3956(75)90026-6 (1975).
85 Nasreddine, Z. S. *et al.* The Montreal Cognitive Assessment, MoCA: a brief screening tool for mild cognitive impairment. *J Am Geriatr Soc* **53**, 695-699, doi:10.1111/j.1532-5415.2005.53221.x (2005).
86 Wang, Y. P. & Gorenstein, C. Psychometric properties of the Beck Depression Inventory-II: a comprehensive review. *Braz J Psychiatry* **35**, 416-431, doi:10.1590/1516-4446-2012-1048 (2013).
87 Stiasny-Kolster, K. *et al.* The REM sleep behavior disorder screening questionnaire--a new diagnostic instrument. *Mov Disord* **22**, 2386-2393, doi:10.1002/mds.21740 (2007).
88 Kipfer, S., Stephan, M. A., Schupbach, W. M., Ballinari, P. & Kaelin-Lang, A. Resting tremor in Parkinson disease: a negative predictor of levodopa-induced dyskinesia. *Arch Neurol* **68**, 1037-1039, doi:10.1001/archneurol.2011.147 (2011).
89 Devigili, G. *et al.* The diagnostic criteria for small fibre neuropathy: from symptoms to neuropathology. *Brain* **131**, 1912-1925, doi:10.1093/brain/awn093 (2008).
90 Lauria, G. *et al.* EFNS guidelines on the use of skin biopsy in the diagnosis of peripheral neuropathy. *Eur J Neurol* **12**, 747-758, doi:10.1111/j.1468-1331.2005.01260.x (2005).
91 Lauria, G. *et al.* European Federation of Neurological Societies/Peripheral Nerve Society Guideline on the use of skin biopsy in the diagnosis of small fiber neuropathy. Report of a joint task force of the European Federation of Neurological Societies and the Peripheral Nerve Society. *Eur J Neurol* **17**, 903-912, e944-909, doi:10.1111/j.1468-1331.2010.03023.x (2010).

92 Provitera, V. *et al.* A multi-center, multinational age- and gender-adjusted normative dataset for immunofluorescent intraepidermal nerve fiber density at the distal leg. *Eur J Neurol* **23**, 333-338, doi:10.1111/ene.12842 (2016).
93 Roberts, R. F., Wade-Martins, R. & Alegre-Abarrategui, J. Direct visualization of alpha-synuclein oligomers reveals previously undetected pathology in Parkinson's disease brain. *Brain* **138**, 1642-1657, doi:10.1093/brain/awv040 (2015).
94 Sekiya, H. *et al.* Wide distribution of alpha-synuclein oligomers in multiple system atrophy brain detected by proximity ligation. *Acta Neuropathol* **137**, 455-466, doi:10.1007/s00401-019-01961-w (2019).
95 Ruffmann, C. *et al.* Detection of alpha-synuclein conformational variants from gastro-intestinal biopsy tissue as a potential biomarker for Parkinson's disease. *Neuropathol Appl Neurobiol* **44**, 722-736, doi:10.1111/nan.12486 (2018).
96 Fahn S, E. R., UPDRS program members. Unified Parkinsons Disease Rating Scale. In: Fahn S, Marsden CD, Goldstein M, Calne DB, editors. . Recent developments in Parkinsons disease, vol 2. . *Florham Park, NJ: Macmillan Healthcare Information*, 153-156 (1987).
97 Sletten, D. M., Suarez, G. A., Low, P. A., Mandrekar, J. & Singer, W. COMPASS 31: a refined and abbreviated Composite Autonomic Symptom Score. *Mayo Clin Proc* **87**, 1196-1201, doi:10.1016/j.mayocp.2012.10.013 (2012).
98 Beck AT, S. R., Brown GK. BDI-II: Beck Depression Inventory Manual. (1996).
99 Stiasny-Kolster, K. *et al.* The REM sleep behavior disorder screening questionnaire - A new diagnostic instrument. *Movement Disord* **22**, 2386-2393, doi:10.1002/mds.21740 (2007).
100 Tomlinson, C. L. *et al.* Systematic Review of Levodopa Dose Equivalency Reporting in Parkinson's Disease. *Movement Disord* **25**, 2649-2653, doi:10.1002/mds.23429 (2010).
101 Tansey, M. G. & Romero-Ramos, M. Immune system responses in Parkinson's disease: Early and dynamic. *Eur J Neurosci* **49**, 364-383, doi:10.1111/ejn.14290 (2019).
102 Sulzer, D. *et al.* T cells from patients with Parkinson's disease recognize alpha-synuclein peptides. *Nature* **546**, 656-661, doi:10.1038/nature22815 (2017).
103 Koliha, N. *et al.* A novel multiplex bead-based platform highlights the diversity of extracellular vesicles. *J Extracell Vesicles* **5**, 29975, doi:10.3402/jev.v5.29975 (2016).
104 Dragovic, R. A. *et al.* Sizing and phenotyping of cellular vesicles using Nanoparticle Tracking Analysis. *Nanomedicine* **7**, 780-788, doi:10.1016/j.nano.2011.04.003 (2011).
105 Scardoni, G., Tosadori, G., Pratap, S., Spoto, F. & Laudanna, C. Finding the shortest path with PesCa: a tool for network reconstruction. *F1000Res* **4**, 484, doi:10.12688/f1000research.6769.2 (2015).
106 Scardoni, G. *et al.* Biological network analysis with CentiScaPe: centralities and experimental dataset integration. *F1000Res* **3**, 139, doi:10.12688/f1000research.4477.2 (2014).
107 Di Silvestre, D. *et al.* Proteomics-based network analysis characterizes biological processes and pathways activated by preconditioned mesenchymal stem cells in cardiac repair mechanisms. *Biochim Biophys Acta Gen Subj* **1861**, 1190-1199, doi:10.1016/j.bbagen.2017.02.006 (2017).
108 Sereni, L. *et al.* Lentiviral gene therapy corrects platelet phenotype and function in patients with Wiskott-Aldrich syndrome. *J Allergy Clin Immunol* **144**, 825-838, doi:10.1016/j.jaci.2019.03.012 (2019).
109 Huang da, W., Sherman, B. T. & Lempicki, R. A. Systematic and integrative analysis of large gene lists using DAVID bioinformatics resources. *Nat Protoc* **4**, 44-57, doi:10.1038/nprot.2008.211 (2009).
110 Burrello, J. *et al.* The Primary Aldosteronism Surgical Outcome Score for the Prediction of Clinical Outcomes After Adrenalectomy for Unilateral Primary Aldosteronism. *Ann Surg* **272**, 1125-1132, doi:10.1097/SLA.0000000000003200 (2020).
111 Yang, Y. *et al.* Classification of microadenomas in patients with primary aldosteronism by steroid profiling. *J Steroid Biochem Mol Biol* **189**, 274-282, doi:10.1016/j.jsbmb.2019.01.008 (2019).
112 Vacchi, E. *et al.* Immune profiling of plasma-derived extracellular vesicles identifies Parkinson disease. *Neurol Neuroimmunol Neuroinflamm* **7**, doi:10.1212/NXI.0000000000000866 (2020).
113 Thery, C., Amigorena, S., Raposo, G. & Clayton, A. Isolation and characterization of exosomes from cell culture supernatants and biological fluids. *Curr Protoc Cell Biol* **Chapter 3**, Unit 3 22, doi:10.1002/0471143030.cb0322s30 (2006).
114 Koliha, N. *et al.* Melanoma Affects the Composition of Blood Cell-Derived Extracellular Vesicles. *Front Immunol* **7**, 282, doi:10.3389/fimmu.2016.00282 (2016).

115 Doppler, K. Detection of Dermal Alpha-Synuclein Deposits as a Biomarker for Parkinson's Disease. *J Parkinsons Dis* **11**, 937-947, doi:10.3233/JPD-202489 (2021).
116 Litvinchuk, A. *et al.* Complement C3aR Inactivation Attenuates Tau Pathology and Reverses an Immune Network Deregulated in Tauopathy Models and Alzheimer's Disease. *Neuron* **100**, 1337-1353 e1335, doi:10.1016/j.neuron.2018.10.031 (2018).
117 Donadio, V. *et al.* In Vivo Diagnosis of Synucleinopathies: A Comparative Study of Skin Biopsy and RT-QuIC. *Neurology* **96**, e2513-e2524, doi:10.1212/WNL.0000000000011935 (2021).
118 Donadio, V. *et al.* Skin alpha-synuclein deposits differ in clinical variants of synucleinopathy: an in vivo study. *Sci Rep* **8**, 14246, doi:10.1038/s41598-018-32588-8 (2018).
119 Peng, C., Trojanowski, J. Q. & Lee, V. M. Protein transmission in neurodegenerative disease. *Nat Rev Neurol* **16**, 199-212, doi:10.1038/s41582-020-0333-7 (2020).
120 Oueslati, A. Implication of Alpha-Synuclein Phosphorylation at S129 in Synucleinopathies: What Have We Learned in the Last Decade? *J Parkinsons Dis* **6**, 39-51, doi:10.3233/JPD-160779 (2016).
121 Isonaka, R., Gibbons, C. H., Wang, N., Freeman, R. & Goldstein, D. S. Association of innervation-adjusted alpha-synuclein in arrector pili muscles with cardiac noradrenergic deficiency in autonomic synucleinopathies. *Clin Auton Res* **29**, 587-593, doi:10.1007/s10286-019-00644-6 (2019).
122 Beach, T. G. *et al.* Unified staging system for Lewy body disorders: correlation with nigrostriatal degeneration, cognitive impairment and motor dysfunction. *Acta Neuropathol* **117**, 613-634, doi:10.1007/s00401-009-0538-8 (2009).
123 Braak, H., Rub, U., Gai, W. P. & Del Tredici, K. Idiopathic Parkinson's disease: possible routes by which vulnerable neuronal types may be subject to neuroinvasion by an unknown pathogen. *J Neural Transm (Vienna)* **110**, 517-536, doi:10.1007/s00702-002-0808-2 (2003).
124 Stokholm, M. G., Danielsen, E. H., Hamilton-Dutoit, S. J. & Borghammer, P. Pathological alpha-synuclein in gastrointestinal tissues from prodromal Parkinson disease patients. *Ann Neurol* **79**, 940-949, doi:10.1002/ana.24648 (2016).
125 Espay, A. J. *et al.* Disease modification and biomarker development in Parkinson disease: Revision or reconstruction? *Neurology* **94**, 481-494, doi:10.1212/WNL.0000000000009107 (2020).
126 Miller, I. N. & Cronin-Golomb, A. Gender differences in Parkinson's disease: clinical characteristics and cognition. *Mov Disord* **25**, 2695-2703, doi:10.1002/mds.23388 (2010).
127 Samuelsson, K., Kostulas, K., Vrethem, M., Rolfs, A. & Press, R. Idiopathic small fiber neuropathy: phenotype, etiologies, and the search for fabry disease. *J Clin Neurol* **10**, 108-118, doi:10.3988/jcn.2014.10.2.108 (2014).
128 Tomlinson, P. R. *et al.* Identification of distinct circulating exosomes in Parkinson's disease. *Ann Clin Transl Neurol* **2**, 353-361, doi:10.1002/acn3.175 (2015).
129 Ohmichi, T. *et al.* Quantification of brain-derived extracellular vesicles in plasma as a biomarker to diagnose Parkinson's and related diseases. *Parkinsonism Relat D* **61**, 82-87, doi:10.1016/j.parkreldis.2018.11.021 (2019).
130 Tofaris, G. K. Lysosome-dependent pathways as a unifying theme in Parkinson's disease. *Mov Disord* **27**, 1364-1369, doi:10.1002/mds.25136 (2012).
131 Tofaris, G. K. A Critical Assessment of Exosomes in the Pathogenesis and Stratification of Parkinson's Disease. *J Parkinson Dis* **7**, 569-576, doi:10.3233/Jpd-171176 (2017).
132 Shah, R., Patel, T. & Freedman, J. E. Circulating Extracellular Vesicles in Human Disease. *N Engl J Med* **379**, 958-966, doi:10.1056/NEJMra1704286 (2018).
133 Balducci, C. *et al.* Toll-like receptor 4-dependent glial cell activation mediates the impairment in memory establishment induced by beta-amyloid oligomers in an acute mouse model of Alzheimer's disease. *Brain Behav Immun* **60**, 188-197, doi:10.1016/j.bbi.2016.10.012 (2017).
134 Hall, S. *et al.* Cerebrospinal fluid concentrations of inflammatory markers in Parkinson's disease and atypical parkinsonian disorders. *Sci Rep* **8**, 13276, doi:10.1038/s41598-018-31517-z (2018).
135 La Vitola, P. *et al.* Alpha-synuclein oligomers impair memory through glial cell activation and via Toll-like receptor 2. *Brain Behav Immun* **69**, 591-602, doi:10.1016/j.bbi.2018.02.012 (2018).
136 Elgueta, R. *et al.* Molecular mechanism and function of CD40/CD40L engagement in the immune system. *Immunol Rev* **229**, 152-172, doi:10.1111/j.1600-065X.2009.00782.x (2009).
137 Chen, J. *et al.* CD146 coordinates brain endothelial cell-pericyte communication for blood-brain barrier development. *Proc Natl Acad Sci U S A* **114**, E7622-E7631, doi:10.1073/pnas.1710848114 (2017).

138 Rapanotti, M. C. *et al.* Minimal residual disease in melanoma: circulating melanoma cells and predictive role of MCAM/MUC18/MelCAM/CD146. *Cell Death Discov* **3**, doi:ARTN 17005

10.1038/cddiscovery.2017.5 (2017).
139 Bose, A., Petsko, G. A. & Eliezer, D. Parkinson's Disease and Melanoma: Co-Occurrence and Mechanisms. *J Parkinsons Dis* **8**, 385-398, doi:10.3233/JPD-171263 (2018).
140 Menon, R. *et al.* Gender-based blood transcriptomes and interactomes in multiple sclerosis: involvement of SP1 dependent gene transcription. *J Autoimmun* **38**, J144-155, doi:10.1016/j.jaut.2011.11.004 (2012).
141 Gratuze, M., Joly-Amado, A., Vieau, D., Buee, L. & Blum, D. Mutual Relationship between Tau and Central Insulin Signalling: Consequences for AD and Tauopathies? *Neuroendocrinology* **107**, 181-195, doi:10.1159/000487641 (2018).
142 Neri, C. Role and therapeutic potential of the pro-longevity factor FOXO and its regulators in neurodegenerative disease. *Front Pharmacol* **3**, doi:UNSP 15

10.3389/fphar.2012.00015 (2012).
143 Thery, C. *et al.* Minimal information for studies of extracellular vesicles 2018 (MISEV2018): a position statement of the International Society for Extracellular Vesicles and update of the MISEV2014 guidelines. *J Extracell Vesicles* **7**, 1535750, doi:10.1080/20013078.2018.1535750 (2018).
144 Agosta, F. *et al.* Myeloid microvesicles in cerebrospinal fluid are associated with myelin damage and neuronal loss in mild cognitive impairment and Alzheimer disease. *Ann Neurol* **76**, 813-825, doi:10.1002/ana.24235 (2014).
145 Verderio, C. *et al.* Myeloid microvesicles are a marker and therapeutic target for neuroinflammation. *Ann Neurol* **72**, 610-624, doi:10.1002/ana.23627 (2012).
146 Tietje, A., Maron, K. N., Wei, Y. & Feliciano, D. M. Cerebrospinal fluid extracellular vesicles undergo age dependent declines and contain known and novel non-coding RNAs. *PLoS One* **9**, e113116, doi:10.1371/journal.pone.0113116 (2014).
147 Reinert, K. R., Umphlet, C. D., Quattlebaum, A. & Boger, H. A. Short-term effects of an endotoxin on substantia nigra dopamine neurons. *Brain Res* **1557**, 164-170, doi:10.1016/j.brainres.2014.02.005 (2014).
148 Pott Godoy, M. C., Tarelli, R., Ferrari, C. C., Sarchi, M. I. & Pitossi, F. J. Central and systemic IL-1 exacerbates neurodegeneration and motor symptoms in a model of Parkinson's disease. *Brain* **131**, 1880-1894, doi:10.1093/brain/awn101 (2008).
149 Yang, Y. *et al.* Inflammation leads to distinct populations of extracellular vesicles from microglia. *J Neuroinflammation* **15**, 168, doi:10.1186/s12974-018-1204-7 (2018).
150 Slomka, A., Urban, S. K., Lukacs-Kornek, V., Zekanowska, E. & Kornek, M. Large Extracellular Vesicles: Have We Found the Holy Grail of Inflammation? *Front Immunol* **9**, 2723, doi:10.3389/fimmu.2018.02723 (2018).
151 Sankowski, R., Mader, S. & Valdes-Ferrer, S. I. Systemic inflammation and the brain: novel roles of genetic, molecular, and environmental cues as drivers of neurodegeneration. *Front Cell Neurosci* **9**, 28, doi:10.3389/fncel.2015.00028 (2015).
152 Guerriero, J. L. Macrophages: Their Untold Story in T Cell Activation and Function. *Int Rev Cell Mol Biol* **342**, 73-93, doi:10.1016/bs.ircmb.2018.07.001 (2019).
153 Stalter, R. D. in *Measuring Immunity - Basic Biology and Clinical Assessment* (ed Michael T. Lotze and Angus W. Thomson) Ch. 1, 3-11 (2005).
154 Rock, K. L., Reits, E. & Neefjes, J. Present Yourself! By MHC Class I and MHC Class II Molecules. *Trends Immunol* **37**, 724-737, doi:10.1016/j.it.2016.08.010 (2016).
155 Galiano-Landeira, J., Torra, A., Vila, M. & Bove, J. CD8 T cell nigral infiltration precedes synucleinopathy in early stages of Parkinson's disease. *Brain* **143**, 3717-3733, doi:10.1093/brain/awaa269 (2020).
156 Rossi, E., Bernabeu, C. & Smadja, D. M. Endoglin as an Adhesion Molecule in Mature and Progenitor Endothelial Cells: A Function Beyond TGF-beta. *Front Med (Lausanne)* **6**, 10, doi:10.3389/fmed.2019.00010 (2019).
157 Lastres, P. *et al.* Regulated expression on human macrophages of endoglin, an Arg-Gly-Asp-containing surface antigen. *Eur J Immunol* **22**, 393-397, doi:10.1002/eji.1830220216 (1992).

158 Walker, D. G., Lue, L. F., Beach, T. G. & Tooyama, I. Microglial Phenotyping in Neurodegenerative Disease Brains: Identification of Reactive Microglia with an Antibody to Variant of CD105/Endoglin. *Cells* **8**, doi:10.3390/cells8070766 (2019).

159 Bechmann, I., Peter, S., Beyer, M., Gimsa, U. & Nitsch, R. Presence of B7--2 (CD86) and lack of B7--1 (CD(80) on myelin phagocytosing MHC-II-positive rat microglia is associated with nondestructive immunity in vivo. *FASEB J* **15**, 1086-1088, doi:10.1096/fj.00-0563fje (2001).

160 Issazadeh, S., Navikas, V., Schaub, M., Sayegh, M. & Khoury, S. Kinetics of expression of costimulatory molecules and their ligands in murine relapsing experimental autoimmune encephalomyelitis in vivo. *J Immunol* **161**, 1104-1112 (1998).

161 Zeinstra, E., Wilczak, N. & De Keyser, J. Reactive astrocytes in chronic active lesions of multiple sclerosis express co-stimulatory molecules B7-1 and B7-2. *J Neuroimmunol* **135**, 166-171, doi:10.1016/s0165-5728(02)00462-9 (2003).

162 Agliardi, C. *et al.* Oligomeric alpha-Syn and SNARE complex proteins in peripheral extracellular vesicles of neural origin are biomarkers for Parkinson's disease. *Neurobiol Dis* **148**, 105185, doi:10.1016/j.nbd.2020.105185 (2021).

10. Abbreviations

- αSyn = αSynuclein
- αSyn-5G4 = Aggregated alpha-Synuclein detected by 5G4 antibody
- αSyn-PLA = Oligomeric alpha-Synuclein detected by proximity ligation assay
- AP = Atypical parkinsonism
- APOA1 = Apolipoprotein A1
- AP-Syn = Atypical parkinsonism with synucleinopathies
- AP-Tau = Atypical parkinsonism with tauopathies
- AUC = Area under the curve
- BDI-II = Beck depression inventory scale II
- CBD = Corticobasal degeneration
- CI = confident interval
- COMPASS-31 = Composite Autonomic Symptom Score 31
- CSF = Cerebrospinal fluid
- DLB = Dementia with Lewy Body
- EVs = Extracellular vesicles
- FITCH = Fluorescein isothiocyanate
- GCI = Glial cytoplasmic inclusions
- GLMM = Generalized linear mixed model
- H&Y = Hoen & Yahr scale
- HC = Healthy control
- IENFD = Intraepidermal Nerve Fiber Density
- KEGG = Kyoto Encyclopedia of Genes and Genomes pathways
- LB = Lewy Body
- LEDD = Levodopa equivalent daily dose
- LN = Lewy neurites
- MAP = muscle arrector pili
- MDS-UPDRS = Movement Disorder Society Unified Parkinson's Disease Rating Scale
- MMSE = Mini-Mental State Examination
- MoCA = Montreal Cognitive Assessment
- MSA = Multiple system atrophy
- OR = Odds ratio
- P-αSyn = Alpha-Synuclein phosphorylated at Serine 129
- PD = Parkinson’s Disease
- PE = Phycoerythrin
- PGP9.5 = Protein gene product 9.5
- PLA = Proximity Ligation assay
- PNS = Peripheral Nervous system
- PPI = Protein-protein interaction
- PSP = Progressive supranuclear palsy
- RBD = Rem Behaviour Disorder
- RF = Random Forest
- ROC = Receiver operating characteristic
- SE = Standard Error
- SG = Sweat gland
- T0 = Time point 0
- T12 = Time point 12 months
- T24 = Time point 24 months
- TSG101 = Tumor susceptibility gene 101

11. List of publications and other activities

Publications in International Peer-Reviewed Journals

Elena Vacchi, Camilla Senese, Giacomo Chiaro, Giulio Disanto, Sandra Pinton, Sara Morandi, Ilaria Bertaina, Giovanni Bianco, Claudio Stadler, Salvatore Galati, Claudio Gobbi, Alain Kaelin-Lang, Giorgia Melli "Alpha-synuclein oligomers and small nerve fiber pathology in skin are potential biomarkers of Parkinson's disease" npj Parkinson's Disease 2021 DOI: 10.1038/s41531-021-00262-y

Giona Pedrioli & Ester Piovesana & Elena Vacchi, Carolina Balbi "Extracellular Vesicles as Promising Carriers in Drug Delivery: Considerations from a Cell Biologist's Perspective" Biology 2021 DOI: 10.3390/biology10050376

Elena Vacchi & Jacopo Burrello, Alessio Burrello, Sara Bolis, Silvia Monticone, Lucio Barile, Alain Kaelin-Lang, Giorgia Melli "Profiling Inflammatory Extracellular Vesicles in Plasma and Cerebrospinal Fluid: An Optimized Diagnostic Model for Parkinson's Disease" Biomedicines 2021 DOI: 10.3390/biomedicines9030230

Elena Vacchi & Jacopo Burrello, Dario Di Silvestre, Alessio Burrello, Sara Bolis, Pierluigi Mauri, Giuseppe Vassalli, Carlo W. Cereda, Cinthia Farina, Lucio Barile, Alain Kaelin-Lang, Giorgia Melli "Immune profiling of plasma-derived extracellular vesicles identifies Parkinson disease" Neurology, Neuroimmunology & Neuroinflammation 2020 doi: 10.1212/NXI.0000000000000866

Elena Vacchi, Alain Kaelin-Lang, Giorgia Melli "Tau and Alpha-Synuclein Synergistic Effect in Neurodegenerative Diseases: When the Periphery Is the Core" IJMS 2020 DOI: 10.3390/ijms21145030

Elena Vacchi, Sandra Pinton, Alain Kaelin-Lang, Giorgia Melli "Targeting Alpha-Synuclein Aggregates in Cutaneous Peripheral Nerve Fibers by Free-floating Immunofluorescence Assay" JoVE 2019 DOI: 10.3791/59558

Giorgia Melli, Elena Vacchi, Vanessa Biemmi, Salvatore Galati, Claudio Staedler, Roberto Ambrosini, Alain Kaelin-Lang "Cervical skin denervation associates with alpha-synuclein aggregates in Parkinson disease" AnnClinTranslNeurol 2018 DOI: 10.1002/acn3.669

Presentations at National and International congress

Oral presentations

Vacchi E., Kaelin-Lang A., Melli G. "Tau protein characterization in skin biopsies differentiates patients with synucleinopathies and tauopathies" 15th International Conference on Alzheimer's and Parkinson's Diseases, Barcelona, Spain, March 11, 2021

Vacchi E., Burrello J., Di Silvestre D., Burrello A., Bolis S., Farina C., Barile L., Kaelin-Lang L., Melli G. "Plasmatic extracellular vesicle-profiles differentiate Parkinson's Disease and synucleinopathies from tauopathies: a role for the immune system" 15th International Conference on Alzheimer's and Parkinson's Diseases, Vienna, Austria, April 2-5, 2020

Vacchi E., Ambrosini R., Galati S., Staedler C., Melli G., Kaelin-Lang A. "Intra epidermal nerve fiber density as a biomarker of PD progression" 14th International Conference on Alzheimer's and Parkinson's Diseases, Lisbon, Portugal, March 29, 2019

Vacchi E., Pinton S., Biemmi V., Galati S., Staedler C., Melli G., Kaelin-Lang A. "Phosphorylated and oligomeric alpha-synuclein in skin nerve fibers discriminate Parkinson Disease from Atypical Parkinsonism". 8° Giornata della Ricerca della Svizzera Italiana, Lugano. March 9, 2018.

Posters

Vacchi E., Burrello J., Burrello A., Bolis S., Barile L., Kaelin-Lang L., Melli G. "The immune-profiling of plasma- and CSF- derived extracellular vesicles allows the discrimination between Parkinson's Disease and atypical parkinsonisms". 2nd EVIta symposium, Lucca, Italy, September 20-22, 2021

Vacchi E., Senese C. Kaelin-Lang A., Melli G. "αSyn oligomers detection by proximity ligation assay in skin biopsies is a biomarker for Parkinson's disease". 15th International Conference on Alzheimer's and Parkinson's Diseases, Barcelona, Spain, March 9-14, 2021

Vacchi E., Burrello J., Burrello A., Bolis S., Barile L., Kaelin-Lang L., Melli G. "Extracellular Vesicles Immune-profiling in plasma and CSF: a diagnostic tool for Parkinson's Disease". 15th International Conference on Alzheimer's and Parkinson's Diseases, Barcelona, Spain, March 9-14, 2021

Vacchi E., Burrello J., Bolis S., Burrello A., Farina C., Barile L., Kaelin-Lang L., Melli G. "Plasma-derived Extracellular Vesicles profiling as a biomarker for Parkinson's Disease", ISEV2020 Virtual Annual Meeting, July 20-22, 2020

Vacchi E., Burrello J., Bolis S., Burrello A., Barile L., Vassalli G., Kaelin-Lang A., Melli G. "Profiling Extracellular Vesicles is a specific diagnostic tool for Parkinson disease". 1st EVIta symposium, Palermo, Italy, November 6-8, 2019

Vacchi E., Ambrosini R., Galati S., Staedler C., Kaelin-Lang A., Melli G. "Skin differential expression of pathogenic proteins in atypical parkinsonism and Parkinson disease" 14th International Conference on Alzheimer's and Parkinson's Diseases, Lisbon, Portugal, March 29-30, 2019

Vacchi E., Ambrosini R., Galati S., Städler C., Kaelin-Lang A., Melli G. "Intra-Epidermal nerve fiber density as a biomarker of PD progression" 9° Giornata della Ricerca della Svizzera Italiana, Lugano. March 15, 2019.

Vacchi E., Capovani C., Grandi L.C., Kaelin-Lang A., Melli G. "Evaluation of autonomic nerve fiber density in small fiber neuropathy patients by skin biopsy confocal microscope analysis" 21th Swiss Society for Neuroscience Meeting, Campus Biotech, Geneve, Switzerland February 1, 2019

Awards

"De Barjac prize" for the best publication of a biomarker translational medical research project 2021. Annual Assembly of the Swiss Society of Clinical Chemistry, Neuchatel (CH), September 8-10, 2021.

Best Poster Presentation at the 2° EVIta symposium, Lucca (ITA), September 20-22, 2021.